Master Thesis

Effect of Blade Parameters on Wind Turbine Fatigue Loads

Bruno de Carvalho Rocha Ceppas

COWI TU Delft Ørsted

Effect of Blade Parameters on Wind Turbine Fatigue Loads

Master of Science Thesis

Faculty of Civil Engineering and Geosciences

Delft University of Technology

Author	Student Number
Bruno de Carvalho Rocha Ceppas	5768543

Committee Members:

Prof. Dr. Andrei Metrikine	TU Delft - Chairman
Dr. Ir. Alessandro Cabboi	TU Delft
Dr. Ir. Mehmet Ozan Gözcü	Ørsted
Dr. Ir. Oscar Gerardo Castro Ardila	COWI
Ir. Christian Ammitzbøll Madsen	COWI

Cover photo by Chirapriya Thanakonwirakit

COWI TU Delft Ørsted

Acknowledgements

I see this master thesis as a cornerstone of my academic career - and what an incredible journey it was! Living in four different countries led to enriching experiences, countless memories, and amazing friends from all over the world.

Starting from Brazil, I want to thank my four best friends Ney Feijó, Rennan Sanches, Matheus Faillace, and Danniel Silva. The opportunity to have grown up with them, sharing all those unforgettable moments, was priceless. I was extremely happy, and there is only one word which is able to express my feelings: *"saudades"*.

Next, I would like to thank *Colégio de São Bento do Rio de Janeiro*, home where I spent 11 years of my educational journey. This school taught me the value of hard work and became the keystone of my academic background, allowing me to pursue my career goals at top-tier universities and companies.

Moving on to Portugal, I want to thank Virginio Francisco and Mariana Covas. The first experience living abroad and the COVID-19 pandemic posed significant challenges. However, with our strong bonds of friendship, we were able to overcome every obstacle during the Bachelor's.

Then, the Netherlands. Choosing TU Delft was one of the best decisions I have ever made. From a professional perspective, it is incredible how much you can grow when surrounded by high-level colleagues. There are brilliant minds over there, and each one of them offers something valuable to learn. Socially speaking, in Delft, I lived some of the best years of my life. In a few words, I can only say that it was a dream. I made numerous friends from all corners of the globe, but I would especially like to thank my "old" and "new" IP groups, they were like a family to me.

With respect to my thesis, I would like to thank the European Union for granting me a scholarship. Without this help, my project would not have been possible. I am pleased to meet the expectations and deliver meaningful results. Since I was a kid, it was always a dream to give my contribution to accelerate the green energy transition.

During my research, I had the opportunity to count on the guidance of a valuable team of Supervisors. With the privilege of having four postdoc Supervisors onboard this project, I want to thank all of them for always focusing on the physical meaning of the theory and the results obtained. The amazing world behind the formulas will always fascinate and remind me of the reason I studied engineering.

From the companies' side, I would especially like to thank Dr. Ir. Oscar Ardila for his unwavering daily dedication to sharpening my skills. Sharing my routine with a mentor like him was priceless. Likewise, I want to express my gratitude to Dr. Ir. Ozan Gözcü. His enthusiasm for the thesis topic was contagious, and it always sparked my desire to go the extra mile. Lastly, I would like to thank Ir. Christian Madsen for the unique attention he gave me. With his trademark positive spirit, he made me feel comfortable in a new type of environment, allowing me to deliver my very best.

From the university side, I would like to start by thanking Prof. Dr. Andrei Metrikine. He was the best Professor I had. With his mesmerising classes and a remarkable ability to explain complex phenomena and complicated problems in a clear way, he opened my eyes to the beauty of the structural dynamics. Moreover, I would like to express my gratitude to Dr. Ir. Alessandro Cabboi, who was always available to help and engage in discussions. His experience in reviewing research papers played an important role in sharpening the quality of my thesis report.

Lastly, from my family, I would like to thank my grandparents, Tonico and Marilia, for their continued interest in following every step of my academic career.

But most importantly, I want to thank my parents, Bruno and Claudia, for their limitless love and support. They were the best gift I could have ever received. I have never seen parents like them.

The picture below is my favourite of our family. I believe it perfectly summarises all the effort they made during this journey and all the support they gave me to chase my dreams.

Exactly 14 years after this picture was taken, on 28$^{\text{th}}$ August 2024, I received the green light to defend my master thesis, titled "Effect of Blade Parameters on Wind Turbine Fatigue Loads".

Thank you for absolutely everything.

Te amo pai! Te amo mãe!

Bruno de Carvalho Rocha Cepparo

Copenhagen, September 2024

Science Fair Project

Wind Energy

28$^{\text{th}}$ August 2010
Rio de Janeiro, Brazil

Abstract

Offshore wind turbines are complex systems that exhibit intricate interactions among the loads, the environment, and the turbine structure. Therefore, wind turbine design significantly relies on the ability to understand this coupled system and accurately estimate the in-service design loads.

A review of the available literature indicates that most of the current understanding of the structural dynamics of offshore wind turbines stems from research on 5 MW turbines. However, as the wind sector progresses towards taller turbines with larger rotor diameters, the interaction between the rotor and support structure becomes more relevant. In addition, with blades more slender, flexible, and lighter than ever before, the complexity of the turbine dynamics significantly increases. Accentuated geometric nonlinear effects, combined with a more sophisticated blade geometry and anisotropic material behavior, contribute to the challenging structural response of modern blades. Hence, there is a need for further investigation into the influence of modern blades on the turbine response and resulting design loads.

In this context, the present study performs a sensitivity analysis on the IEA 15 MW Reference Wind Turbine to investigate which blade parameters have the greatest influence on fatigue loads during normal turbine operation under turbulence. The sensitivities of different blade parameters are ranked, a reflection on the type of relationship (i.e., either monotonic, quasi-monotonic, or non-monotonic) between each blade parameter and the model response is provided, as well as an indicator of the change caused in the magnitude of the loads. One of the goals of this research is to support blade manufacturers in improving their blade designs by tuning the parameters in new blade models to achieve lower fatigue loads at different positions of the turbine structure. Furthermore, this study aims to highlight parameters that should receive special attention during the manufacturing phase, as slight deviations in their values from the original blade design may considerably increase the fatigue loads.

In this work, aeroelastic simulations are performed with HAWC2, and fatigue loads are quantified using Damage Equivalent Loads, while the first-order Elementary Effects method is employed to assess the parameters' individual effects on the turbine response. Lastly, two strategies are adopted to ensure that the causes of changes in the dynamic response of the turbine are mainly attributed to variations in blade parameters: turbulence files are generated only once per wind condition and reused in all simulations, and the controller is retuned with HAWCStab2 each time a blade parameter is altered.

The findings reveal a dominant influence of the shear centre on the flapwise moment at the blade root, as well as on the fore-aft moments at the tower-top and tower-bottom across different wind speeds. These moments are critical with respect to fatigue loads since they align with the wind direction and experience a high number of load cycles during turbine operation. This research also unveils that even slight differences in the shear centre position along the chord can have a significant impact on the fatigue loads. For the torsional moment at the blade root - a challenging load component in modern blades due to their increasing length, slenderness, and flexibility - the flapwise bending stiffness, followed by the edgewise bending stiffness, exhibit the highest importance levels at below and near rated wind speeds. In contrast, at above rated wind speeds, the importance of the edgewise swept increases significantly, surpassing the influence of both flapwise and edgewise bending stiffness. Lastly, the torsional stiffness typically plays an important role at near and especially above rated wind speeds in several load components at the tower.

Although the findings may vary based on the size, type, and control of the wind turbine evaluated, the results of this thesis are expected to contribute to the load analysis of other turbines.

Contents

List of Figures

List of Tables

Abbreviations

Acronym	Definition
AAT	All-At-A-Time
BEM	Blade Element Momentum
COV	Coefficient Of Variation
DEL	Damage Equivalent Load
DLB	Design Load Basis
DLC	Design Load Case
DYN	Dynamic method
DTU	Technical University of Denmark
EE	Elementary Effects
FEM	Finite Element Method
FRP	Fibre-Reinforced Polymer
FVW	Free Vortex Wake method
GDW	Generalized Dynamic Wake
LCT	Load Case Table
OAT	One-At-A-Time
OWT	Offshore Wind Turbine
PM	Palmgren–Miner
QS	Quasi-Static method
RB	Rigid Body
RFC	Rainflow Counting
RWT	Reference Wind Turbine
TSR	Tip Speed Ratio

1 Introduction

1.1. Background

The growth of energy consumption combined with the constraints of the Paris Agreement on reducing greenhouse gas emissions by 43% by 2030 has stimulated interest in renewable sources [1]. As a result, due to its cost competitiveness and the widespread availability of wind as a natural resource, wind power has been in the spotlight among renewable energies.

Offshore wind farms are a particularly promising area of the wind energy sector. Although it is currently more expensive than onshore wind farms, it also comes with a broad range of benefits. Wind speeds at the sea are not only significantly stronger than inland but also do not face obstacles on the earth's surface such as vegetation, buildings, or mountains. Furthermore, the wide offshore space availability allows for the installation of bigger turbines, with longer blades. These advantages translate into larger power generation capacities, contributing to the industry's primary goal of reducing per-megawatt project costs. Finally, installing wind turbines offshore also mitigates the social costs entailed in placing them near populated areas.

The cost reduction of offshore wind energy can also be achieved by optimizations on different stages such as the structural design, fabrication, and installation. However, offshore wind turbines (OWTs) are complex systems that exhibit significant interactions between the loads, the environment, and the different subsystems as illustrated in Figure 1.1.

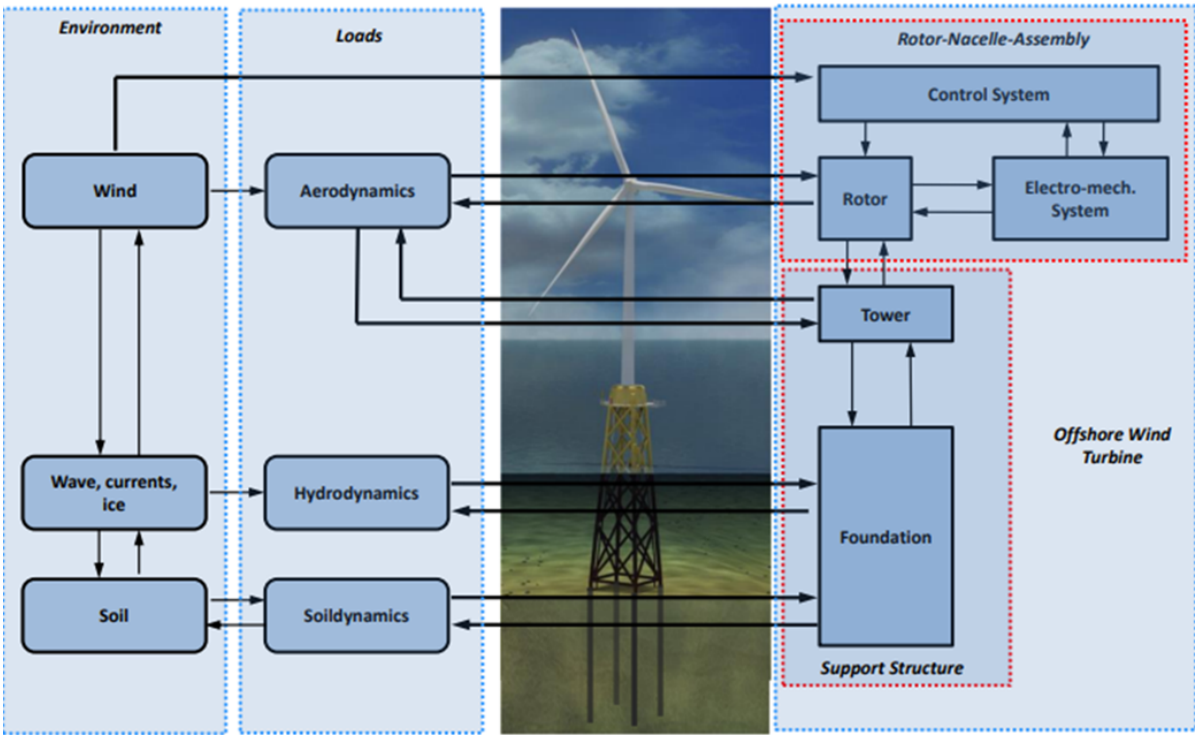

Figure 1.1: Interactions between the loads, the environment, and the different OWT subsystems [2].

Thus, due to the complex interactions introduced by the OWTs, any optimization of the individual subsystems requires proper consideration of the dynamics of the whole system. The understanding of this coupled system is especially relevant when designing the rotors and support structures of OWTs, as they significantly rely on the accurate estimation of the in-service design loads.

1.2. Motivation and Research Gap

Even though much has been accomplished in terms of cost reductions, there are still opportunities for further progress. The wind speed typically increases with altitude, and by employing larger rotor diameters, more energy can be harnessed, thereby reducing per-megawatt project costs.

Therefore, since the realisation of the world's first offshore wind farm in 1991 off the coast of Vindeby, Denmark, the turbine's height and energy output has been increasing rapidly, as shown in Figure 1.2. The largest announced OWTs under development are reaching 22 MW, compared to the 0.45 MW turbines commissioned by Ørsted at Vindeby [3] [4].

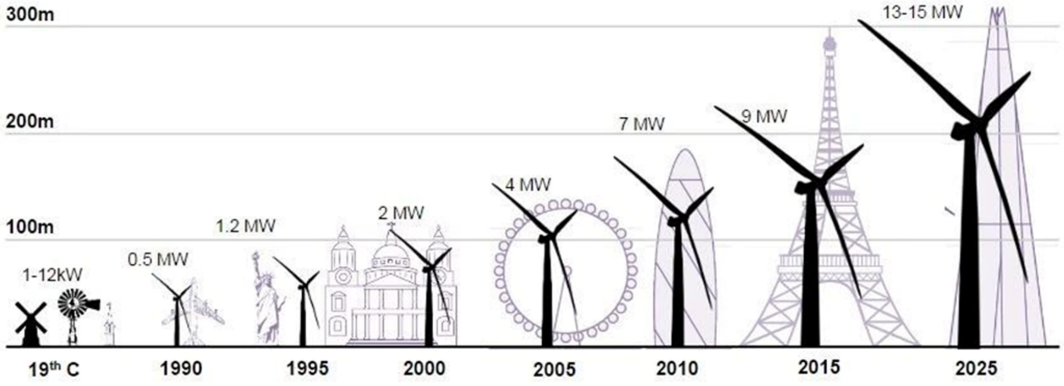

Figure 1.2: Evolution of wind turbine heights and energy output [5].

A review of the available literature indicates that most of the current understanding of the structural dynamics of OWTs stems from research on 5 MW turbines. Nevertheless, as the wind sector progresses towards taller turbines with larger rotor diameters, the interaction between the rotor and support structure becomes more relevant. Moreover, as depicted in Figure 1.3, the blades are becoming more slender, flexible, and lighter than ever before, significantly increasing the complexity of the turbine dynamics [6] [7].

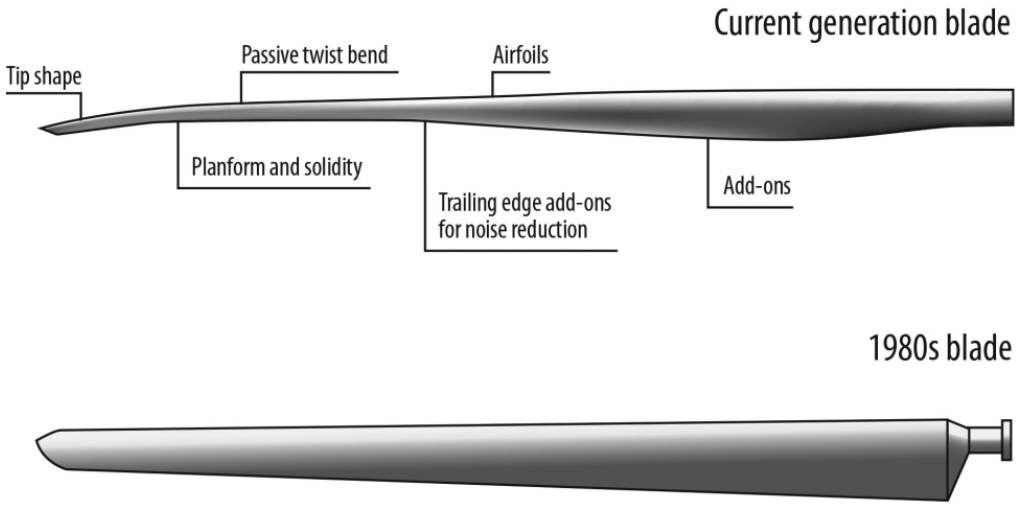

Figure 1.3: Comparison of a modern blade (top) and a commercial blade from the mid-1980s (bottom) scaled to the same length. [7].

The increased gravitational loads and aerodynamic forces experienced by modern, flexible blades induce geometric non-linear effects, such as large rotations and deflections. These effects not only trigger and propagate damage in common stress regions (e.g., spar caps and the leading and trailing edges), but also in more varied and unexpected sections of the blade, often involving more complicated damage mechanisms [8] [9].

Additionally, the more sophisticated blade geometry, as shown in Figure 1.3, combined with the anisotropic material behavior, expand the range of factors contributing to the complex structural response of modern blades [10].

Hence, there is a need for further investigation into the structural behaviour of the current generation of wind turbines.

1.3. Objective and Research Questions

This thesis gives special attention to the blades' influence on the turbine response and resulting fatigue design loads, aiming to further close the gap between rotor and support structure design.

To achieve this goal, the **main research question** of this thesis can be formulated as follows:

''Which blade parameters have the greatest influence on wind turbine fatigue loads during normal turbine operation under turbulence?''

In order to better frame the problem, several sub-questions are proposed:

- What is the most appropriate Wind Turbine Simulation Tool to be used?
- What is the most suitable Fatigue Evaluation Method to be utilised?
- What is the most proper Sensitivity Analysis Approach to be adopted?

Thus, this thesis is expected to rank the sensitivities of different blade parameters with respect to fatigue loads, indicating which are the most important parameters to be examined in more detail in future work.

The insights provided by this research aim to support blade manufacturers in two distinct phases:

1) In the **design phase**, by providing an initial understanding towards potential blade parameter modifications.

   The first goal is to support blade manufacturers in improving their blade designs by tuning the parameters in new blade models to achieve lower fatigue loads at different positions of the turbine structure, increasing the turbine lifetime.

2) In the **manufacturing phase**, by providing an initial understanding of which parameters are critical to having their deviations from the original design minimised.

   Due to the unavoidable deviations between designed and fabricated blades [11], the second goal of this work is to indicate parameters that, when subjected to slight mismatches, have potential to considerably increase the fatigue loads, decreasing the turbine lifetime.

1.4. Scope

This research is focused on the IEA 15 MW Reference Wind Turbine (models are publicly available on GitHub [12]) and does not consider specific site conditions.

The blade parameters under evaluation in this thesis are listed in Table 1.1. These parameters were selected based on available literature and previous simulation experiences from experts at COWI and Ørsted, which suggested their likely greater level of importance compared to other options.

Furthermore, in this work, each blade parameter is considered independent across the full range, and only the dependence on wind speed is studied.

Table 1.1: Blade parameters.

Parameter	**Units**
Flapwise bending stiffness	Nm^2
Edgewise bending stiffness	Nm^2
Torsional stiffness	Nm^2
Shear centre	m
Edgewise swept	m

Nm^2	Newton square metre	m	metres

The fatigue loads are investigated at three critical regions in wind turbines, namely the blade root, tower-top, and tower-bottom. The load components under evaluation are the moments M_x, M_y, M_z at the three regions, besides the forces F_x, F_y, F_z at the tower-top and tower-bottom. At the blade-root, the forces are not considered. This is because the moments are the dominant loads at this position [13]. Thus, the forces are usually not contemplated when designing blades against fatigue [13].

The global coordinate system adopted in this research is illustrated in Figure 1.4, with the wind direction aligned along the y axis.

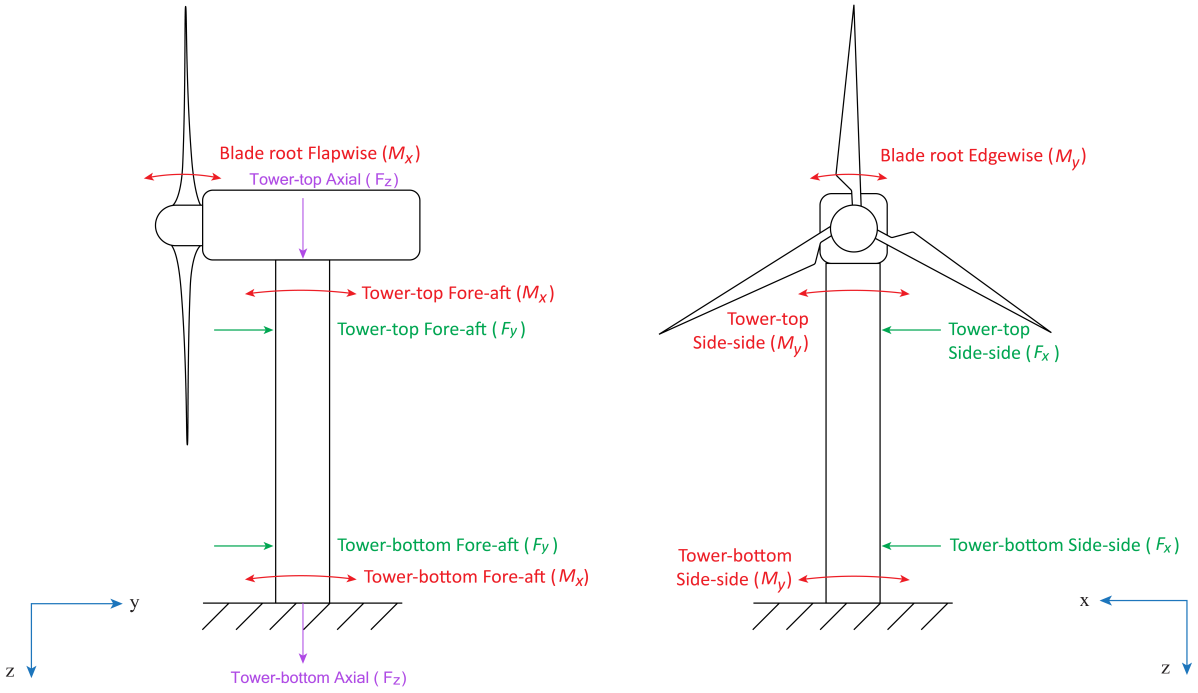

Figure 1.4: Global coordinate system and loads. (Adapted from [14])

Lastly, the load analysis is based on the Design Load Case (DLC) 1.2 of the IEC 61400-1 [15], which is a standard that outlines minimum and fundamental design requirements to guarantee the structural integrity of wind turbines [16]. In the DLC 1.2, only normal operation under turbulence is considered, whereas gusts, start-ups, shut-downs, and parked/idling events are not contemplated. The DLC 1.2 is the main contributor to the fatigue limit state [17], accounting for more than 90% of the total fatigue damage based on industry experience.

1.5. Research Methodology

Among the available versions of the IEA 15 MW Reference Wind Turbine (IEA 15 MW RWT), this research utilises the onshore version. This simplification is adopted since it maintains the validity of the study while reducing unnecessary complexity. In other words, the offshore version would require an additional modelling component with respect to hydrodynamic loads, which can be avoided since this would not significantly alter the effect of blade parameters on fatigue loads.

In this thesis, the onshore IEA 15 MW RWT and the DLC 1.2 are used as inputs for the wind turbine simulation tool. Next, a code is introduced to process the simulation output (i.e., the dynamic response of the wind turbine) and extract the fatigue loads. The sensitivity analysis begins by altering the blade parameters, repeating the simulation and fatigue evaluation phases, and comparing the outputs to assess the effect of blade parameters on fatigue loads during normal turbine operation under turbulence. Figure 1.5 illustrates how these different research tools are intertwined to obtain the desired results.

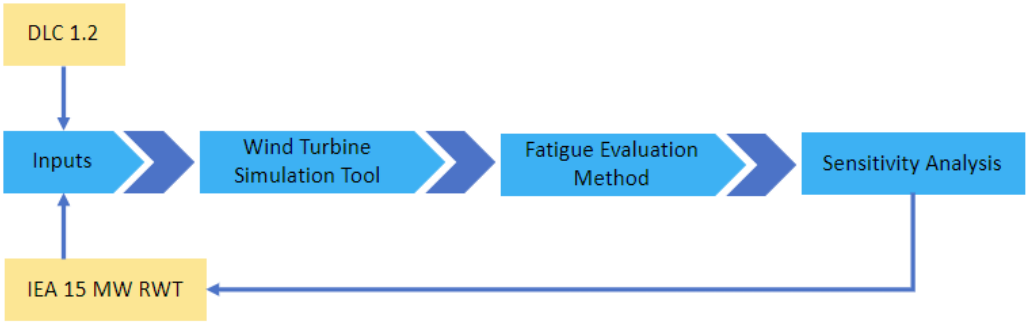

Figure 1.5: Methodology overview.

1.6. Thesis Outline

This report initially started in **Chapter 1** with an introduction to offshore wind energy and the industry's strategies to make it more cost-competitive against other energy sources. Subsequently, a research gap was identified and motivations for the study were presented. Finally, the objectives, scope and research methods of this master thesis were specified.

In **Chapter 2** a literature review is developed to delve into the fundamental components of this thesis. It starts by explaining the selected blade parameters and their relevance to the topic. Then, a summary of some of the available simulation tools in the industry is presented, accompanied by an examination of relevant evaluation methods regarding wind turbine fatigue loads. In the end, this chapter investigates different sensitivity analysis approaches, in which the main trade-offs are highlighted.

Chapter 3 provides a detailed description of the case study. It presents the characteristics of the IEA 15 MW RWT, outlines the procedure for modeling turbulence, and explains the verification process for the turbine model. Additionally, it addresses the proposed sub-questions for this research, explains the importance of the controller tuning process for this study, and defines the blade parameter ranges to be considered in the sensitivity analysis.

Chapter 4 explains the selected sensitivity analysis method, presents the results of the study, and discuss the findings.

Lastly, the conclusions of the thesis and recommendations for future studies are stated in **Chapter 5**.

2
Literature Review

2.1. Blade Parameters

2.1.1. The Aerofoil Shape

Aerofoils, the cross-sectional shape of wind turbine blades, are the foundation of blade designs. When the aerofoil shape is exposed to an incident wind velocity (W) with an angle of attack (α), two aerodynamic forces are generated on the blade section - lift force (f_L) and drag force (f_D) – as illustrated in Figure 2.1. The former is perpendicular to the incident wind velocity and generates a positive contribution to the aerodynamic torque, whereas the latter is parallel to the incident wind velocity and generates a negative contribution to the aerodynamic torque. In other words, lift induces rotation, while drag resists rotation. Hence, the combination of these forces results in a net aerodynamic force that causes the blades to rotate.

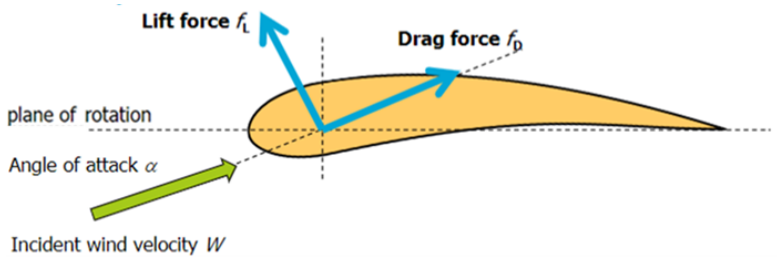

Figure 2.1: Aerodynamic forces on aerofoil shapes [18].

However, using a single aerofoil profile along the whole blade results in poorer efficiency of the blade design. An efficient design consists of several aerofoil profiles, with distinct chords and thicknesses, blended at an angle of twist terminating at a circular blade root [19]. The chord is defined as an imaginary straight line from the leading edge to the trailing edge of the aerofoil. The thickness is the distance between the upper and lower surfaces, measured perpendicular to the chord line. Lastly, the angle of twist is described as the angle between the tip aerofoil and the local aerofoil in analysis [19].

Figure 2.2 depicts two distinct aerofoil profiles utilised in an arbitrary turbine model, along with their corresponding chord and thickness measurements. Whereas Figure 2.3 shows the twist angle distribution across a typical blade.

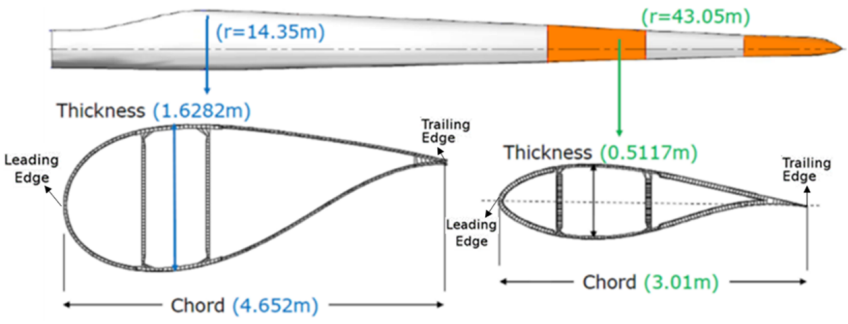

Figure 2.2: Different aerofoil profiles used in an arbitrary turbine model. (Adapted from [20])

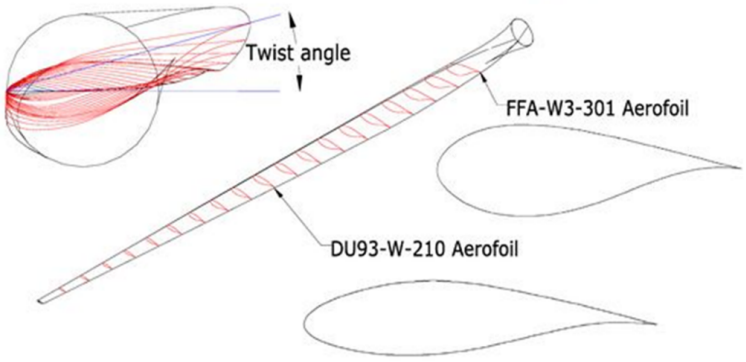

Figure 2.3: The twist angle distribution along a typical blade [13].

2.1.2. Parameters Related to Structural Stiffness and Geometry

This section describes the blade parameters under evaluation in this thesis, which are listed in Table 1.1

By definition, the bending stiffness of a structure refers to its ability to resist a deformation caused by bending moments. A wind turbine blade can be subjected to two different bending moments: the flapwise and edgewise bending moments. The flapwise bending moment predominantly arises from aerodynamic forces, whereas the edgewise bending moment is primarily attributed to the gravitational effects [13].

The flapwise and edgewise bending stiffnesses are essential to avoid excessive deformations in these respective directions. For instance, sufficient flapwise bending stiffness is important to prevent the blades from crashing into the tower [21]. Moreover, for larger turbines with rotor diameters bigger than 70 meters, loads resulting from the mass of the blade become critical [22]. Therefore, satisfactory edgewise bending stiffness is required to avoid increased fatigue loads on the turbine structure and, consequently, prevent structural failure.

Furthermore, the flapwise and edgewise deformations experienced by the blades lead the blade to twist along its longitudinal axis. In other words, a torsional load component is provoked due to flapwise and edgewise loads. This component has a major influence on localized deformations (and strains/stresses), especially at the root and transition zone of the blade [23], as indicated in Figure 2.4.

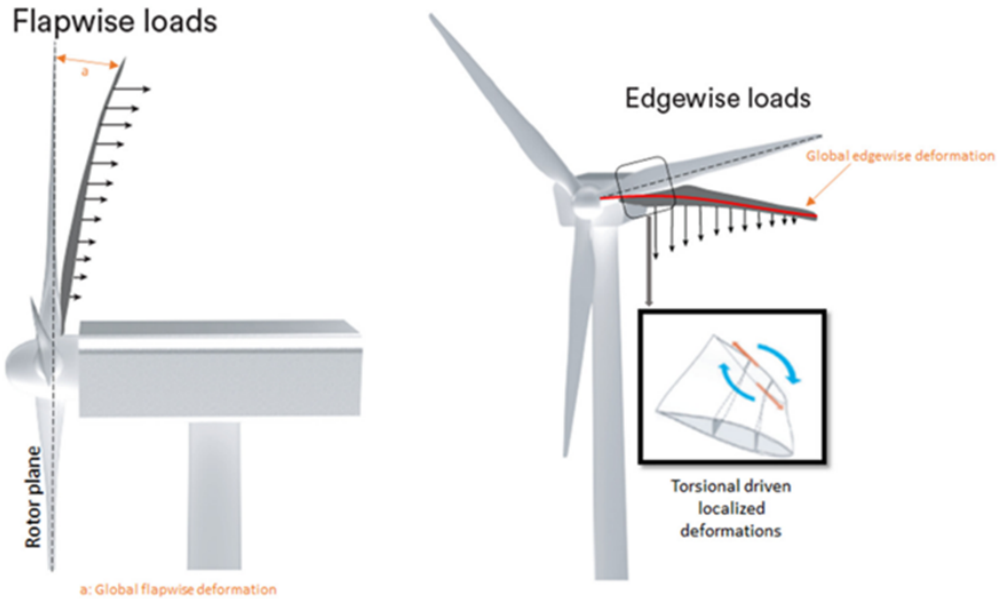

Figure 2.4: Torsional load component caused by flapwise and edgewise loads [23].

The torsional stiffness parameter describes the ability of the structure to resist a twisting deformation caused by a torsional load. The task of dealing with these torsional components and generated localized deformations is considered one of the current main challenges faced by the industry due to the increasing length, slenderness, and flexibility of modern blades.

Although not a major design concern for smaller wind turbines in the past, the phenomenon of flutter has emerged as a noteworthy challenge to overcome when developing long and flexible modern wind turbine blades. This is due to the fact that as blade lengths rise, there is a greater chance that the local wind velocity on rotating blade sections will surpass critical limitations [24]. Additionally, blade flutter has also become a problem owing to the reduced torsional and bending stiffness of modern blades [25].

Flutter has been acknowledged as a dangerous phenomenon encountered in flexible structures in the presence of incident aerodynamic forces since it was first seen in airplanes during World War I. It is described as an unfavourable aerodynamic coupling between flapwise and torsional vibrations of blades when subjected to these kinds of forces [26]. This aeroelastic instability causes the amplitudes of the flapwise and torsional motions to escalate, which increases the risk of fatigue failure of the blades [26].

The next parameter contemplated in this thesis is the shear centre, which is commonly used to describe cross-sections. It is characterised as the point at which a force (F) applied parallel to the plane of the cross-section will produce no torsional deformation ($\kappa_z = 0$) [27], as illustrated in Figure 2.5.

Moreover, the shear centre has a tied relationship with torsional load components and with the torsional stiffness parameter. The magnitude of the root torsional moment is predominantly influenced by the way the load is applied in the shear centre [23]. This is because, when the blade is in operation, its deflection is a consequence of the combination of flapwise loads, edgewise loads, and blade dynamics during rotation. These movements cause forces to not precisely act at the shear centre of the blade, thereby producing an arm that generates a torsional moment at the root [28]. Lastly, the torsional stiffness is defined with respect to the shear centre [29].

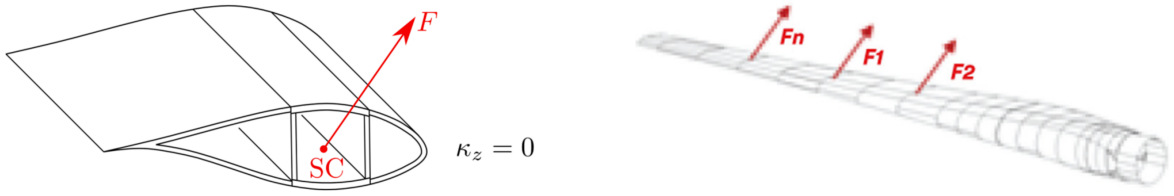

(a) The shear centre at a blade section [21].

(b) Applied combined load vectors in the shear centre at different sections [23].

Figure 2.5: The shear centre across the blade span.

Lastly, the edgewise swept parameter refers to blades that are not straight but manufactured with an intentional sweep in the edgewise direction (i.e., perpendicular to the rotor axis), typically in the outboard portion of the blade. Figure 2.6 compares a straight blade and a backward swept blade.

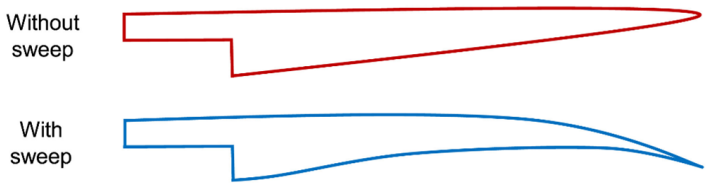

Figure 2.6: Sweeping adaptability of wind turbine blades. (Adapted from [30])

Previous studies have shown that introducing a moderate amount of sweep can effectively mitigate fatigue loads since it produces a structural coupling between flapwise bending and torsion [31] [32]. Based on the swept direction, the induced coupling can either reduce loads on the turbine structure by decreasing the angle of attack (backward sweep) or increase the power output of the turbine by increasing the angle of attack (forward sweep) [32].

2.2. Wind Turbine Simulation Tools

Although Computational Fluid Dynamics calculations are frequently used to study wind turbines, aeroelastic codes provide the benefit of being computationally much cheaper while offering a satisfactory level of agreement with more detailed modelling and experimental results. Thus, the aeroelastic codes enable the exploration of a diverse set of parameters at a reasonable computational cost [33].

Several aeroelastic tools are available to determine the loads and dynamic response of the turbine. OpenFAST [34], HAWC2 [35], and Bladed [36] are examples of these codes. They employ different modelling approaches for the structure and aerodynamics, with the latter two providing linearization features, as depicted in Table 2.1.

Table 2.1: Summary of numerical simulation tools capabilities used to model OWTs [37] [38] [6].

Software	Structure	Aerodynamics	Linearization
OpenFAST	RB + Modal / FEM + DYN / QS	BEM + GDW / FVW	-
HAWC2	FEM + DYN	BEM + GDW	HAWCStab2
Bladed	Modal	BEM + GDW	Bladed (lin.)

RB:	Rigid Body	BEM:	Blade Element Momentum
FEM:	Finite Element Method	GDW:	Generalized Dynamic Wake
DYN:	Dynamic method	FVW:	Free Vortex Wake method
QS:	Quasi-Static method		

For the aerodynamics, all tools can use the BEM theory and the GDW method. Nevertheless, there are several differences between the codes that should be highlighted. For instance, in terms of structural blade models, HAWC2 and OpenFAST directly employ the reference 6x6 mass and stiffness matrices as a basis for an exact model of the geometric coupling effects. In contrast, Bladed utilises beam properties derived from the 6x6 matrices which include coupling effects arising from offsets between the shear and elastic centres. Furthermore, both Bladed and HAWC2 employ a multibody segmentation to account for geometrically non-linear effects, whereas OpenFAST opts for a direct internal non-linear finite element analysis. Finally, Bladed and HAWC2/HAWCStab2 provide a feature to linearize their models around a non-linear equilibrium point, which is the standard approach for stability assessment, but the state-of-the-art OpenFAST does not offer similar functionality [6].

2.3. Fatigue Evaluation Methods

Fatigue is defined as the progressive structural damage that occurs when a material is subjected to cyclic or fluctuating loads [39]. In this phenomenon, the material cracks after bearing a certain number of load cycles, while a single load of equal magnitude would not have caused a failure [40]. Thus, fatigue failure occurs due to damage accumulation and is especially common in structures and components exposed to time-variable loads (i.e., dynamic loads). In wind turbines, fatigue significantly impacts the lifetime of the tower, blades, and drivetrain, becoming a major design driver [41].

Fatigue evaluation methods can be divided into two categories, namely time-domain methods and frequency-domain methods.

Time-domain methods are the classical approaches. In this type of analysis, the response of the structure is expressed as a load history (stress and strain histories are also used), with fatigue damage occurring due to variations in the load over time, referred to as cycles. Given this load record, a counting method is applied to allow the identification of cycles with different amplitudes and mean values. Next, the total fatigue damage is estimated by aggregating the contributions of each damage cycle.

Cycle identification is straightforward if, for instance, a simple sinusoidal signal is under evaluation, as the number of cycles and their respective amplitudes and mean values are evident. However, during their service life, wind turbines often exhibit highly complex load responses, because the external loads, such as wind and waves, have an irregular and random nature. The Rainflow Counting (RFC) algorithm developed by Matsuishi and Endo [42] is the standard technique for the decomposition of complex load time series [41], as it is considered the most accurate method among the common cycle counting algorithms [40].

Then, the total damage is typically assessed using the Palmgren–Miner (PM) rule [43], which is based on a linear damage accumulation hypothesis. In this formulation, each cycle of constant load range produces a specific amount of damage, which accumulates linearly with the number of load cycles applied, leading to material failure. However, this method does not account for the sequential impact of the load history. The crack propagation rate is influenced by the chronological order of load cycles, but this cannot be captured by a linear damage accumulation hypothesis [40]. Moreover, this approach overlooks the material's potential for regeneration, as cracks may have the ability to heal under compressive loads [40].

Despite these limitations, the combination of the RFC technique and the PM rule has been thoroughly tested and is recognised as a well-established time-domain approach [40]. For this reason, the main standards and guidelines of wind turbines, including the IEC 61400-3 [44], IEC 61400-1 [15], DNV-2011 [45], GL-2010 [46], and GL-2012 [47], suggest their application for fatigue assessment.

Finally, the combination of the RFC algorithm and the PM rule can be seen as a process that converts an irregular signal into a cyclical load of constant amplitude [48] [49]. In other words, the goal would consist of achieving a cyclical load with a constant amplitude that causes an amount of damage which is equivalent to the damage caused by the original complex signal. The peak-to-peak constant amplitude illustrated in Figure 2.7 is found by the PM rule and is called the Damage Equivalent Load (DEL). This quantity, therefore, describes the damage accumulation in a component.

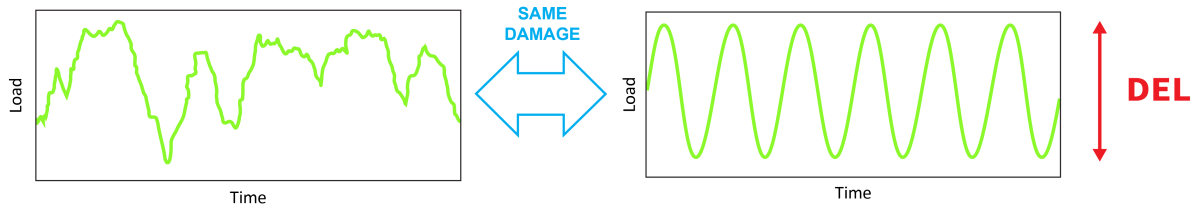

Figure 2.7: Fatigue estimation: from complex signal to cyclical load of constant amplitude. (Adapted from [50])

The main advantage of using the RFC technique, along with the PM rule and the DEL quantity, is that it allows for a straightforward comparison of the fatigue damage from different load histories, as the time-domain data is translated into a single number [50] [48]. In contrast, multiple load records are typically required to develop reliable statistical considerations about the distribution of rainflow cycles, the fatigue damage, and the system service life [51]. Hence, time-domain analyses become significantly time-consuming.

To overcome the computational cost of time-domain analyses, **frequency-domain methods** were introduced. In this approach, the irregular load time series are modelled as random phenomena and viewed as realisations of a stationary Gaussian process [40] [52]. The process is described in the frequency-domain by a power spectral density function, which provides an overview of the power distribution over frequencies.

The main benefit of this approach is the ability to obtain analytical expressions that allow the estimation of cycle distribution and fatigue damage using a specific cycle counting algorithm (e.g., the RFC technique), without requiring knowledge of each load time series [52]. However, loads usually have a broad-band spectral density, and currently there is no clear theoretical framework for this case [51]. The relationship between the rainflow cycle distribution and spectral density is still under discussion due to the complexity of the RFC algorithm's cycle extraction rules [51]. For this reason, the methods proposed in the literature are all approximate and based on empirical solutions, utilising best-fitting techniques [40][51].

2.4. Sensitivity Analysis Approaches

Sensitivity analysis is defined as the study of how variation in model output can be attributed to different input variations [53]. It identifies which input parameters have the most influence on the model response and assesses how the model reacts to slight changes in input parameters. Additionally, it can detect specific input values that trigger sudden changes in the model response and evaluate the impact of input inaccuracies on the model output [54]. Thus, sensitivity analysis studies provide deeper insights into the model behavior.

Sensitivity analysis approaches can be divided into three categories, namely local sensitivity analysis, global sensitivity analysis, and screening methods.

Local sensitivity analysis examines the relationship between input and model response at a point (or set of points) of the input space [54]. The goal of this type of analysis is to assess the effect of a single parameter on the model output at a time. This is achieved using the One-At-A-Time (OAT) technique, where one factor changes at a time while the remaining input parameters are fixed. As a result, this approach reduces the number of simulations required to assess the sensitivity of a given parameter, which is typically evaluated through finite differences or partial derivatives of output functions [54]. However, the results of local sensitivity methods are only valid at a specific point (or set of points), as local methods do not account for the interaction between the parameters [55]. Therefore, the results cannot be proved across the entire input space, leading to relevant limitations, especially when dealing with non-linear models [55].

To overcome the limitations of local methods, **global sensitivity analysis** was introduced to explore the relationship between input and model response across the entire input space [54]. The goal of this type of analysis is to assess the effect of each input factor and their combination on the model response. This is achieved using the All-At-A-Time (AAT) technique, where all input factors are perturbed at the same time, and the response is studied based on statistical analyses. Several statistical methods can be employed to assess global sensitivity, such as variance decomposition (Sobol indices), standardized regression coefficient analysis (linear regression of Monte Carlo simulations), and partial correlation coefficient analysis. However, global sensitivity analysis is typically computationally expensive since it employs a high number of data points throughout the complete input domain, and it fails to answer which part of the input space results in the largest change in the model response [54].

Screening methods are used to rank the importance of input parameters using a relatively small number of data points across the input space [56]. These methods are particularly valuable in the initial stage of a sensitivity analysis to select a few key input parameters for further detailed evaluation and delete parameters that have little effect on the output. This exclusion step is important to reduce the complexity of the model and the computational cost of the simulations, especially if a more sophisticated method is to be applied in the next stage [57].

The most popular screening method is the Elementary Effects (EE) method proposed by Morris [58], which is based on the OAT technique. From the sampled data points, first-order finite differences are calculated as a measure of how the output changes when one input changes. This first-order EE method is often seen as a local sensitivity analysis since it calculates the influence of each parameter without considering interactions with other parameters [59] [60]. Lastly, the first-order EE method can detect non-linearity and interaction effects between the parameters [59] [61].

However, the first-order EE method can be extended in order to account for the interaction between the parameters [59] [60]. This extension, called as second-order EE method, investigates how the response changes for a given input parameter at several locations (points) in the input parameter hyperspace. In this formulation, only one parameter is changed at a time, but this variation is carried out repeatedly using different values for the remaining input parameters. Thus, the second-order EE method is treated as a global sensitivity analysis [60].

The EE method has gained recognition as an effective approach for ranking multiparameter systems. It has been frequently used in wind energy investigations across the world, especially by researchers at the National Renewable Energy Laboratory in the United States. In 2018, this group employed the EE method to assess the sensitivity of wind parameters on ultimate and fatigue wind turbine loads [62].

Then, in 2019, they extended their research by also investigating the sensitivity of turbine properties on wind turbine loads [60]. Finally, in 2023, the group included other modelling parameters that are relevant to floating offshore wind turbine loads in their study [63].

Thus, the choice between local sensitivity analysis, global sensitivity analysis, and screening methods should be based on the requirements and assumptions of the problem under analysis. Factors such as desired calculation time, linearity, dependency, and the number of input parameters under evaluation should guide this decision-making process.

3
Case Study Description

3.1. Simulation Tools

3.1.1. Aeroelastic Simulations with HAWC2

Aeroelasticity is the field of physics and engineering that studies the interactions between inertial, elastic, and aerodynamic forces that occur when an elastic body interact with fluid flow [64]. Wind turbines are elastic bodies subjected to these forces, and thus, aeroelastic simulations are required to guarantee the safety and reliability of their design. Consequently, these simulations are crucial instruments for promoting the growth of wind energy by offering models that can simulate the behaviour of wind turbines under a wide range of configurations and operational conditions [65].

As previously seen in Chapter 2, a variety of aeroelastic codes is available. For this thesis, **HAWC2** is the preferred choice due to license availability reasons, and version 13.0.5 is used to perform the turbine analyses.

HAWC2 is intended for calculating wind turbine response in the time-domain and has a structural model based on a multibody formulation, as illustrated in Figure 3.1. In this approach, all the main components of a wind turbine, such as the blades and the tower, are represented as independent main bodies and connected through different kinds of algebraic constraints. These constraints either fix or allow specific translations and rotations, imposing limitations on the bodies' motion [66]. Then, each main body is divided into sub-bodies, with every sub-body consisting of an assembly of Timoshenko beam elements, which account for shear deformation and rotational inertia effects [67].

The multibody segmentation enables the modelling of complex structures such as modern flexible blades. The Timoshenko beam elements add flexibility to each sub-body, where the formulation is linear and deformations are assumed to be small. The structural non-linear effects, such as rotations and deformations, are captured through the coupling constraints in between the sub-bodies. As a result, large blade deflections are included using a sufficient number of sub-bodies [66].

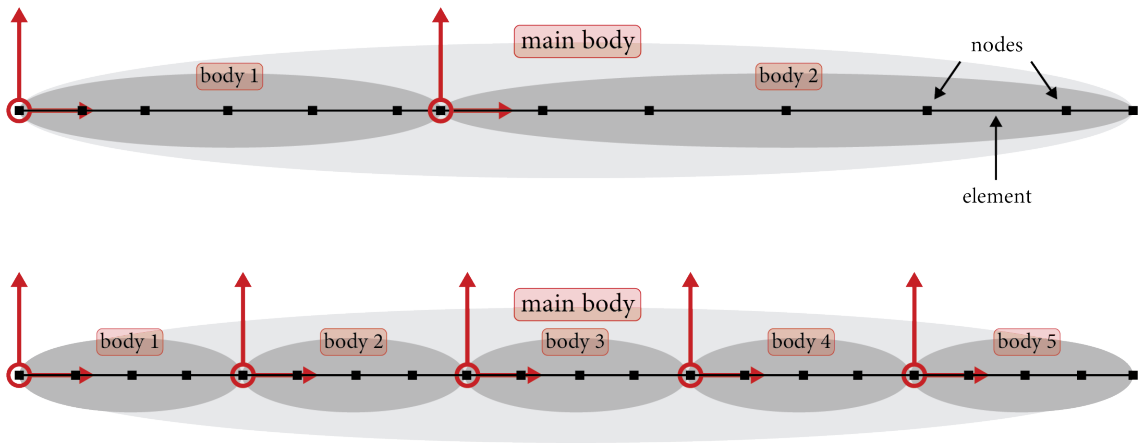

Figure 3.1: Arbitrary main bodies based on a multibody formulation [68].

The aerodynamic model of the HAWC2 code is based on the Blade Element Momentum (BEM) theory, as described by Glauert in his work on propellers [69]. This classical approach offers a framework to model the aerodynamic interaction between a turbine and a fluid flow. However, HAWC2 extends this formulation to handle dynamic inflow, dynamic stall, shear effects on induction, tip loss, skew inflow, and impacts of large blade deflections [70].

More detailed information about HAWC2 can be found in the latest version of the manual [70].

3.1.2. Controller Tuning with HAWCStab2

As rotor sizes and rated powers keep increasing, the role of the controller becomes more crucial in wind turbine performance. Its location is depicted in Figure 3.2, and its operation is described as a continuous regulation process aimed at achieving the optimal turbine performance. A practical example of this regulation procedure is provided in Section 3.2.3.

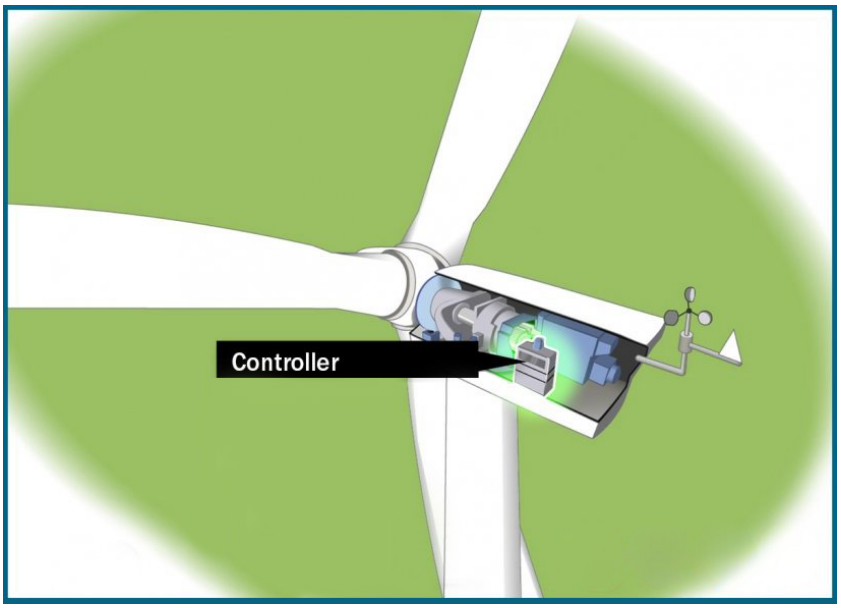

Figure 3.2: The location of the controller in an arbitrary turbine. (Adapted from [71])

In this thesis, the controller tuning is performed with **HAWCStab2** version 2.15.7. HAWCStab2 is selected due to its license availability and for consistency purposes, as the technical report of the IEA 15 MW RWT specifies its use for controller tuning [72].

Unlike HAWC2, the HAWCStab2 code uses linear aeroelastic models of wind turbines. This tool implements an analytical linearization of a non-linear finite beam element model. Additionally, the beam model is integrated with an unsteady BEM model of the blade aerodynamics [73].

More detailed information about HAWCStab2 and its controller tuning feature can be found in the latest version of the manual [73].

Lastly, the importance of the controller tuning process for this research is highlighted in Section 3.3.3.

3.2. IEA 15 MW Reference Wind Turbine

RWTs have become more significant in recent years due to their various roles within the wind sector. They are open benchmarks, specified with design parameters accessible to the public, serving as starting points for different research projects. This facilitates collaboration between the wind industry and academia, enabling the industry to safeguard its intellectual property while collaborating with outside parties. Lastly, RWTs function as a gateway and educational tool for newcomers to the wind energy field, providing insight into essential design principles and system trade-offs [72].

3.2.1. Model Description

This thesis focuses on the onshore IEA 15 MW RWT. This model is fixed in translation and rotation at the bottom of the tower, 15 metres above the mean water level, and it uses the same tower as the offshore model [74]. With a rotor diameter of 240 metres and a hub height of 150 metres, the key features of this turbine are given in Table 3.1, while Figure 3.3 depicts the model in HAWC2 visualization tool.

Table 3.1: Key specifications of the IEA 15 MW RWT. (Adapted from [72])

Parameter	**Value**	**Units**
Power rating	15	MW
Turbine class	IEC Class 1B	-
Specific rating	332	W/m^2
Control	Variable speed	-
Control	Collective pitch	-
Cut-in wind speed	3	m/s
Rated wind speed	10.59	m/s
Cut-out wind speed	25	m/s
Minimum rotor speed	5.0	rpm
Maximum rotor speed	7.56	rpm
Rotor diameter	240	m
Aerofoil series	FFA-W3	-
Hub height	150	m
Hub diameter	7.94	m
Hub overhang	11.35	m
Drivetrain	Direct drive	-
Shaft tilt angle	6	deg
Rotor nacelle assembly mass	1,017	t
Tower mass	860	t
Tower-base diameter	10.0	m
Tower-base thickness	41.058	mm
Tower-top diameter	6.5	m
Tower-top thickness	23.998	mm

W/m^2	watts per square metre	t	metric tons	m/s	metres per second
MW	megawatts	rpm	revolutions per minute	deg	degrees
m	metres	mm	millimetres		

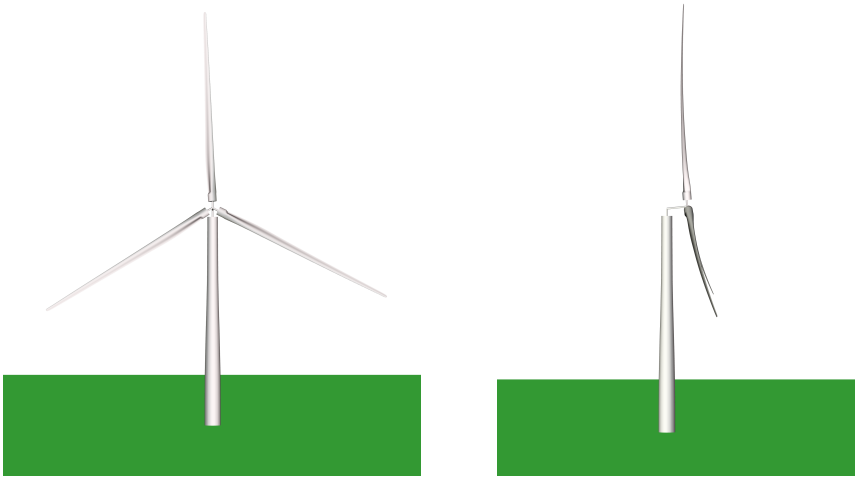

(a) Front view. (b) Side view.

Figure 3.3: The onshore IEA 15 MW RWT represented in HAWC2 visualization tool.

Figure 3.4 shows the type of blade under analysis and its main properties are presented in Table 3.2. In this context, C_P and C_T represent the power coefficient and thrust coefficient, respectively. The former is defined as the ratio of the power extracted by the wind turbine relative to the energy available in the wind stream at a specific wind speed [75]. The power coefficient is also often seen as a measure of wind turbine efficiency and it is utilised in the upcoming analyses in this thesis.

Table 3.2: Key specifications of the IEA 15 MW RWT blade. (Adapted from [72])

Parameter	**Value**	**Units**
Blade length	117	m
Root diameter	5.20	m
Root cylinder length	2.34	m
Max chord	5.77	m
Max chord spanwise position	27.2	m
Tip prebend	4.00	m
Precone	4.00	deg
Blade mass	65,250	kg
Blade center of mass	26.8	m
Design tip-speed ratio	9.00	-
Maximum tip speed	95	m/s
First flapwise natural frequency	0.555	Hz
First edgewise natural frequency	0.642	Hz
Design C_P	0.489	-
Design C_T	0.799	-
Annual energy production	77.4	GWh

GWh	gigawatt-hours	kg	kilograms	deg	degrees
Hz	hertz	m	metres	m/s	metres per second

Figure 3.4: The suction side (top) and trailing edge (bottom) view of the IEA 15 MW RWT blade. (Adapted from [72])

3.2.2. Wind and Turbulence Modelling

The wind model of the HAWC2 code is divided into deterministic and stochastic wind. The former refers to the predictable part of the wind, and their models rely on fundamental principles of physics to predict wind patterns. The latter represents the random, unpredictable fluctuations in wind behavior arising from the inherent variability in the atmosphere and influenced by multiple small-scale factors that are difficult to predict accurately.

The deterministic component defines, for example, the mean wind speed and the vertical wind shear profile. This format is described by the power law [76] according to Equation 3.1, where the wind velocity is a function of height and typically increases with altitude.

$$\overline{u}(z) = \overline{u}(z_{\text{ref}}) \times \left(\frac{z}{z_{\text{ref}}} \right)^{\alpha} \tag{3.1}$$

In this formulation, $\overline{u}(z_{\text{ref}})$ is the mean wind speed at the reference height z_{ref}, while z is the height at which the mean wind speed $\overline{u}(z)$ is to be estimated. The wind shear exponent, symbolized by α, takes the value of 0.2 for slightly rough surfaces, such as hay or pastures, in normal atmospheric conditions [77].

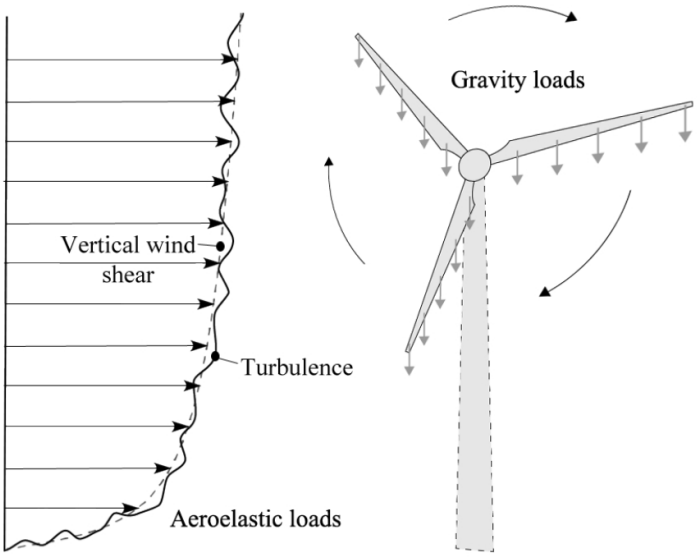

Figure 3.5: Vertical wind shear profile and the effect of turbulence [78].

In the context of fluid dynamics, turbulence refers to the chaotic and irregular motion of air particles [79]. This generates rapid fluctuations in wind speed, and it disturbs the wind shear profile, as illustrated in Figure 3.5.

Given their inherently unpredictable nature, turbulent motions are generally treated statistically rather than deterministically [80]. They are modeled using statistical methods to capture the probabilistic characteristics of wind behavior. However, the model for the IEA 15 MW RWT, which is publicly available on GitHub [12], does not include this stochastic component of the wind.

The main research question of this thesis asks for an investigation of the effects of blade parameters on fatigue loads during normal turbine operation, emphasising the need to include turbulence in the evaluation process. Turbulence, by chaotically disturbing wind direction and velocity, becomes a significant source of fluctuations in wind turbine loading. For this reason, turbulence is widely recognised as one of the major contributors to fatigue loads [81] and must be included in this research.

This thesis utilises the Mann turbulence model [82] to account for turbulence. The Mann model is build on Rapid Distortion Theory [80] and generates a three-dimensional turbulent wind field. This method is recommended by the IEC 61400-1 standard [15] and it is the default turbulence simulator for HAWC2 [83] [84] [85].

The Mann model relies on the generation of turbulence boxes for different wind speeds and turbulence intensities [33]. The procedure utilised to create these boxes is described in the following subsection and further detailed in [84].

3.2.2.1. Mann Turbulence Box

The turbulence box is a three-dimensional grid that contains a wind velocity vector at each grid point [84]. In this research, all turbulence boxes have 8192 x 32 x 32 grid points in the u, v, and w directions, respectively. The v-w plane is parallel to the rotor, while the u direction corresponds to the length of the turbulence box, as depicted in Figure 3.6.

The distance between the grid points in the v and w directions is determined based on the rotor diameter [84], which is 240 metres for the IEA 15 MW RWT [72]. Typically, the spacing is set to create a mesh that is 10% to 20% larger than the rotor diameter. In this work, a conservative approach is adopted, and a 20% larger mesh is utilised. Consequently, the height and width of the Mann Turbulence Box are 288 metres, with a spacing of 9 metres between the grid points.

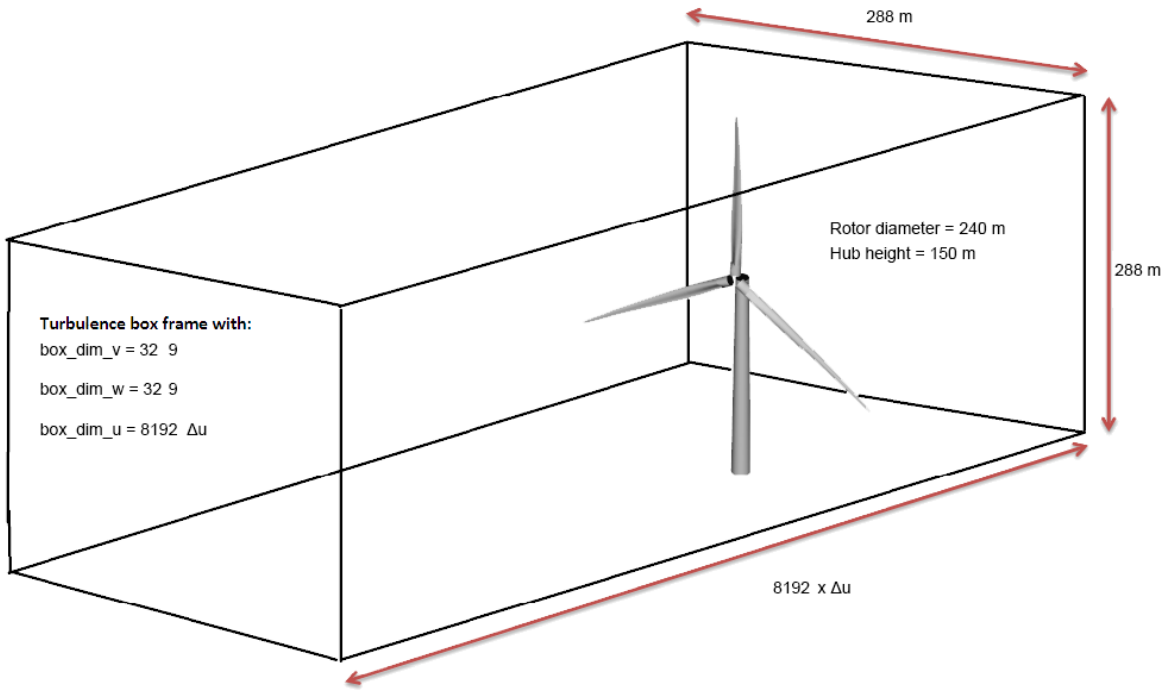

Figure 3.6: Schematic of the Mann Turbulence Box framework. (Adapted from [86])

Lastly, the distance between the grid points in the u direction, denoted by Δu, is determined based on the Equation 3.2 [83] [87].

$$\Delta u = wsp \times \left(\frac{T}{N_u}\right) \tag{3.2}$$

In this formulation, wsp is the mean wind speed in metres per second, T denotes the simulation length (excluded the time for initial transients) in seconds, and N_u symbolizes the number of grid points in the u direction, which is 8192 for this thesis. This configuration ensures that the length of the turbulence box corresponds to the simulation length [87].

The code created for the Mann Turbulence Boxes is incorporated into the IEA 15 MW RWT model, resulting in an updated model. Before utilising it for the investigations in this research, the updated model must be verified to ensure that it delivers the expected performance. This task is executed in the next section.

3.2.3. Model Verification

Simulation models are powerful tools for improving the design and optimization of complex systems, but they need to be verified before they can be trusted and used for decision-making. The verification process consists of checking whether the computational model accurately represents the developer's conceptual description of the model and delivers its expected performance. It involves trying to ensure that the simulation model is correctly implemented, free of errors, and able to produce reliable results. Thus, the model verification process aims to guarantee that the model does what it is intended to do.

3.2.3.1. Simulation Setup for the Model Verification

The turbine is assessed using the Design Load Basis (DLB) - Revision 00 [88]. This report describes the full DLB used for load calculations at DTU Wind Energy for onshore wind turbines and is based on the third edition of the IEC 61400-1 standard [15].

As previously stated, this thesis relies on the DLC 1.2, which aims to represent power production in normal turbulence conditions. DTU describes the DLC 1.2 as ''simulations of power production without faults performed for wind speeds in the entire operational range with normal turbulence according to the IEC class. Yaw errors during normal operation are set to +/- 10 degrees. Six seeds per wind speed and yaw error are used.'' [88].

In the model verification process for this research, two strategies are adopted to decrease the required calculation time. First, two yaw error turbulence seeds are utilised, resulting in six turbulence seeds per wind speed, which follows the minimum requirement set out in the IEC standard [15]. Additionally, the wind speed of 26 m/s is excluded from the analysis since it occurs very rarely and does not significantly contribute to fatigue loads in real life.

The simulation period is set to 800 seconds, with the initial 200 seconds allocated for the initialization of the wind turbine response. This initial phase is excluded from the load analysis.

Finally, Table 3.3 depicts the simulation setup for this task.

Table 3.3: Simulation setup for the Model Verification Process.

Simulation	Length: 600 s
Setup	Wind: 4 - 24 m/s with steps of 2 m/s
	Yaw: -10/0/+10 degrees
	Turbulence: NTM, 2 seeds per wind speed and yaw error
	Shear: vertical and exponent of 0.2
	Gust: None
	Fault: None

The Load Case Table (LCT), which includes turbulence intensity, mean wind speed, yaw misalignment, and turbulence seed values used in the model verification process, can be found in Appendix A. The turbulence intensity values are based on data from COWI's experience and cannot be disclosed in this version of the report due to confidentiality reasons.

3.2.3.2. Target Model Performance

In this work, the verification process is based on the controller regulation trajectory and power curve. The technical report developed within IEA Wind Task 37 [72] defines the IEA 15 MW RWT, specifying the steady-state performance of the rotor as a function of wind speed.

Figure 3.7 illustrates the behaviour of key performance parameters: blade pitch, rotor speed, generator torque, and Tip Speed Ratio (TSR). The TSR is defined as the ratio between the tangential speed of the blade at its tip and the wind speed [89], while the blade pitch is defined as the angle between the chord line and the plane of rotation of the blade [90]. In simple words, the blade pitch refers to the angle at which the blades are set relative to the oncoming wind. Next, Figure 3.8 shows the generator power during rotor operation.

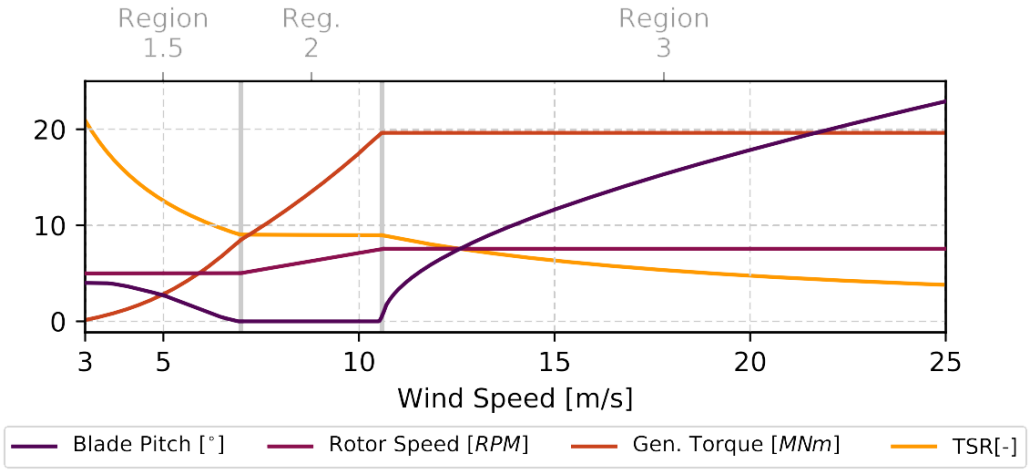

Figure 3.7: Controller regulation trajectory of the IEA 15 MW RWT presented in the technical report [72].

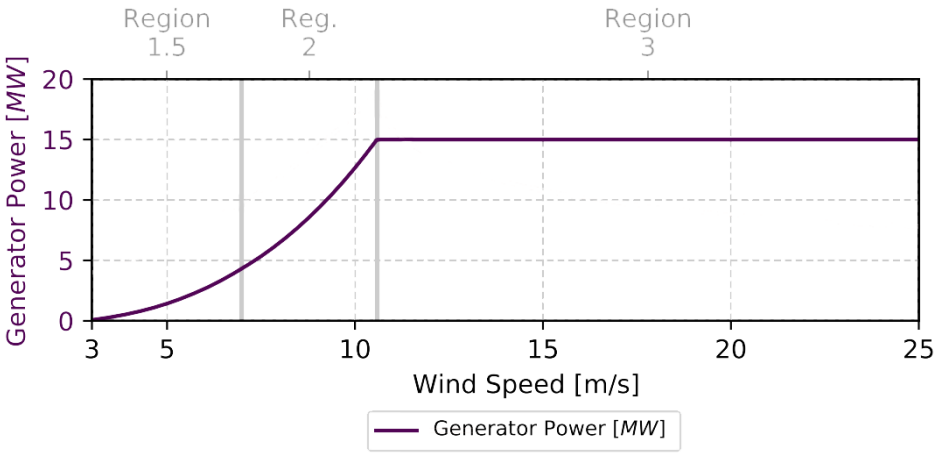

Figure 3.8: Power curve of the IEA 15 MW RWT presented in the technical report. (Adapted from [72])

Wind turbine controllers typically use two actuation techniques. A generator torque controller manages generator power, whereas a blade pitch controller regulates rotor speed. These actuation techniques are often divided into several operational regions.

Regions 1 and 4 are below the cut-in wind speed and above the cut-out wind speed, respectively. In other words, in Region 1, wind speeds are not strong enough to turn the blades, while in Region 4, wind speeds are extremely high, triggering a shutdown maneuver and pitching the blades to reduce rotor thrust to zero. Thus, these regions do not hold specific interest for standard control purposes and are not depicted in Figures 3.7 and 3.8.

Hence, as illustrated in Figures 3.7 and 3.8, the controller operation for the IEA 15 MW RWT can be distinguished by three regions [72] [91]:

- **Region 1.5 ($3\,\mathrm{m/s} \leq$ wind speed $\leq 6.98\,\mathrm{m/s}$)**
  The wind speed is above the turbine's cut-in wind speed, but the turbine is still unable to operate at its optimal TSR. At this point, both controllers actuate concurrently aiming to maintain a defined minimum rotor speed and maximize power output. This is achieved by modifying the generator torque and adjusting the blades to their minimum allowable blade pitch angle so that the power coefficient (C_P) is maximized.
- **Region 2 ($6.98\,\mathrm{m/s} \leq$ wind speed $\leq 10.59\,\mathrm{m/s}$)**
  The wind speed reaches a level where the turbine can operate at its optimal TSR, but it is still below rated. At this stage, the goal of the generator torque controller is to maximize power output as much as possible, with the blade pitch angle kept constant at the position where the blades are typically designed to be the most aerodynamically efficient.
- **Region 3 ($10.59\,\mathrm{m/s} \leq$ wind speed $\leq 25\,\mathrm{m/s}$)**
  The wind speed is above rated. The blade pitch controller regulates the rotor speed to its rated value, whereas the generator torque controller is saturated at rated torque. Thus, constant power output is achieved.

3.2.3.3. Achieved Model Performance

After performing the simulation defined in Table 3.3 on the computational model assembled for this thesis, the average results of the key performance parameters are obtained and shown in Figure 3.9. Likewise, the achieved generator power as a function of wind speed is depicted in Figure 3.10.

In **Region 1.5**, the minimum rotor speed constraint of around 5 RPM is present to avoid resonance effects [72]. This constraint results in high, and consequently, non-optimal TSRs, as expected. Moreover, positive blade pitch angles are observed at low wind speeds, and they decrease as wind speed increases, thereby matching the target model performance.

In **Region 2**, the design point for the blade is achieved, with an optimal TSR of around 9 and a blade pitch angle of about 0°, as described by the turbine developer [72].

Lastly, in **Region 3**, a rated power of around 15 MW, a rated torque of about 20 MNm, and a rated rotor speed of approximately 7.55 RPM are reached.

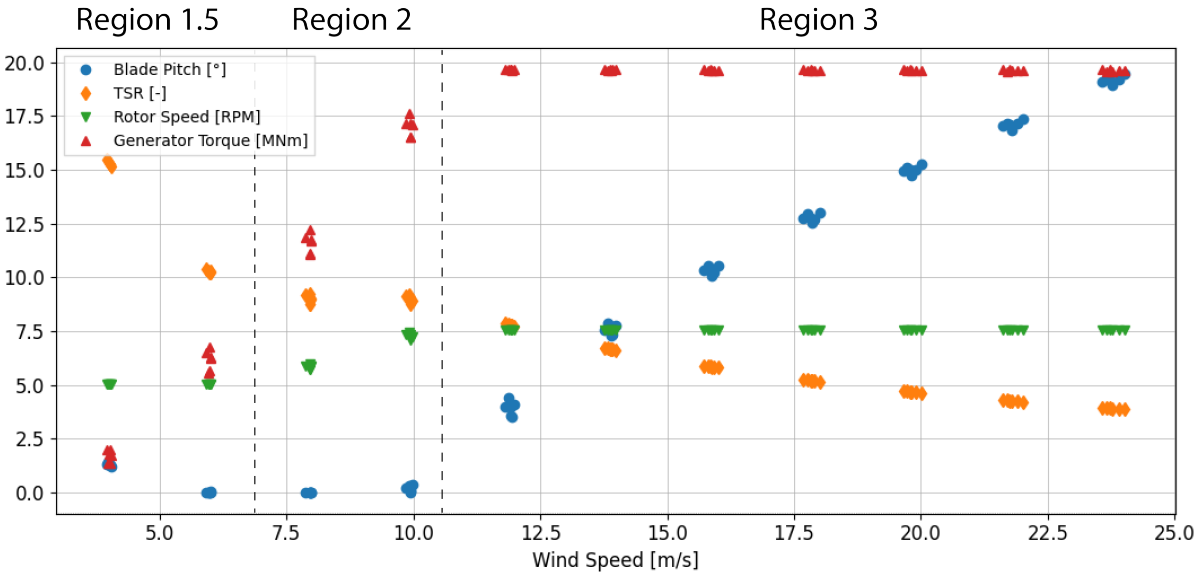

Figure 3.9: Controller regulation trajectory of the simulation model developed for this research.

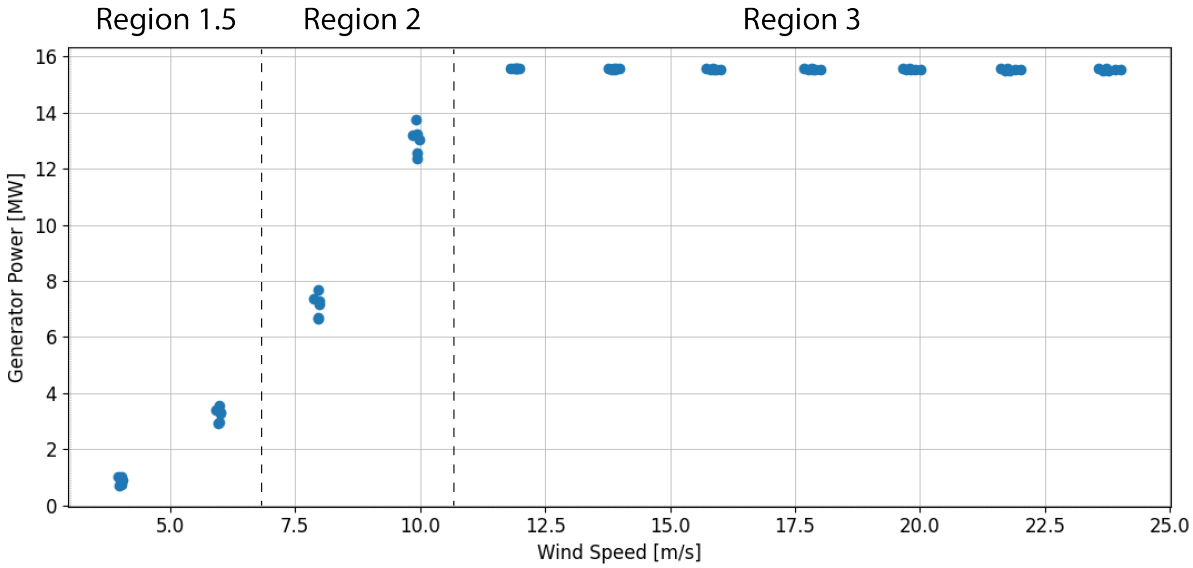

Figure 3.10: Power curve of the simulation model developed for this research.

Small differences between the target and achieved model performance may arise from two main reasons.

First, due to the distinct nature of the simulations. The results provided by the turbine developer for the controller regulation trajectory and power curve are based on steady-state simulations, while the results obtained in this thesis are based on dynamic simulations.

Steady-state simulations assume that the system has reached an equilibrium stage, where the effect of the initial conditions has become negligible. In this type of simulation, the input conditions do not change, leading to a stable and unvarying output. In contrast, dynamic simulations analyse how the system responds to changing input conditions. Thus, steady-state simulations do not account for factors such as turbulence, yaw misalignment, or the wind shear profile, which are considered in dynamic simulations.

Second, due to the use of different simulation software and controllers for the calculations. The developer of the IEA 15 MW RWT employs OpenFAST with the NREL Reference OpenSource Controller (ROSCO) [72], whereas this thesis utilises HAWC2 with the Basic DTU Wind Energy controller.

Despite the slight differences, the obtained behaviour of the key performance parameters and generator power are consistent with the expected outcomes across all three regions of the controller operation. Therefore, the computational model assembled for this research delivers its expected performance. At this stage, the updated model is verified and ready to be utilised in the sensitivity analysis study.

3.3. Methods & Discussions

3.3.1. Fatigue Analysis

In Chapter 2, different fatigue evaluation methods were examined and the key trade-offs were discussed.

For this thesis, **time-domain analysis** is preferred because the calculations in HAWC2 are performed in the time-domain, and because, as previously seen in the literature review, frequency-domain methods are not yet considered a well-established approach.

Next, the combination of the RFC technique, along with the PM rule and the DEL quantity, is adopted because it allows a straightforward comparison between the fatigue damage of different load histories. This is particularly useful for this thesis, as the comparison of the effect of each blade parameter on fatigue loads is simplified to the analysis of a single quantity, the DEL. Lastly, this approach is the standard procedure followed in the design of wind turbines [44] [15] [45] [46] [47].

Hence, the fatigue estimation framework for this research is summarised in Figure 3.11

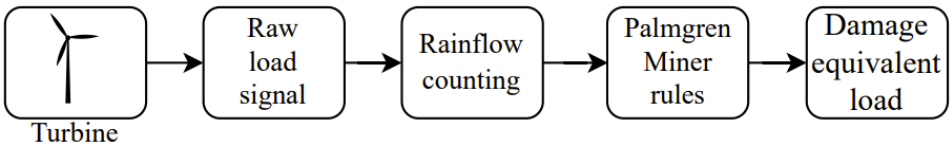

Figure 3.11: Schematic of the fatigue analysis framework. (Adapted from [92]).

Given a load time series, the RFC technique computes the number of cycles n_i and their corresponding amplitudes S_i. Then, by applying the PM rule, the DEL can be calculated using the Wöhler exponent m, which corresponds to the slope of the S-N curve for a specific material. Thus, fatigue loads expressed in terms of DELs are obtained according to Equation 3.3 [92].

$$\mathrm{DEL} = \left(\sum_{i=1}^{n} \frac{n_i S_i^m}{N_{eq}} \right)^{\frac{1}{m}} \tag{3.3}$$

A wind turbine tower is made of steel, and for this material, m is equal to 3 for low-cycle fatigue and 5 for high-cycle fatigue [93]. The blades are usually made of composite materials, but the blade root connection to the turbine hub, as well as the bolts, are typically made of steel. Therefore, this research follows the common practice adopted in the industry when analysing the turbine as a whole, which consists of considering $m = 5$, as turbines tend to fail after a high number of cycles.

Lastly, N_{eq} corresponds to the number of equivalent cycles, with amplitude denoted by DEL, that causes an amount of damage equal to that caused by the cycles derived from the raw load signal. This work follows the convention of using a 1 Hz DEL for easier quantification and comparison of DELs.

3.3.2. Simulation setup for the Sensitivity Analysis

During the sensitivity analysis study in this research, several simulations need to be executed in order to assess the effect of each blade parameter on cyclic loads. The simulation setup defined in Table 3.3 for model verification is computationally expensive, especially for a sensitivity analysis, which involves multiple simulations. Thus, this subsection aims to build a new, less expensive simulation setup for the sensitivity analysis, which helps to address the main research question of this thesis without compromising the quality of the results.

3.3.2.1. Wind Speeds

In terms of wind speeds, the goal of simulating normal operation conditions can be achieved by using one representative wind speed for each region of the controller operation. For this research, the wind speeds of 4, 8, and 18 m/s are chosen, as illustrated in Figure 3.12.

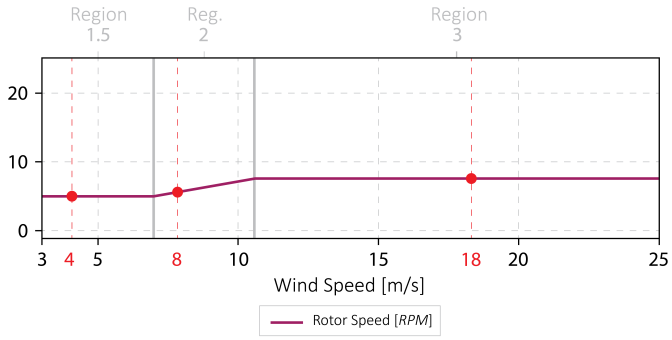

Figure 3.12: Chosen representative wind speed for each region of the controller operation. (Adapted from [72])

3.3.2.2. Number of Turbulence Seeds

The choice of two yaw error turbulence seeds utilised in the model verification process is the least computationally expensive option. However, a convergence study is required to choose a suitable number of seeds that not only reduces the calculation time but also guarantees an accurate DEL estimation.

The convergence study consists of calculating the DEL for each load component employing 2, 3, 4, and 5 seeds per yaw error per wind speed, which translates to 6, 9, 12, and 15 seeds per wind speed, respectively. Then, the resulting DELs are compared, and percentage errors for each load component with respect to the 6 seeds alternative are calculated according to Equation 3.4.

$$\text{Percentage Error}_{6\ \text{Seeds}} = \left(\frac{|\text{DEL}_{6\ \text{Seeds}} - \text{DEL}_{\text{i Seeds}}|}{\text{DEL}_{6\ \text{Seeds}}} \right) \times 100\% \quad \text{for } i = 9, 12, 15. \tag{3.4}$$

The load component with the biggest difference in DELs is the side-side moment at the tower-bottom. In this case, when comparing the DEL obtained using 6 seeds to the DEL obtained using 15 seeds, the error is around 17.5% at a wind speed of 8 m/s, as shown in Figure 3.13b. Hence, the option of using 6 seeds is discarded given the high error obtained.

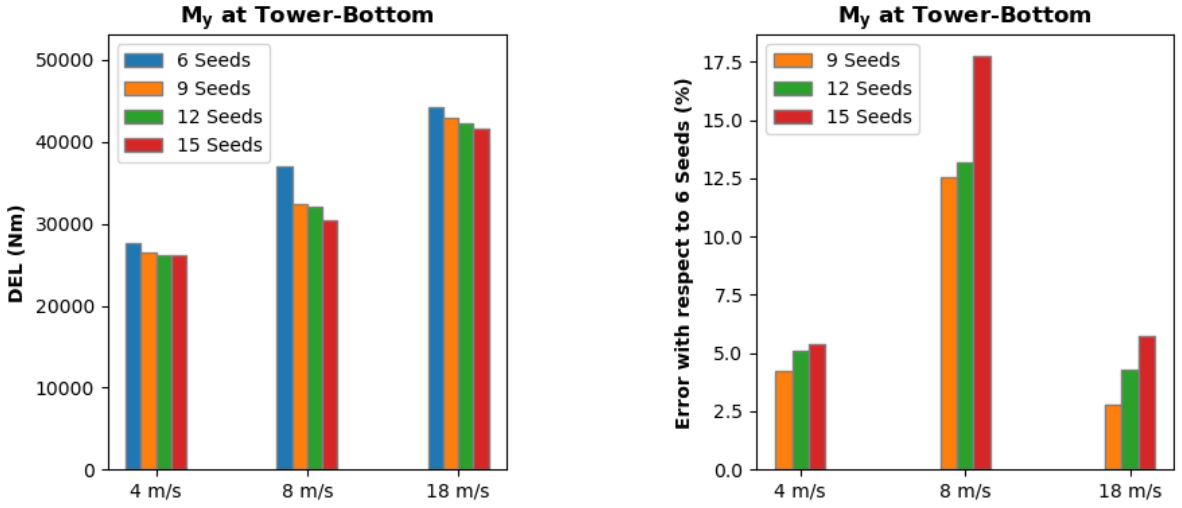

(a) (b)

Figure 3.13: Convergence study for side-side moment, M_y, at the tower-bottom: DELs and errors with respect to the 6 seeds alternative.

At this stage, the convergence study moves towards the 9 seeds alternative, and the errors for each load component are calculated according to Equation 3.5.

$$\text{Percentage Error}_{9\ \text{Seeds}} = \left(\frac{|\text{DEL}_{9\ \text{Seeds}} - \text{DEL}_{\text{i Seeds}}|}{\text{DEL}_{9\ \text{Seeds}}} \right) \times 100\% \quad \text{for } i = 12, 15. \tag{3.5}$$

At this moment, when comparing the DEL obtained using 9 seeds to the DEL obtained using 15 seeds, the error reduces to around 6% for the side-side moment at the tower-bottom at a wind speed of 8 m/s, as illustrated in Figure 3.14.

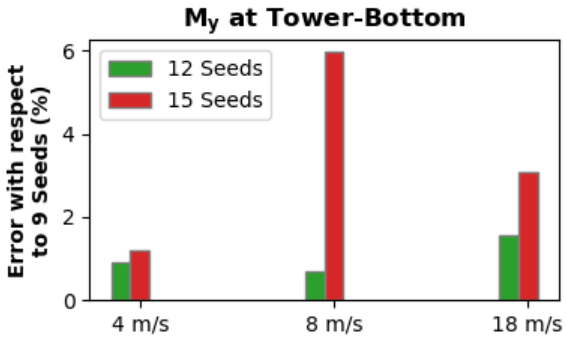

Figure 3.14: Convergence study for side-side moment, M_y, at the tower-bottom: errors with respect to the 9 seeds alternative.

For all other load components, the error is below 6% at the three wind speeds considered. Thus, 9 seeds per wind speed are adopted for the sensitivity analysis in this research, as it keeps calculation time affordable while delivering an acceptable error in DEL estimation.

The complete results of the convergence study are presented in Appendix B. Lastly, Table 3.4 depicts the simulation setup for the sensitivity analysis, whereas the complete LCT can be found in Appendix C.

Table 3.4: Simulation setup for the Sensitivity Analysis.

Simulation	Length: 600 s
Setup	Wind: 4 m/s, 8 m/s, and 18 m/s
	Yaw: -10/0/+10 degrees
	Turbulence: NTM, 3 seeds per wind speed and yaw error
	Shear: vertical and exponent of 0.2
	Gust: None
	Fault: None

3.3.3. Controller Tuning Relevance

3.3.3.1. Theory and Background

As previously stated, the controller operation is defined as a continuous adjustment process focused on attaining the turbine's optimal performance.

Figure 3.15 illustrates the design point for the blades of the IEA 15 MW RWT, which corresponds to a TSR of 9.0 and a blade pitch angle of 0°. At this design point, which is inside the region where C_P is maximized, the IEA 15 MW RWT reaches its optimal performance. The controller of the IEA 15 MW RWT, through its actuation techniques (i.e., blade pitch and torque control), adjusts the turbine during operation so that the turbine can achieve this specific design point.

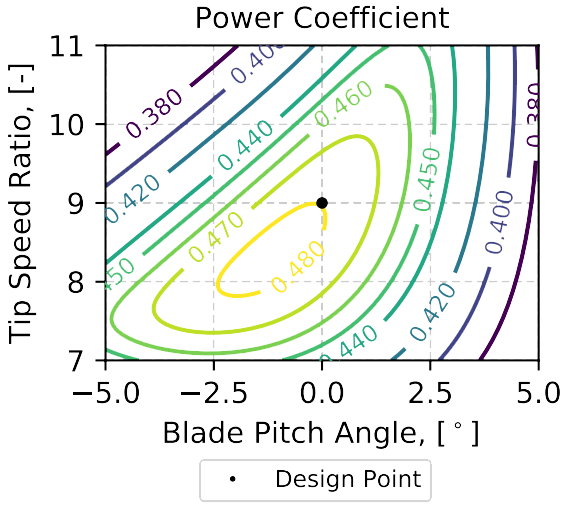

Figure 3.15: The design point for the blades of the IEA 15 MW RWT. (Adapted from [72])

In this research, when a certain blade parameter is changed, a different turbine is obtained. This modified turbine, therefore, has a different design point where its performance is optimal.

In other words, using the same controller of the IEA 15 MW RWT for the new turbine would adjust the new turbine to reach the design point of the IEA 15 MW RWT, instead of its own design point. Thus, the new turbine would achieve the configuration in which the IEA 15 MW RWT reaches its optimal performance, instead of reaching the setup of its own optimal performance. Hence, a new turbine requires a different controller, which will regulate the new turbine during operation so that it can achieve its design point, where its performance is optimal.

The new controller is obtained through the controller tuning process, which is inherently important for this thesis. At first glance, it may be assumed that small changes in blade parameter values would result in minor differences in controller tuning parameters. However, the latter can lead to significant DEL variations, which is not desired. The following subsection presents an indicator of this risk. Finally, using different controllers for different blades is consistent with real-life practice.

3.3.3.2. Risk Indicator

This subsection aims to provide an indicator of the potential impact on DEL results when the controller is not tuned after a certain blade parameter is changed.

To investigate this effect, the torsional stiffness parameter of the IEA 15 MW RWT is increased by 10% at all cross-sections defined in the `IEA_15MW_RWT_Blade_st_noFPM.st` file. The torsional stiffness parameter is defined as the product of the shear modulus of elasticity G (N/m^2) and the torsional stiffness constant I_p (m^4). In this task, the 10% increase in the torsional stiffness parameter is achieved by increasing the torsional stiffness constant by 10% at each cross-section, while the shear modulus of elasticity remains the same.

The study is conducted in two phases: one simulation without tuning the controller after modifying the torsional stiffness, and another with the controller tuned to the new torsional stiffness values. The simulation setup employed is based on Table 3.4 and it is important to highlight that both simulations use the same turbulence files. The goal of this approach is to avoid variations in the results caused by the utilisation of different turbulence files. Lastly, the resulting DELs are compared, and percentage errors for each load component are calculated according to Equation 3.6.

$$\text{Percentage Error}_{\text{controller tuning}} = \left(\frac{|\text{DEL}_{\text{with controller tuning}} - \text{DEL}_{\text{without controller tuning}}|}{\text{DEL}_{\text{with controller tuning}}} \right) \times 100\% \quad (3.6)$$

The load components with percentage errors greater than 1% at a wind speed of 8 m/s are depicted in Figure 3.16.

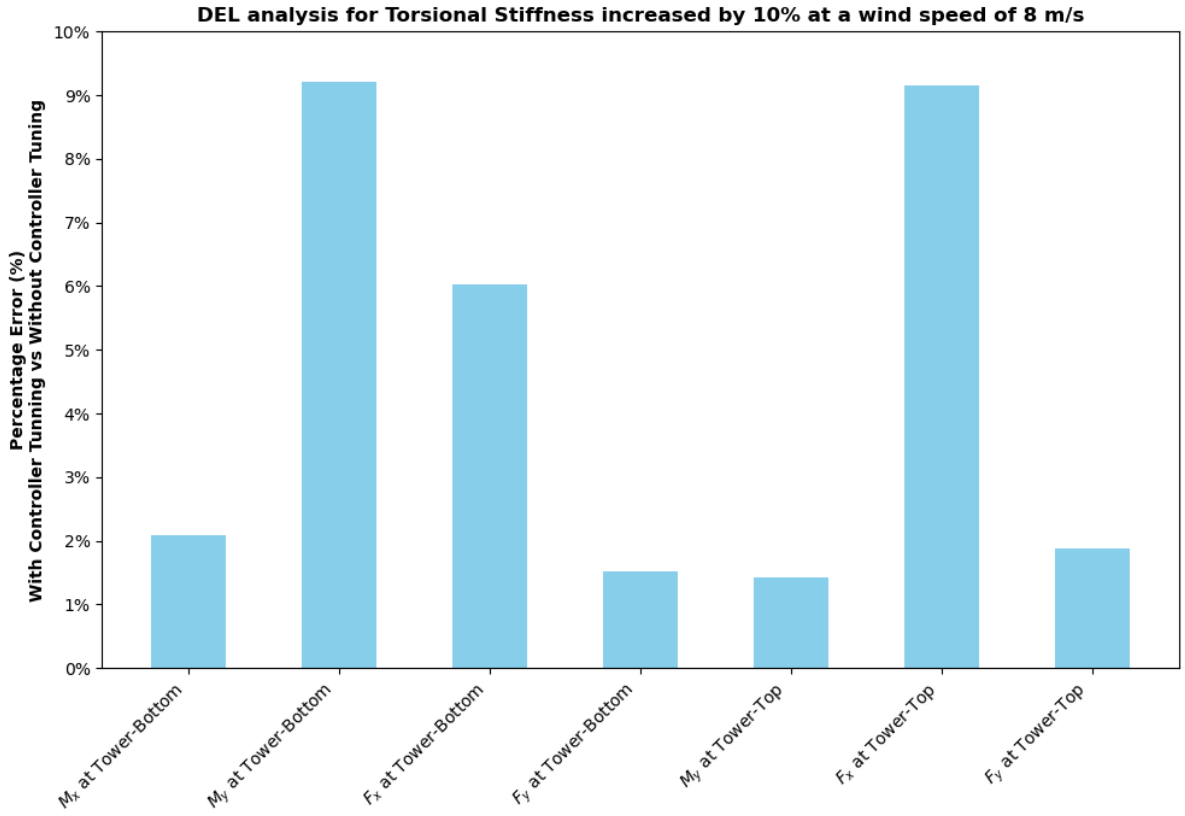

Figure 3.16: Percentage errors in DEL results when comparing simulations with controller tuning and without controller tuning.

Notably, two load components, the side-side moment at the tower-bottom and the side-side force at the tower-top, exhibited differences of around 9%, indicating significant DEL variations. It is noteworthy to observe that the side-side force at the tower-top highly contributes to the side-side moment at the tower-bottom. Hence, if a significant error is present in the side-side force at the tower-top, it is expected that a similar error will manifest in the side-side moment at the tower-bottom, as noticed in the results. Lastly, these errors are especially relevant because, based on industry experience, wind speeds with the highest probabilities of occurrence in offshore wind farms typically range between 8 and 12 m/s.

Therefore, throughout this research, every time a blade parameter is changed, the controller must be tuned. This can be seen as another strategy to ensure, as much as possible, that variations in the dynamic response of the turbine arise from changes in blade parameter values rather than from other sources.

The controller tuning parameters are described in Table F.1. Their initial values for the computational model assembled for this thesis are listed in the IEA 15 MW RWT row of Tables F.6 and F.7. Likewise, the results for these parameters after tuning the controller for the case of 10% increase in the torsional stiffness are shown in the IEA 15 MW RWT increased by 10% row.

3.3.4. Sensitivity Analysis Study

In Chapter 2, different sensitivity analysis approaches were reviewed and the main trade-offs were highlighted. For this thesis, the **first-order EE method** is chosen due to three key reasons: time constraints, the necessity of tuning the controller, and the assumption that each parameter is considered independent.

First, the LCT for the sensitivity analysis defined in Appendix C requires approximately 6 hours of simulation. Consequently, a method that utilises a large number of data points across the input space is not feasible for this research due to the extensive number of simulations needed. Similarly, employing a high number of data points would demand multiple controller tuning sessions, as each new data point corresponds to a new blade parameter value, thereby requiring a new controller tuning process.

Second, in this work, the simulations are conducted in HAWC2, whereas the controller tuning is performed in HAWCStab2. Therefore, this thesis demands a method that does not rely on an iterative loop of simulations to cover different data points. Instead, it requires a method that provides flexibility by allowing the execution of the controller tuning process in between the several simulations.

Third, this thesis considers that the parameters are independent. Hence, it requires a method that does not account for the interaction between the parameters.

Thus, the first-order EE method unfolds as the most suitable choice for this research. As discussed in Chapter 2, this method is based on the OAT technique, which consists of changing one parameter at a time, while keeping other parameters constant. This technique does not account for the interaction between the parameters, which translates to a relatively low number of data points across the input space, reducing the total number of simulations and controller tuning sessions. Lastly, the first-order EE method provides the required flexibility to include the controller tuning process in between the simulations.

3.3.4.1. Limitation

This subsection aims to illustrate the limitation of using the OAT technique in non-linear models.

Figure 3.17 depicts the response of a non-linear model given the range of two input parameters, namely x_1 and x_2. In this case, the OAT technique is divided into two steps:

1) Figure 3.17a shows the first step, in which the parameter x_1 is fixed at its nominal value of 100, while different data points are sampled across the range of x_2.
2) Figure 3.17b displays the second step, in which the parameter x_2 is fixed at its nominal value of 120, whereas different data points are sampled across the range of x_1.

Figure 3.17c represents the combination of data points sampled in the OAT procedure.

This practical example demonstrates that the OAT technique only partially explores the model's parametric space. In this case, the darker blue areas, which indicate regions where the model response is higher, are not included in the evaluation process.

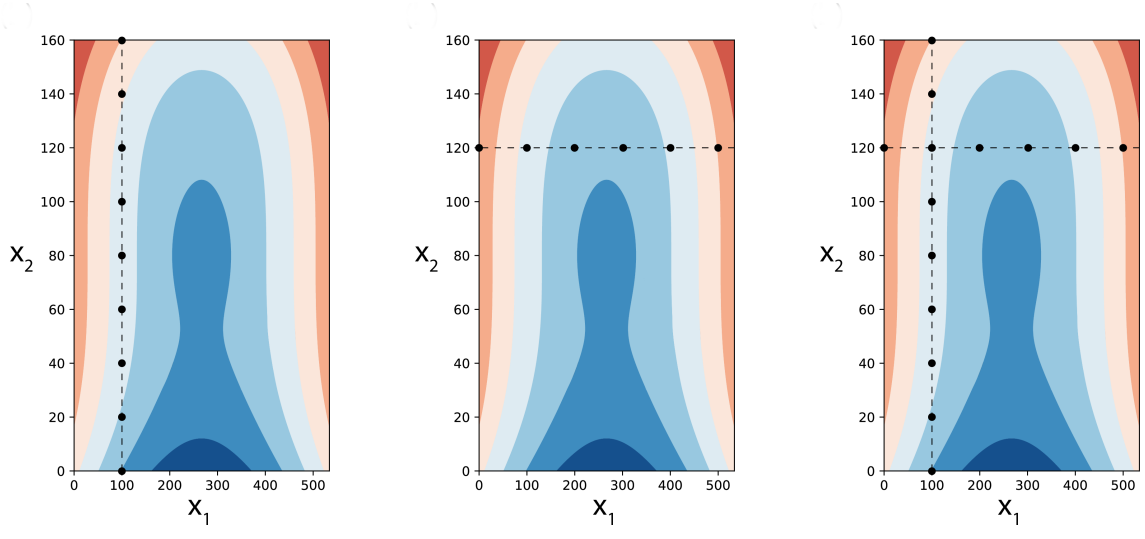

(a) (b) (c)

Figure 3.17: OAT technique in an arbitrary non-linear model. (Adapted from [55])

Given this limitation, this research serves as a preliminary, low-cost analysis of the parameters' individual effects. The first-order EE method satisfies the goal of this thesis to provide an initial understanding of which parameters are most important. However, this research should be complemented with more sophisticated methods (e.g., second-order EE method) that account for the interaction between the parameters, thereby providing a more comprehensive understanding of the model response.

Lastly, it is recommended that future sensitivity analysis studies utilise methods that can incorporate the controller tuning process, as its importance for achieving more robust results was highlighted in Section 3.3.3.

3.3.5. Blade Parameter Analysis

This section starts by introducing the system of coordinates adopted in this research to define the blade parameters. Next, it conducts a study among different turbine models to select the parameter ranges to be considered in the sensitivity analysis.

3.3.5.1. System of Coordinates

This thesis adopts the HAWC2 coordinate system scheme [70] to define the blade parameters, and below two examples are given.

The shear centre is given with respect to the local coordinate system, which has its origin at the half-chord point of the aerofoil. In this formulation, the x axis is aligned with the chord line and points towards the leading edge, while the y axis points towards the aerofoil's suction side, as illustrated in Figure 3.18.

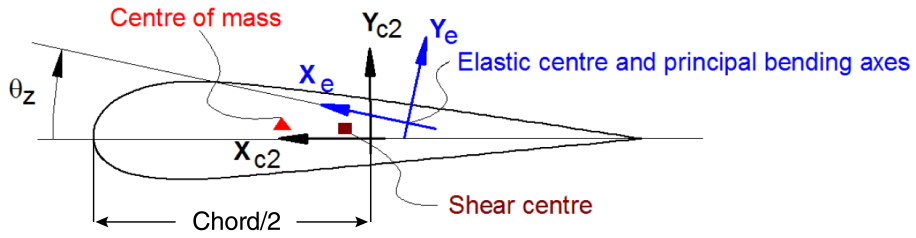

Figure 3.18: The local system of coordinates used by the HAWC2 code to calculate the locations of different centres. (Adapted from [70])

The edgewise swept, denoted by dx, is specified based on the local coordinate system and the main body coordinate system, as depicted in Figure 3.19. In the main body coordinate system, the z axis points from the blade root towards the tip, whereas the x axis follows the tangential direction of rotation, and the y axis points from the pressure side towards the suction side of the aerofoil.

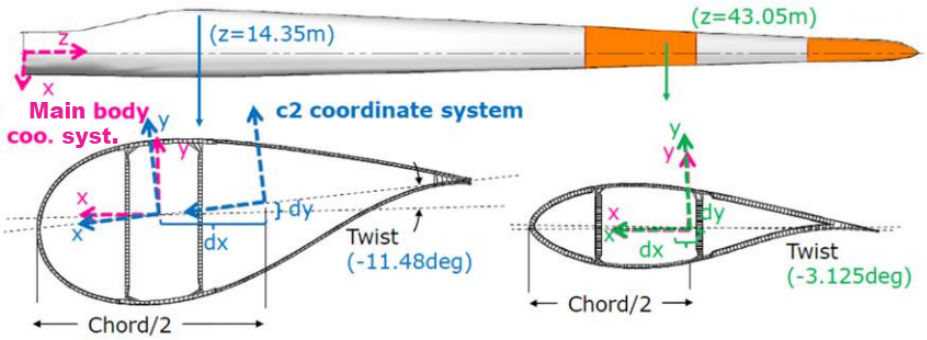

Figure 3.19: The quantification of edgewise swept in an arbitrary turbine model using the HAWC2 coordinate system scheme. (Adapted from [20])

3.3.5.2. Blade Parameter Ranges

To understand what are the minimum and maximum values that each parameter can assume across the blade span, data is collected from four different turbine models, namely the COWI 8.6 MW Turbine, DTU 10 MW RWT, IEA 15 MW RWT, and IEA 22 MW RWT. The data from the first turbine is provided by COWI and is based on engineering judgement from in-house experts, while the data from the RWTs is publicly available on GitHub [94] [12] [95].

To allow a fair comparison between the different types of blades, a three-step procedure is employed:

1) **Normalization Stage**

The different types of blades have distinct lengths. Therefore, the blade span of each model is normalized.

2) **Interpolation Stage**

The parameters are defined at several cross-sections of a blade model. However, each blade model has its own set of cross-sections where the parameters are defined. Hence, the IEA 15 MW RWT cross-sections are used as the reference, and cubic spline interpolation is employed to determine parameter values of the other turbines at these reference cross-sections.

3) **Scaling Stage**

The different turbine models have distinct rotor dimensions and power outputs. To better align with the IEA 15 MW RWT rotor, the rotors of the COWI 8.6 MW Turbine and DTU 10 MW RWT are upscaled, while the IEA 22 MW RWT rotor is downscaled. The set of scaling laws used in this research is detailed by Chaviaropoulos [96] and further discussed in [97].

The results of this three-step procedure for the blade parameters under evaluation in this research are illustrated in Figures 3.20 and 3.21.

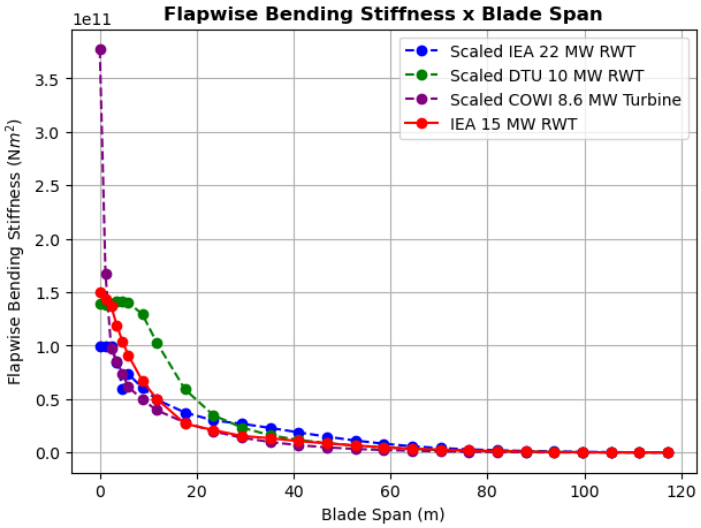

(a)

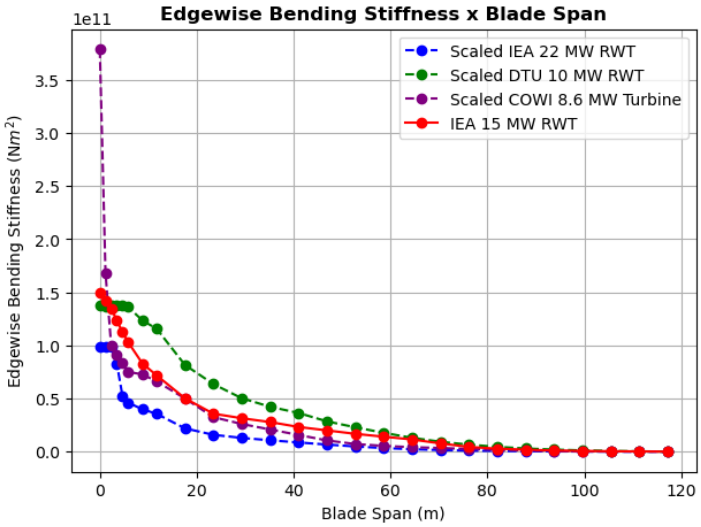

(b)

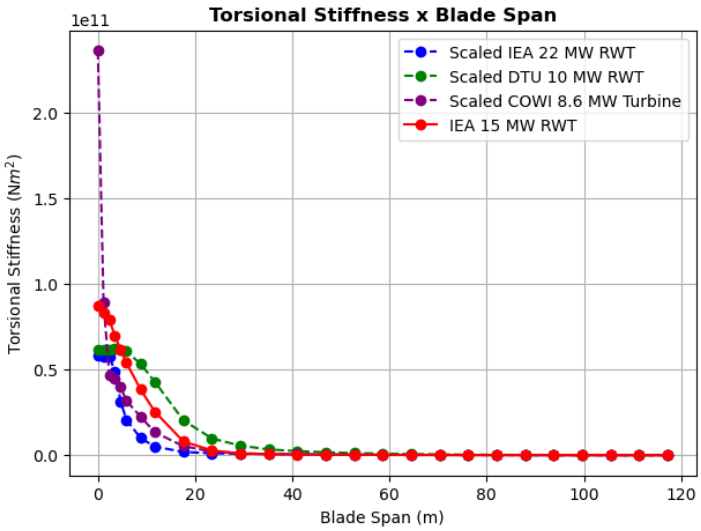

(c)

Figure 3.20: Flapwise, edgewise, and torsional stiffnesses across the blade span for different types of blades.

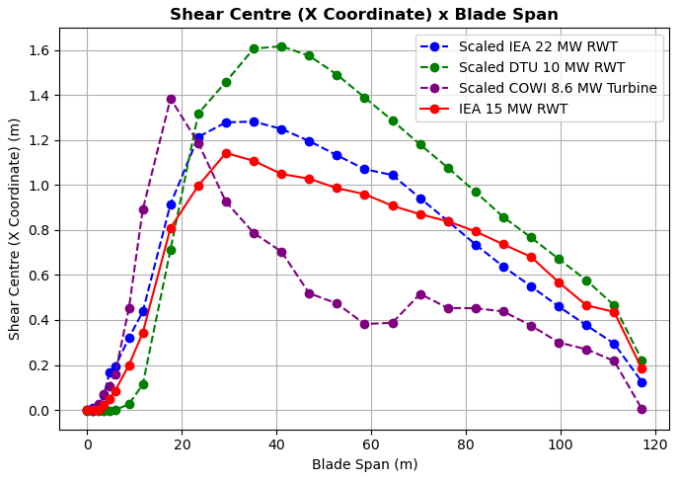

(a)

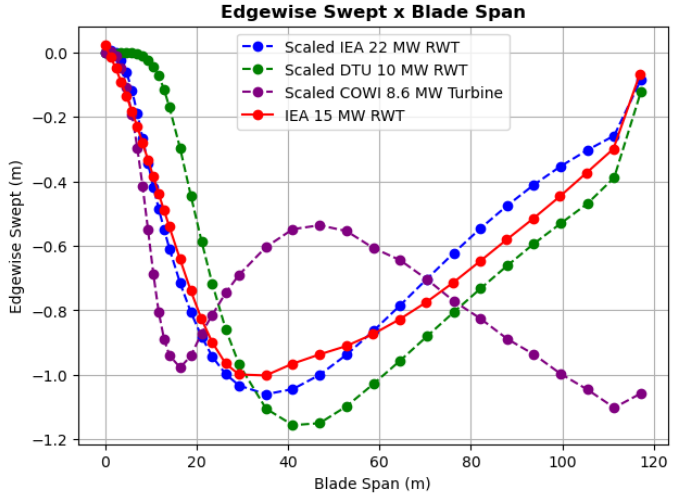

(b)

Figure 3.21: Shear Centre (x coordinate) and edgewise swept across the blade span for different types of blades.

The y coordinate of the shear centre is disregarded in this research since its values are approximately 10 times lower than the x coordinate values across the blade span of the IEA 15 MW RWT. Hence, more significant variations in DELs are expected when perturbing the x coordinate of the shear centre.

Given the references provided by Figures 3.20 and 3.21, Table 3.5 summarises the ranges selected for this research. These ranges consider, as much as possible, the different types of blades in a symmetric way, as shown in Figures 3.22 and 3.23. A reduction in torsional stiffness exceeding 9% is not supported by the IEA 15 MW RWT model, as this modification caused aeroelastic instabilities during the simulations.

Table 3.5: Blade parameter ranges for the Sensitivity Analysis.

Parameter	**Minimum**	**Maximum**
Flapwise bending stiffness	IEA 15 MW RWT decreased by 40%	IEA 15 MW RWT increased by 40%
Edgewise bending stiffness	IEA 15 MW RWT decreased by 40%	IEA 15 MW RWT increased by 40%
Torsional stiffness	IEA 15 MW RWT decreased by 8%	IEA 15 MW RWT increased by 8%
Shear centre (x coordinate)	IEA 15 MW RWT decreased by 10%	IEA 15 MW RWT increased by 10%
Edgewise swept	IEA 15 MW RWT decreased by 10%	IEA 15 MW RWT increased by 10%

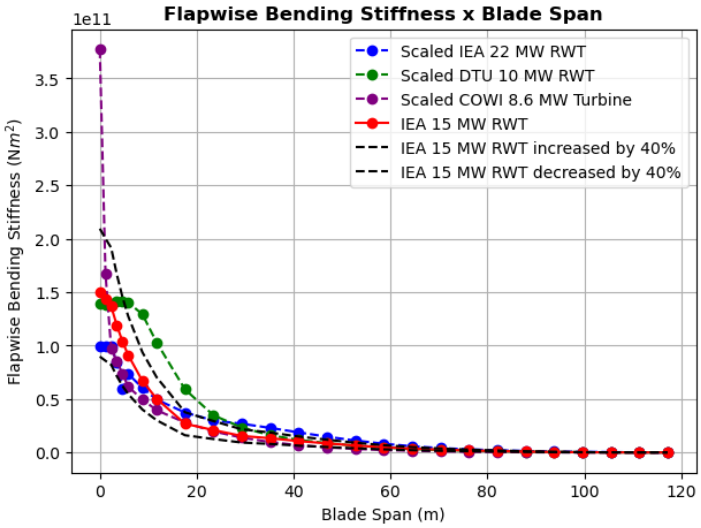

(a)

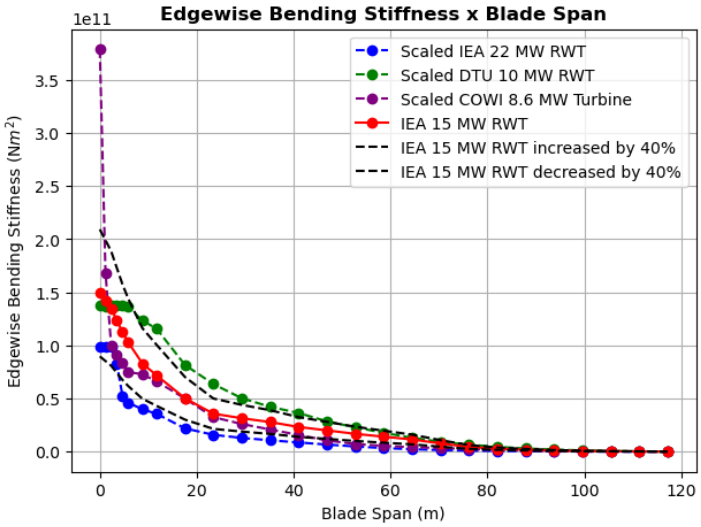

(b)

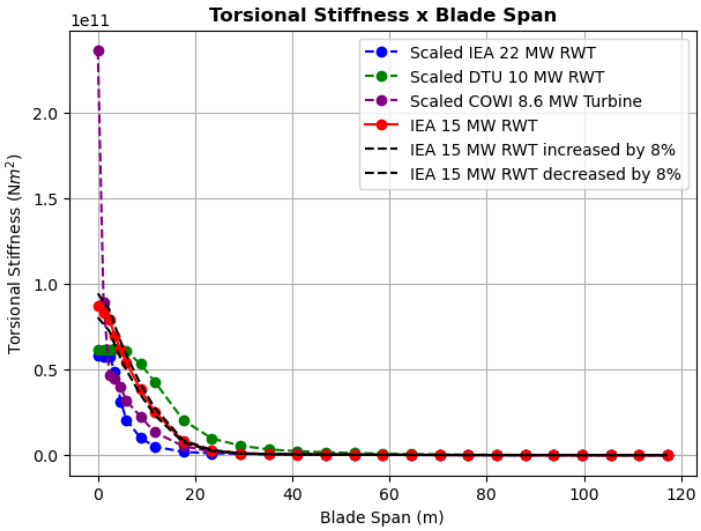

(c)

Figure 3.22: Ranges for flapwise, edgewise, and torsional stiffnesses across the blade span.

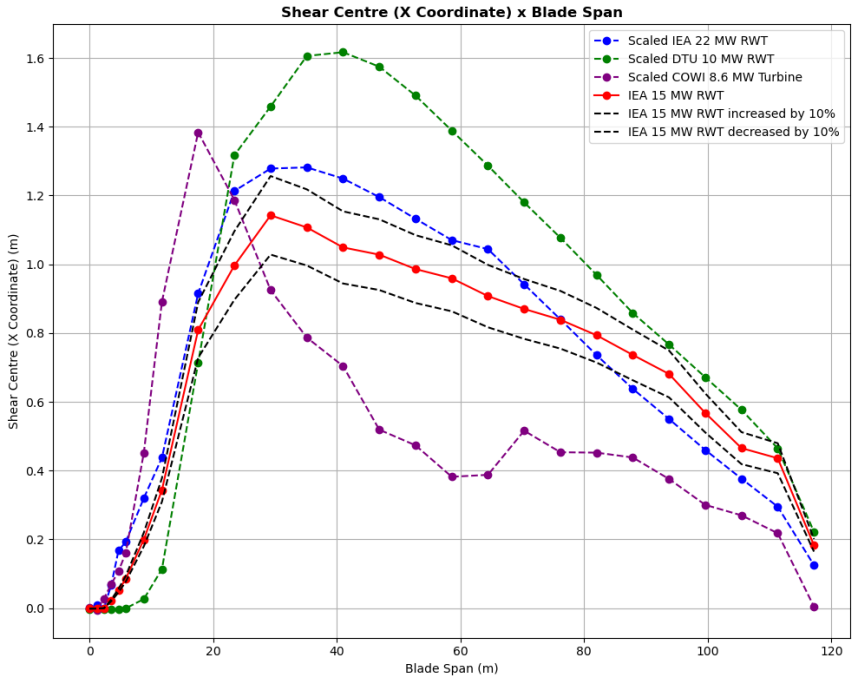

(a)

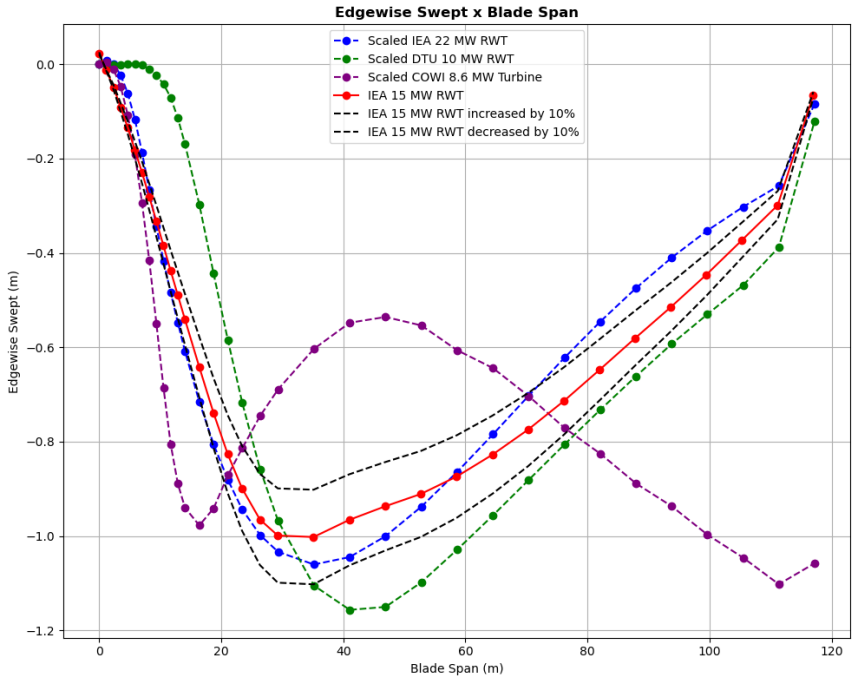

(b)

Figure 3.23: Ranges for shear centre (x coordinate) and edgewise swept across the blade span.

3.3.5.3. Sampling Strategy

Typically, sensitivity analysis problems involve inputs that have fixed values as the boundaries of their ranges (e.g., an arbitrary parameter x_1 takes values in $[5, 20]$). Data points are then sampled within these ranges for evaluation. However, as shown in Figures 3.22 and 3.23, the boundaries of the input ranges in this research are not fixed values but curves, because the parameters vary across the blade span. Thus, this thesis requires a set of curves within the parameter ranges, instead of a set of points.

For this research, nine equally spaced curves within each parameter range are selected. By ensuring a uniform distribution of the curves, the model response can be better captured. The selected curves for each parameter under evaluation in this thesis are depicted in Figures 3.24 and 3.25.

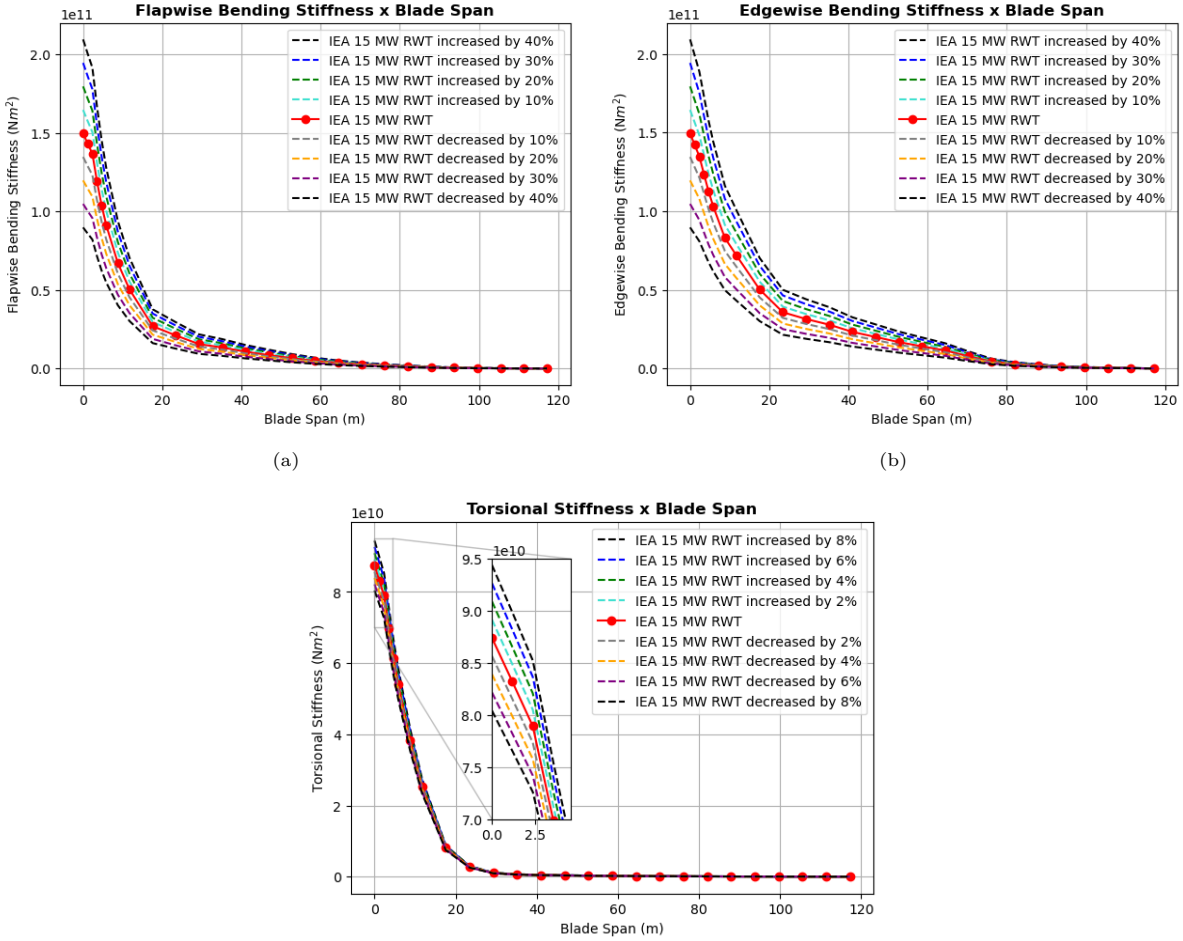

Figure 3.24: Set of selected curves within the flapwise, edgewise, and torsional stiffness ranges.

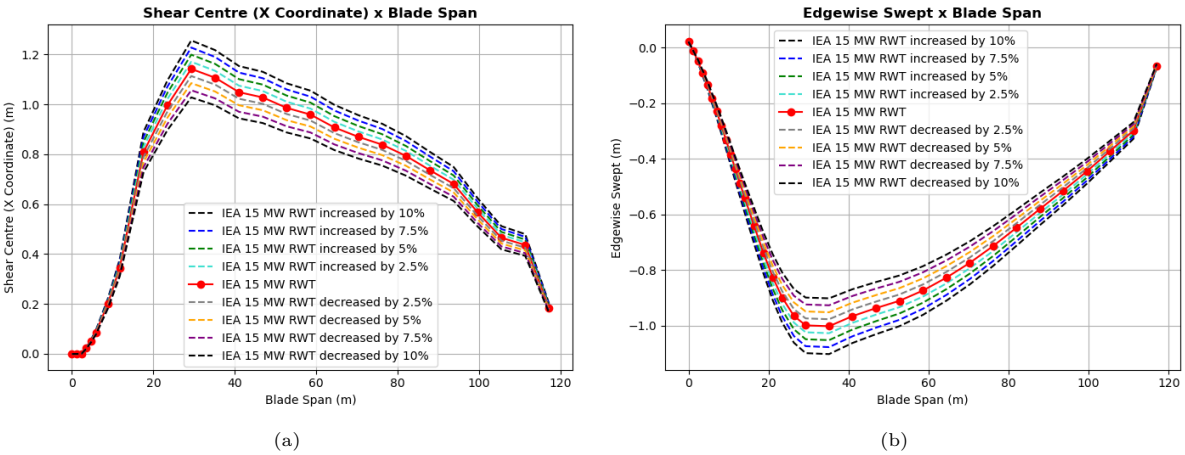

Figure 3.25: Set of selected curves within the shear centre (x coordinate) and edgewise swept ranges.

4
Sensitivity Analysis

4.1. First-Order Elementary Effects Method Description

This thesis employs the first-order EE method [59] for the sensitivity analysis study. As previously discussed, this method is based on the OAT technique, which evaluates the influence of each parameter without considering interactions with other parameters.

The original EE approach proposed by Morris [58] has been refined over the years to enhance the sensitivity assessment [60]. Additionally, modifications to the standard approach are often implemented to better accommodate the specific characteristics of each problem [60].

This section provides a step-by-step description of the first-order EE method and outlines the strategies used in this research to address the unique characteristics of the problem under evaluation. Based on this, the procedure employed in this work can be described as follows:

1) **The input parameters are selected and their respective ranges are defined**

   The parameters under analysis in this research were listed in Table 1.1, with their ranges defined in Section 3.3.5 and summarised in Table 3.5.

2) **A set of initial curves r is chosen and generated across the input parameter space**

   As discussed in Section 3.3.5, this thesis requires a set of initial curves within the parameter ranges, rather than a set of points. For this work, nine equally spaced curves within each parameter range were selected, as shown in Figures 3.24 and 3.25. This approach enables an investigation uniformly distributed across the model response without necessitating an unfeasible number of simulations.

3) **Each initial curve is perturbed by a fixed step size denoted by Δ_i**

   Studies [60] [62] [63] typically set a delta value equal to 10% of the input parameter range. For example, an arbitrary parameter i that takes values in the range [5, 20] would result in $\Delta_i = +0.15$.

   As discussed in Section 3.3.5, the boundaries of the input ranges in this research are not fixed values but curves. However, a delta value equal to 10% of the input range can still be implemented. For instance, as shown in Table 3.5, the adopted range for the flapwise bending stiffness parameter varies from a 40% decrease to a 40% increase of the IEA 15 MW RWT original values. Hence, the total range corresponds to an 80% variation, which results in $\Delta_i = +8\%$. Thus, for example, the initial curve that represents a 10% increase in flapwise bending stiffness is altered by $\Delta_i = +8\%$, leading to a perturbed curve that represents an 18% increase in flapwise bending stiffness.

   In this research, each generated curve, whether initial or perturbed, corresponds to a change in the original IEA 15 MW RWT blade. Thus, the controller must be tuned for each of these modifications before starting the simulations, as discussed in Section 3.3.3. The static calibration results for each initial and perturbed curve are provided in Section F.1.2.

4) **Simulations are performed for each initial and perturbed curve**

   In this thesis, once the simulation outputs are obtained (i.e., the dynamic responses of the wind turbine), Equation 3.3 is used to calculate the DEL for a specific load component at each wind speed.

5) Calculation of the elementary effects

In the original first-order EE approach [59], a first-order finite difference is calculated to measure how the output changes when one input changes. Thus, the EE of the i^{th} input parameter is given by Equation 4.1. In this formulation, f denotes the output in study, x_i is the i^{th} input variable, and Δ_i expresses the increment for this variable i.

$$EE_i = \frac{f(x_1, \ldots, x_{i-1}, x_i + \Delta_i, x_{i+1}, \ldots, x_k) - f(x_1, \ldots, x_{i-1}, x_i, x_{i+1}, \ldots, x_k)}{\Delta_i} \tag{4.1}$$

The original formulation of the first-order EE method assumes that inputs are dimensionless and take values in the range [0, 1] [58] [98]. However, in many real-life problems, the inputs have dimensions and take values in non-unit intervals. To address this, recent studies [60] [62] [63] have normalized all input parameters, ensuring all variables are dimensionless and fall within the range [0, 1].

Given the unique characteristics of the problem evaluated in this thesis, where the boundaries of the input ranges are not fixed values but curves, this research chooses to implement the normalization directly in the EE_i calculation.

The EE method is based on the ratio of the variation of the model output to the variation of the input parameter. Thus, the EE_i formulation can be rewritten, as expressed in Equation 4.2, where x_a refers to the reference input value, x_b to the incremented input value, f_a to the output generated by x_a, and f_b to the output generated by x_b.

$$EE_i = \frac{f_b - f_a}{x_b - x_a} \tag{4.2}$$

At this stage, the normalization is introduced with respect to the reference input and output, resulting in Equation 4.3.

$$EE_i = \frac{\dfrac{f_b - f_a}{f_a}}{\dfrac{x_b - x_a}{x_a}} \tag{4.3}$$

Next, x_b can be rewritten as $x_a + \Delta_i$, which leads to Equation 4.4.

$$EE_i = \frac{\dfrac{f_b - f_a}{f_a}}{\dfrac{\Delta_i}{x_a}} \tag{4.4}$$

As mentioned in step 3, studies [60] [62] [63] typically set a delta value equal to 10% of the input parameter range. Nevertheless, the boundaries of the input ranges in this research are not fixed values but curves. Hence, this thesis uses the maximum and minimum values at the cross-section where the widest range for the parameter is observed.

The identification of these cross-sections is straightforward when analysing Figures 3.24 and 3.25. Specifically, for the flapwise, edgewise, and torsional stiffnesses, the blade root is clearly the location with the largest range.

Table 4.1 summarises the largest range for each parameter and the respective blade cross-section where it occurs. The values are rounded to two decimal places.

Table 4.1: Widest range for each blade parameter.

Parameter	**Blade Cross-Section**	**Widest Range (c_i)**
Flapwise bending stiffness	0.00 m	1.20×10^{11} Nm^2
Edgewise bending stiffness	0.00 m	1.20×10^{11} Nm^2
Torsional stiffness	0.00 m	1.40×10^{10} Nm^2
Shear centre (x coordinate)	29.29 m	0.23 m
Edgewise swept	35.13 m	0.20 m

In the context of this thesis, where the output of interest is the DEL for a specific load component at a given wind speed, the EE_i formulation for a parameter i, given a certain initial curve, can be expressed as shown in Equation 4.5.

$$EE_i = \frac{\dfrac{\text{DEL}_{\text{perturbed curve}} - \text{DEL}_{\text{initial curve}}}{\text{DEL}_{\text{initial curve}}}}{\dfrac{0.1\, c_i}{x_a}} \tag{4.5}$$

At this point, the example introduced in step 3 is further elaborated.

Given the initial curve representing a 10% increase in flapwise bending stiffness, $DEL_{\text{initial curve}}$ denotes the DEL generated by this curve for a specific load component at a given wind speed. Similarly, $DEL_{\text{perturbed curve}}$ refers to the DEL produced by the corresponding perturbed curve, which, in this case, represents an 18% increase in flapwise stiffness, for the same load component and wind speed under analysis.

Finally, the reference input value x_a corresponds to the flapwise bending stiffness of the initial curve at the cross-section where the widest range is observed. This value is indicated by a blue cross mark in Figure 4.1.

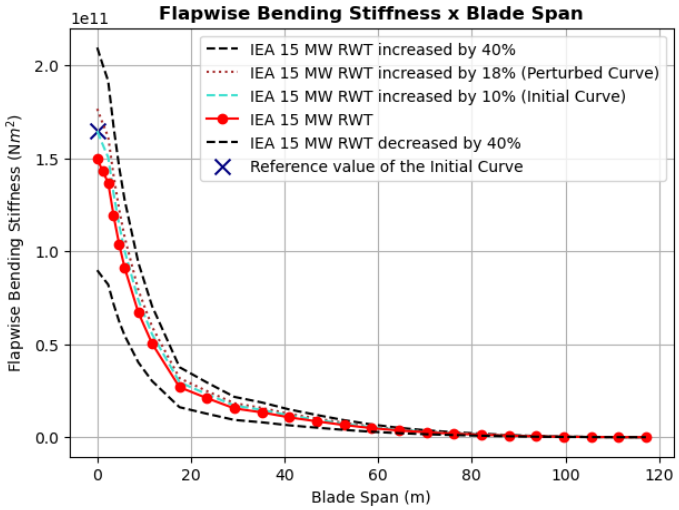

Figure 4.1: Practical example for EE calculation.

6) Calculation of the mean and standard deviation of the elementary effects

Since each parameter in this research is associated with r initial curves, r different EEs are calculated for each parameter. This results in an estimate denoted by EE_{it}, where i refers to the input variable and t is the index of the initial curve under evaluation.

Next, the distribution of effects for each parameter i can be characterised by its mean and standard deviation, as represented by Equation 4.6 and Equation 4.7, respectively [59].

$$\mu_i = \frac{1}{r} \sum_{t=1}^{r} EE_{it} \tag{4.6}$$

$$\sigma_i = \sqrt{\frac{1}{r-1} \sum_{t=1}^{r} \left(EE_{it} - \mu_i\right)^2} \tag{4.7}$$

Lastly, Campolongo and Saltelli in [99] proposed to also consider the mean of absolute elementary effects, according to Equation 4.8. The goal of this approach is to filter out potential cancelling of terms, since some elementary effects can eliminate each other [98].

$$\mu_i^* = \frac{1}{r} \sum_{t=1}^{r} |EE_{it}| \tag{4.8}$$

Therefore, this research employs the first-order EE method [59] and uses the derived statistical quantities for each parameter i to obtain two types of results, which are further detailed below.

- **Ranking of Parameters**

  The first-order EE method [59] ranks the parameters by their level of importance based on either the magnitude of the mean of the effects μ_i or the magnitude of the mean of the absolute effects μ_i^*, as suggested by Campolongo and Saltelli in [99].

  This thesis adopts the quantity μ_i^* and introduces a relative importance evaluation index denoted by $S_{\mu_i^\star}$. This index, as expressed in Equation 4.9 and described in [100], facilitates the comparison between the parameters, as the sum of their importance levels equals 1.

$$S_{\mu_i^\star} = \frac{\mu_i^\star}{\sum_{i=1}^{n} \mu_i^\star} \tag{4.9}$$

- **Coefficient of Variation**

  The index $S_{\mu_i^\star}$ was introduced as a measure of relative importance of a given input factor. This information can be complemented by the coefficient of variation (COV), which is expressed according to Equation 4.10.

$$\rho_i = \frac{\sigma_i}{\mu_i^*} \tag{4.10}$$

  The COV further describes the relationship between an input variable and the model response by indicating the type of effect that this factor has on the output.

The COV ranges which translate each type of effect are summarised in Table 4.2, and a detailed statistical discussion about their definition is provided in [59].

Table 4.2: The information given by the COV [59] [101].

COV Ranges	**Indicator**
$\rho_i \leq 0.5$	the i^{th} input variable has a monotonic effect on the output
$0.5 < \rho_i \leq 1$	the i^{th} input variable has a quasi-monotonic effect on the output
$\rho_i > 1$	the i^{th} input variable has a non-monotonic effect on the output

The term monotonic refers to a consistent, single-direction change. For instance, if an input factor i increases and the output f increases, a monotonic increasing is acknowledged [102]. In contrast, when an input factor i increases and the output f decreases, a monotonic decreasing is recognised [102]. Hence, a monotonic relationship implies that the effect of i on f is consistently increasing or decreasing throughout the range of i.

This type of information is particularly valuable for this research, as it indicates whether a specific blade parameter can be used to achieve a desired DEL in a load component. In other words, if a blade parameter has a monotonic effect on the DEL, it suggests that wind turbine blade manufacturers could adjust (either by increasing or decreasing) the value of this parameter to achieve a desired DEL in the load component under analysis. However, if the parameter has a non-monotonic effect on the DEL, it indicates a more complex relationship, where the DEL may be determined by significant interactions of the parameter with other variables.

4.2. Sensitivity Analysis Results

This section aims to present the main results of the sensitivity analysis and discuss the findings.

The complete results of this study can be found in Appendix G, whereas the simulation setup was defined in Section 3.3.2 and is shown in Table 3.4.

Furthermore, three key aspects can be highlighted for the sensitivity analysis of this thesis:

1) The turbulence files are generated only once per wind condition and reused in all blade parameter simulations. The goal of this approach is to avoid variations in the results caused by the utilisation of different turbulence files.

2) Every time a blade parameter is changed, the controller is tuned. The importance of this procedure for achieving more robust results was highlighted in Section 3.3.3.

3) Rayleigh damping parameters are kept constant and, therefore, are not tuned according to modifications in stiffness values.

By implementing aspects 1 and 2, the causes of changes in the dynamic response of the turbine are mainly reduced to variations in the blade parameters.

Lastly, before starting the sensitivity analysis, two verifications are noteworthy to be conducted:

- **Power Production**

  It is important to verify if the selected blade parameter ranges listed in Table 3.5 do not translate into significant power production differences with respect to the original IEA 15 MW RWT. One of the goals of this research is to provide an initial understanding of potential blade parameter modifications to obtain lower fatigue loads at different positions of the turbine structure. However, the target consists of achieving a relevant decrease in the loads without significantly decreasing the power production, as the power output is an essential criteria for the industry when analysing the financial viability of the turbine.

  The complete results of this comparison task is presented in Appendix D, where it is presented that the proposed blade parameter ranges do not reduce the power production in more than 2%. It is worth noting that despite not being the widest among the parameters in analysis, the **shear centre range** stands out for **producing the most significant difference in power production**. While the variations generated by the different parameter ranges remain below 0.8% for the wind speeds under evaluation, the shear centre range at a wind speed of 8 m/s results in **differences of nearly 2%**. Lastly, the small differences in power production also serves to indicate that the turbine controller was operating properly in each case, effectively guiding the turbine to produce the expected power across the different wind speeds.

- **Controller Activity**

  To assess which blade parameter modification demands more effort from the controller, the standard deviations of blade pitch, rotor speed, and generator torque are calculated for each wind speed and illustrated in Figures E.1, E.2, and E.3 in Appendix E.

  A higher standard deviation compared to that observed in the simulation of the original IEA 15 MW RWT suggests increased regulatory effort from the controller due to changes in the blade parameter in analysis.

  Overall, there is a strong level of agreement between the standard deviations of the different performance parameters for the original and modified cases. Nevertheless, modifications in the shear centre stand out, causing the most notable differences, particularly in blade pitch and generator torque, as depicted in Figures E.1d and E.3d.

  Hence, although the differences remain subtle, the results indicate that **modifications to the shear centre have the greatest impact on the controller's regulatory effort.**

4.2.1. Blade Parameter Effects at the Blade Root, Tower-Top and Tower-Bottom

As highlighted in Chapter 2, addressing torsional loads and the resulting deformations at the blade root is regarded as one of the primary challenges currently faced by the industry due to the increasing length, slenderness, and flexibility of modern blades. Figure 4.2 shows the obtained ranking of parameters by their level of importance with respect to this load component.

The results indicate a **dominant influence** of **flapwise and edgewise bending stiffnesses** compared to other parameters **at** wind speeds of **4 m/s** and **8 m/s**. Moreover, **at** a wind speed of **18 m/s**, there is a notable shift, with the **importance of the edgewise swept increasing significantly** and surpassing the influence of flapwise and edgewise bending stiffnesses.

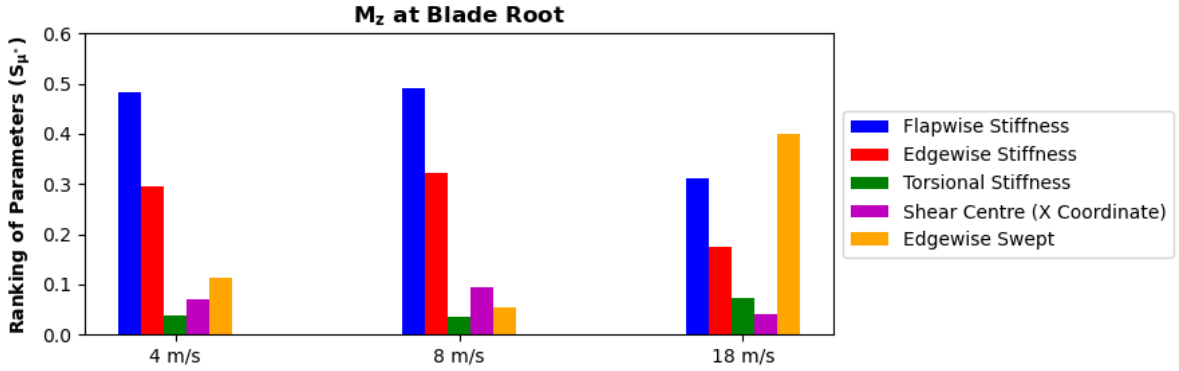

Figure 4.2: Ranking of parameters for torsional moment, M_z, at the blade root.

Subsequently, Figure 4.3 shows the COV results for the torsional moment at the blade root. In this case, the flapwise bending stiffness presents a COV below 0.5 at wind speeds of 4 m/s and 8 m/s, with the latter being within the range of wind speeds most likely to occur in offshore wind farms, based on industry experience. Furthermore, the edgewise bending stiffness exhibits COV levels around 0.5 across the different wind speeds under evaluation.

As previously explained, a COV lower than 0.5 suggests that the parameter has a monotonic effect on the output [59] [101]. Thus, this is an indicator that blade manufacturers could further investigate the flapwise and edgewise bending stiffnesses to tune these parameters in their new blade models, aiming to reduce torsional fatigue at the blade root, which is critical for the long and flexible modern blades.

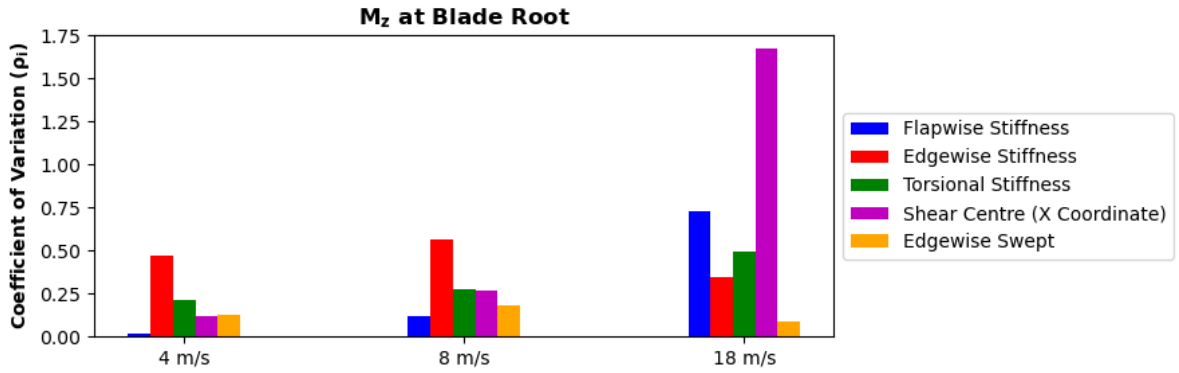

Figure 4.3: COV for torsional moment, M_z, at the blade root.

Next, it is valuable to compare the obtained rankings of parameters for three critical load components: the flapwise moment at the blade root, the fore-aft moment at the tower-top, and the fore-aft moment at the tower-bottom. These components are widely recognised in the industry as the most critical with respect to fatigue loads.

The flapwise moment at the blade root is generated by the aerodynamic forces acting on the blades. Similarly, the fore-aft moments at the tower-top and bottom represent the bending loads on the tower caused by the wind forces. As these load components align with the wind direction, they experience a high number of load cycles during turbine operation, leading to progressive structural fatigue damage.

The results illustrated in Figure 4.4 reveal a consistent, **dominant influence of the shear centre** on the different moments **across most of the wind speeds**.

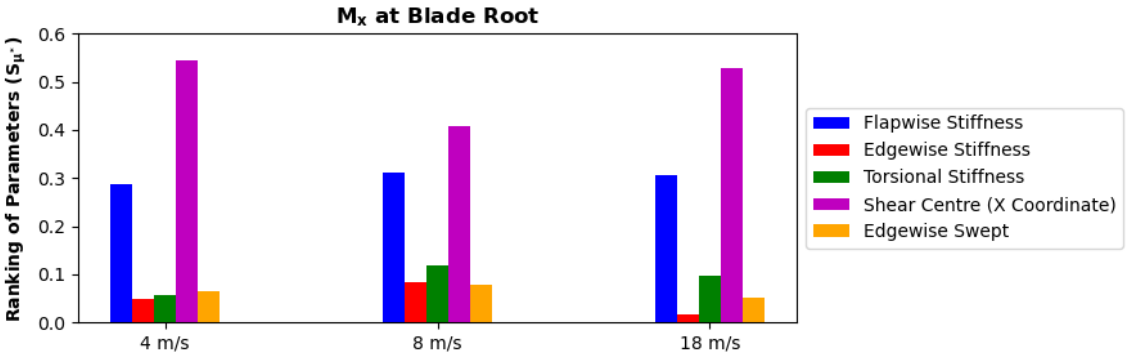

(a)

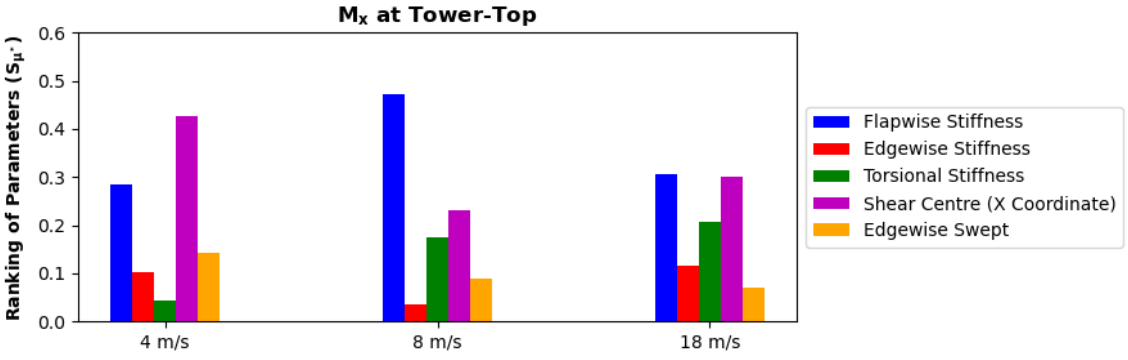

(b)

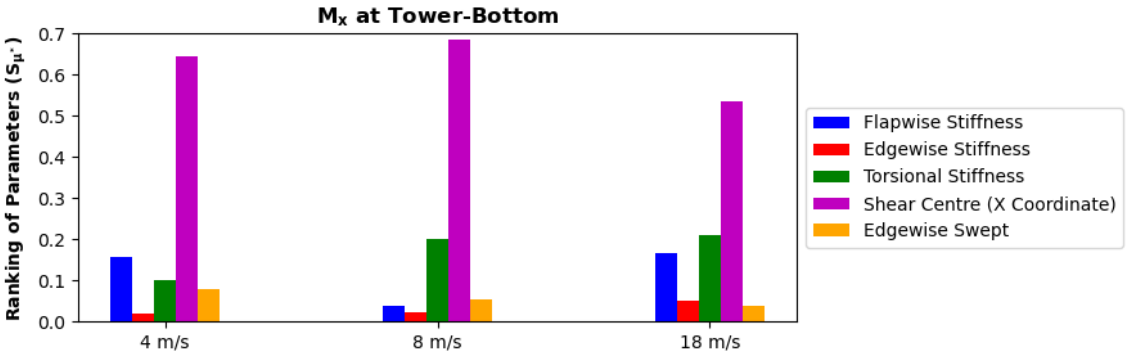

(c)

Figure 4.4: Ranking of parameters for (a) flapwise moment, M_x, at the blade root, (b) fore-aft moment, M_x, at the tower-top, and (c) fore-aft moment, M_x, at the tower-bottom.

In terms of flapwise moment at the blade root, the flapwise bending stiffness plays a significant role as expected, since it contributes to prevent (i.e., higher stiffness) or allow (i.e., lower stiffness) deformations and, consequently, high amplitude load cycles in the flapwise direction. Moreover, the results reveal that the shear centre exerts an even greater influence for this load component across the different wind speeds, surpassing the impact of the flapwise bending stiffness.

With respect to the fore-aft moment at the tower-top, the flapwise bending stiffness reaches a level of importance similar to the shear centre at a wind speed of 18 m/s and surpasses it at 8 m/s.

Concerning the fore-aft moment at the tower-bottom, the findings indicate that the shear centre has a particularly stronger impact compared to the other parameters.

Therefore, the **shear centre**, followed by the **flapwise bending stiffness**, emerge as the parameters with the **greatest influence** on these three critical load components.

Subsequently, Figures 4.5a and 4.5b illustrate the COV results for the flapwise moment at the blade root and the fore-aft moment at the tower-top, respectively. For these load components, the flapwise bending stiffness holds low COVs across the different wind speeds, while the shear centre shows a COV higher than 0.5 only at a wind speed of 8 m/s for the fore-aft moment at the tower-top.

Hence, the simultaneous high importance levels and low COVs exhibited by the shear centre and flapwise bending stiffness across most of the wind speeds suggest that these parameters could be further examined and tuned in future blade models to achieve lower fatigue loads in these critical components.

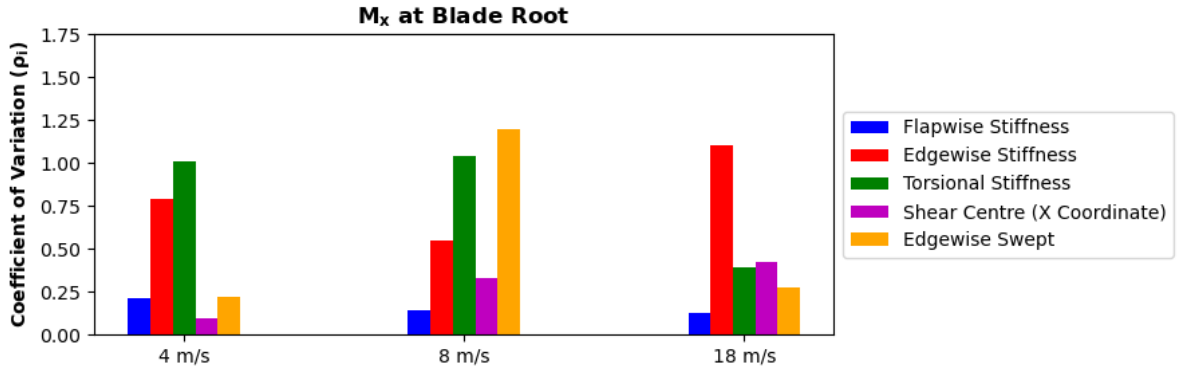

(a)

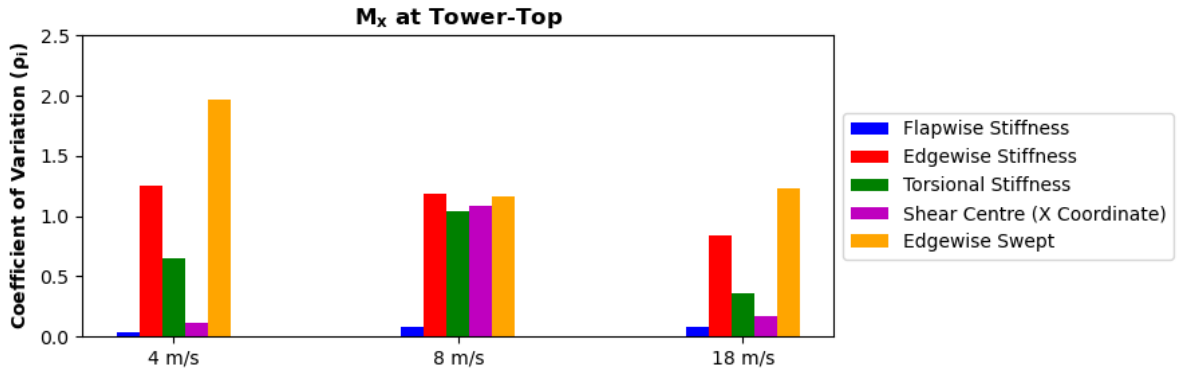

(b)

Figure 4.5: COV for (a) flapwise moment, M_x, at the blade root and (b) fore-aft moment, M_x, at the tower-top.

Then, Figures 4.6a and 4.6b present the obtained ranking of parameters with respect to the side-side and torsional moments at the tower-bottom, respectively. In these load components, the results reveal that the **shear centre** also exerts a **dominant influence** compared to other parameters on the different moments **across the several wind speeds**.

For the side-side moment, torsional stiffness reaches a level of importance comparable to the shear centre at wind speeds of 8 m/s and 18 m/s, while for the torsional moment, flapwise bending stiffness closely follows the influence of the shear centre at these wind speeds.

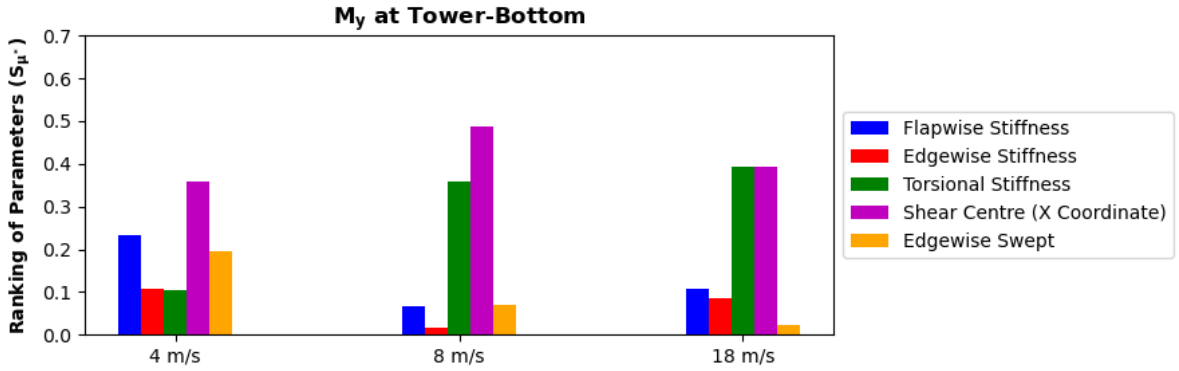

(a)

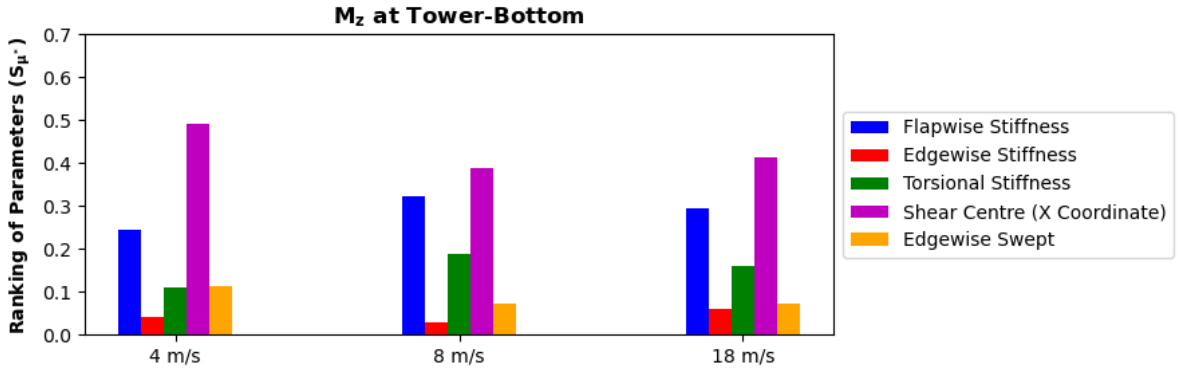

(b)

Figure 4.6: Ranking of parameters for (a) side-side moment, M_y, and (b) torsional moment, M_z, at the tower-bottom.

Furthermore, the fore-aft force at the tower-top highly contributes to the fore-aft moment at the tower-bottom, thus a similar ranking of parameter is expected.

Figure 4.7 and Figure 4.8 show the results for these load components and confirms that the outcomes align with the expectations, as the proportions remain similar between the parameters, with the **shear centre** exerting the **greatest influence across the different wind speeds**.

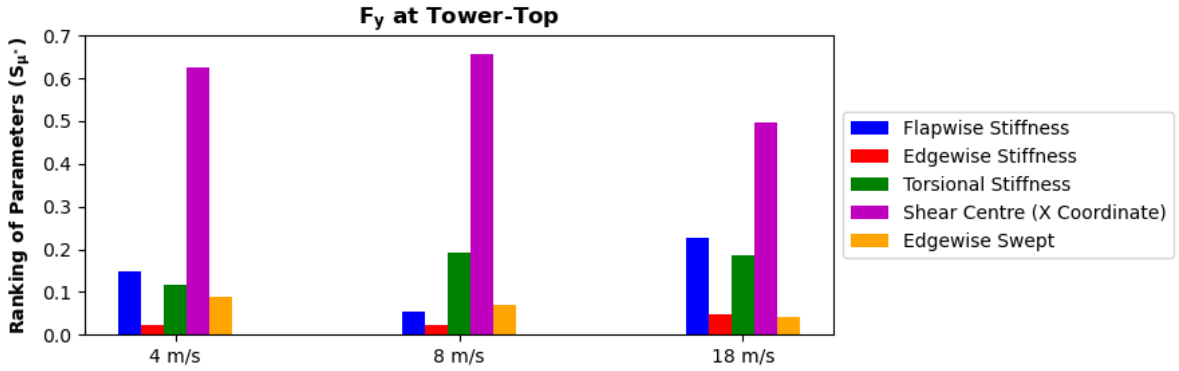

Figure 4.7: Ranking of parameters for fore-aft force, F_y, at the tower-top.

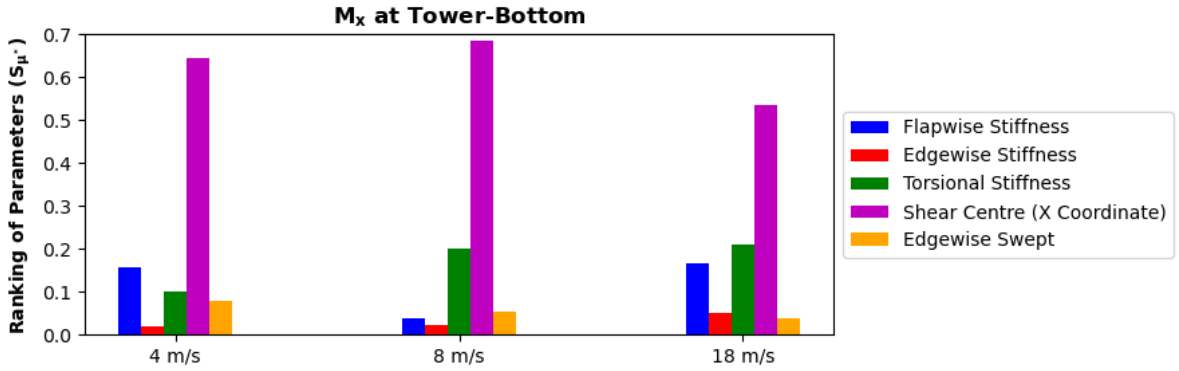

Figure 4.8: Ranking of parameters for fore-aft moment, M_x, at the tower-bottom.

The axial force at the top of the tower is primarily due to the weight of the nacelle and rotor, while at the bottom of the tower, it also includes the contribution of the tower weight. Therefore, variations in blade parameters are not expected to significantly affect the axial forces. Consequently, a similar level of importance among the different parameters is anticipated. This is particularly evident in the results for the wind speeds of 4 m/s and 8 m/s, as depicted in Figure 4.9.

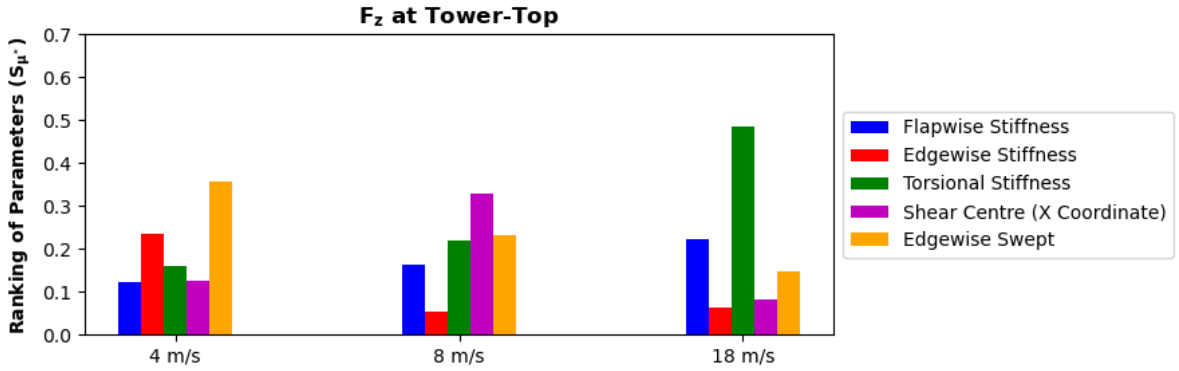

(a)

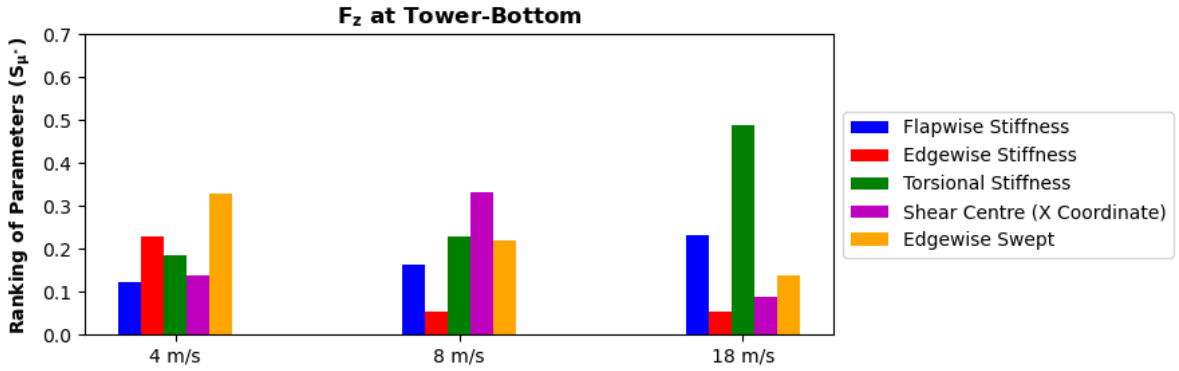

(b)

Figure 4.9: Ranking of parameters for axial force, F_z, at (a) the tower-top and (b) tower-bottom.

Lastly, a similar ranking of parameters is also predicted when comparing the side-side force at the tower-top with the side-side force at the tower-bottom and the torsional moment at the tower-top with the torsional moment at the tower-bottom. These results are illustrated in Figures G.4a, G.10a, G.9a, G.15a, which can be found in Appendix G, and they match the expectations.

The complete results of the sensitivity analysis are presented in Appendix G, including the ranking of parameters and the coefficient of variation outcomes for each load component evaluated in this research.

4.3. Reflection on Main Outcomes

As outlined in the literature review, flapwise and edgewise deformations cause the blade to twist along its longitudinal axis, leading to torsion, especially at the root and transition zone of the blade [23], as illustrated in Figure 4.10. The amount of flapwise and edgewise stiffnesses contributes to prevent (i.e., higher stiffness) or allow (i.e., lower stiffness) deformations in these respective directions, and thus, it also avoids or allows blade twisting. Hence, the high importance for flapwise and edgewise stiffnesses for the torsional moment at the blade root, depicted in Figure 4.2, matches the expectations. The level of these stiffnesses has a tied relationship with the level of fluctuations (i.e., fatigue loads) that the blade experiences in terms of flapwise, edgewise, and torsional moments.

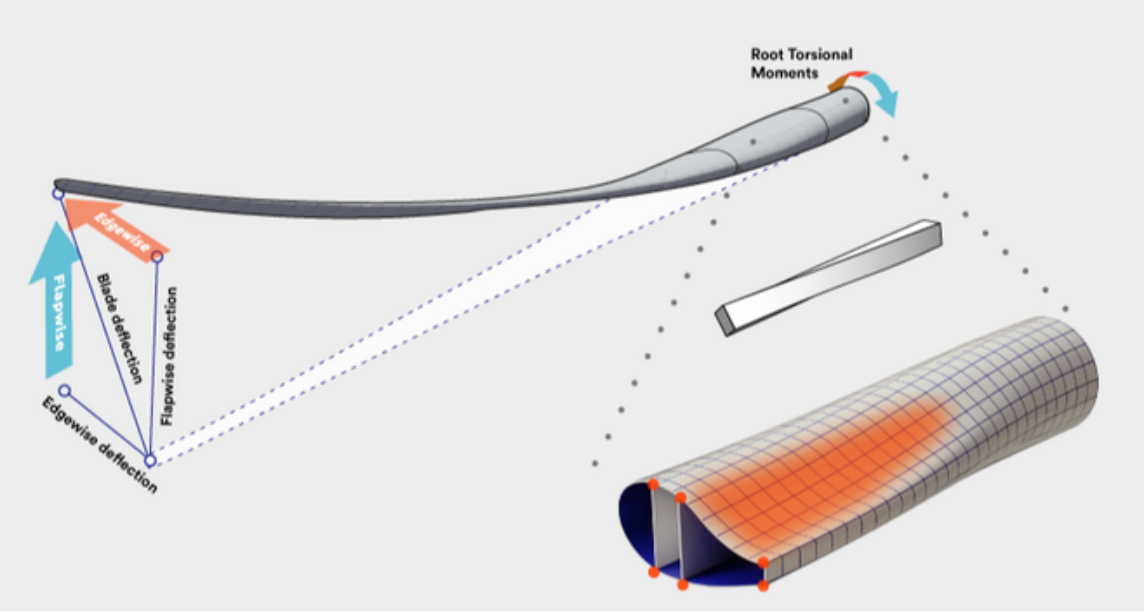

Figure 4.10: Torsion provoked by flapwise and edgewise deformations [103].

As discussed in Chapter 2, a moderate amount of sweep is typically introduced in modern blades because it creates a structural coupling between flapwise bending and torsion, which can be used for load alleviation [31] [32]. As the blade deflects in the flapwise direction, the tip twists towards a lower angle of attack (i.e., twist to feather), reducing aerodynamic loading, and thus, reducing flapwise bending [104], as shown in Figure 4.11.

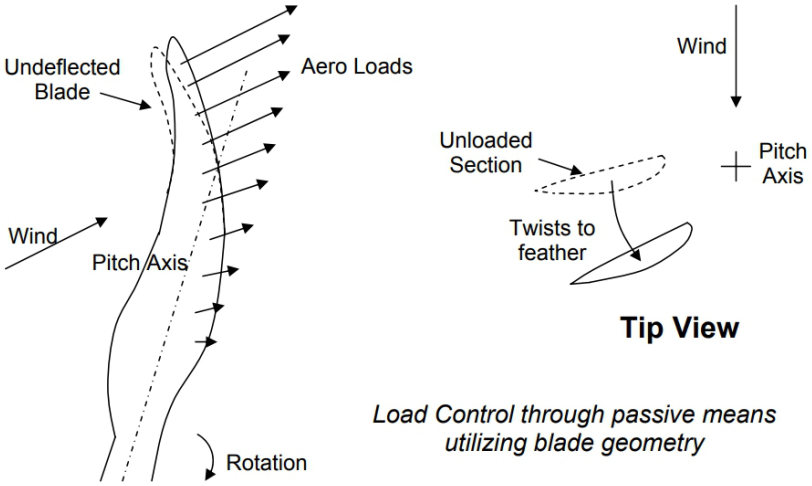

Figure 4.11: Swept blade concept [104].

In contrast, the loads generated at the edgewise swept tip introduce an additional torsional moment about the pitch axis [104]. This effect is especially significant at the blade root as blade length and wind speed increase. Numerous studies [105] [106] [107] have reported an increase in torsional fatigue load at the blade root due to the addition of edgewise swept. The increased aerodynamic loads at higher wind speeds accentuate the coupling between flapwise bending and torsion, increasing torsional loads. Therefore, the significant impact of the edgewise swept on the torsional moment at the blade root for a wind speed of 18 m/s, observed in Figure 4.2, is consistent with the available literature.

Although the results shown in Figure 4.2 and Figure 4.3 suggest a simultaneous high importance and low COV for edgewise swept at a wind speed of 18 m/s, any modification on the amount of edgewise swept to address the high torsional loads at high wind speeds should be carefully evaluated. As discussed, the increased torsion is the price paid for reducing flapwise bending. **Therefore, the effects are coupled and there is no straightforward solution.**

Next, the results displayed in Figure 4.4 indicated a dominant influence of the shear centre across different wind speeds on the most critical components with respect to fatigue loads, namely the flapwise moment at the blade root, and the fore-aft moments at the tower-top and tower-bottom. Hence, it is noteworthy to correlate this outcome with the challenges associated with the shear centre location.

Figure 4.12 illustrates the internal structure of a wind turbine blade. The blades are classified as composite structures since they are made of different materials. Additionally, a significant portion of these materials are also composites, formed by the combination of two or more materials with different mechanical properties. For example, the combination of fibres and polymers, known as fibre-reinforced polymer (FRP) composites, represents the majority of the blade's material composition, typically accounting for 60% to 70% [108].

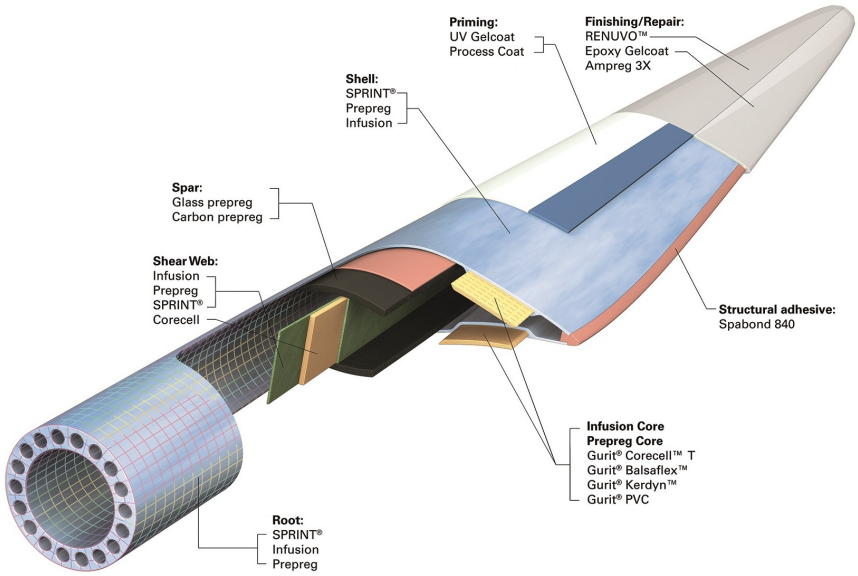

Figure 4.12: Composite materials in a typical wind turbine blade [109].

A material is classified as isotropic if its mechanical properties are uniform in all directions. This implies that its response to applied loads, such as strength, stiffness, and elasticity, does not vary with the direction under evaluation [110]. In contrast, anisotropic materials have properties that vary depending on the direction in which they are measured [110]. For instance, anisotropic materials can demonstrate great strength when force is applied in the same direction as the fibres, and much less strength when force is applied in the perpendicular direction.

For a beam made of isotropic material, the location of the shear centre is primarily dependent on the geometry of the cross-section, whereas for a beam made of anisotropic material, the material properties and configuration (e.g., fibre's orientation) also play a significant role [111] [112]. Composite materials, such as FRP, typically display anisotropic properties [113] and, thus, identifying the shear centre location in composite beams becomes more complex [112].

As wind turbine blades are largely constituted by composite materials [108], which are arranged in different layers and directions as depicted in Figure 4.12, identifying the shear centre location of a blade cross-section becomes an even more challenging task, necessitating advanced methods. Currently, powerful computational tools, such as VABS (Variational Asymptotic Beam Section analysis code) [114] and BECAS (Beam Cross-section Analysis Software) [115], are used to estimate the position of the shear centre and overcome the complexity of the problem.

Briefly explaining this complexity, in isotropic beams, bending and twisting are typically independent (i.e., applying a bending moment causes bending and applying a torsional moment causes twisting). However, in composite beams, bending and twisting are often coupled due to the anisotropic material properties [116] [117]. When a bending moment is applied to a composite beam, the different stiffness in different directions causes the load to produce not only bending but also some twisting. Similarly, an applied torsional moment may cause both twisting and some bending [116] [117].

In Chapter 2, the conventional definition of the shear centre was introduced. It is defined as the point at which a force applied parallel to the plane of the cross-section will produce bending but no twisting deformation [118]. Nevertheless, for composite beams, it is typically not possible to find a closed-form solution for such a point due to the bend-twist coupling effects [119].

In his book titled "Nonlinear Composite Beam Theory for Engineers" [120], Hodges proposes the recognition of a generalised shear centre for anisotropic beams. For beams with bend-twist coupling, such as composite beams, the conventional definition of the shear centre should be generalised by considering only the twist caused by the shear forces and excluding the twist produced by bending moments through the bend-twist coupling.

While existing literature highlights the challenges in finding a closed-form solution for the shear centre location [119] [120] and the unavoidable deviations between designed and fabricated blades [11], the findings of this thesis suggest that even slight differences in the shear centre position can have a meaningful impact on fatigue loads.

For example, Figure 4.13 shows the maximum and minimum fore-aft moments, in terms of DELs, observed at the base of the tower at a wind speed of 8 m/s. The label in Figure 4.13 specifies which modification, among the several modifications executed and simulated for each parameter, led to this respective maximum or minimum value.

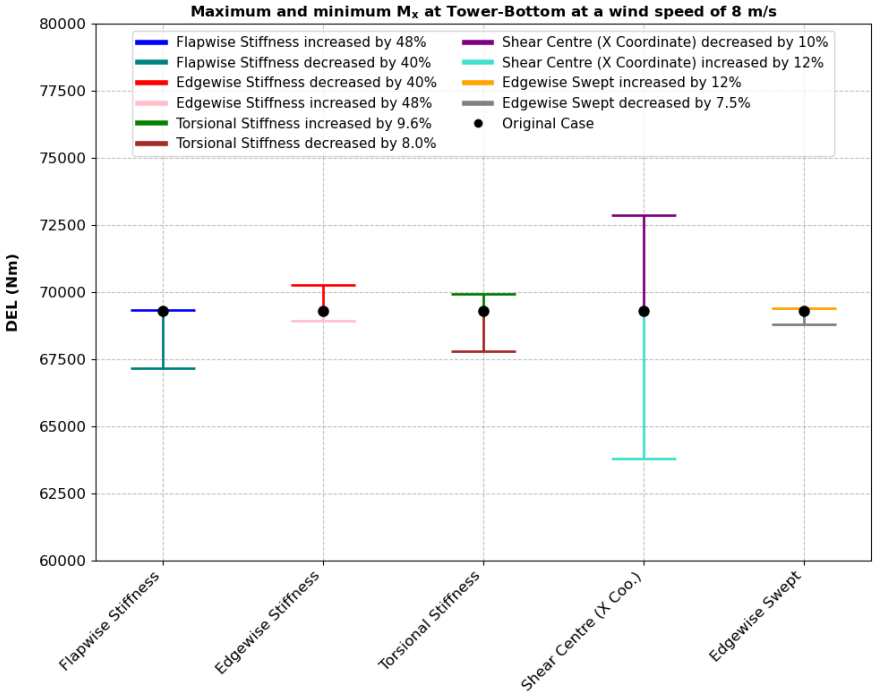

Figure 4.13: Maximum and minimum fore-aft moments, M_x, at the tower-bottom at a wind speed of 8 m/s.

The results indicate that a 12% increase in the original x coordinate values of the shear centre reduces the magnitude of this load component by approximately 8%, while a decrease of 10% increases the magnitude by around 5%. These load differences are especially relevant because they are observed at a wind speed of 8 m/s, which is within the range of wind speeds most likely to occur in offshore wind farms, based on industry experience.

Next, it is noteworthy to observe that, given the x coordinate values of the IEA 15 MW RWT, the 12% increase and 10% decrease in the original values do not result in a change greater than 14 centimetres and 12 centimetres, respectively, for the different cross-sections along the blade span, as depicted in Figure 4.14.

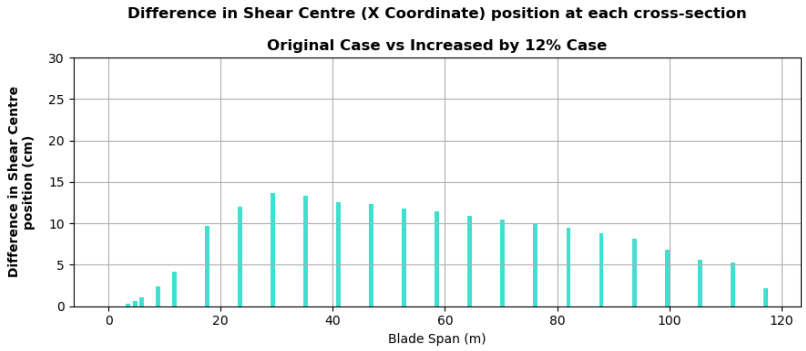

(a)

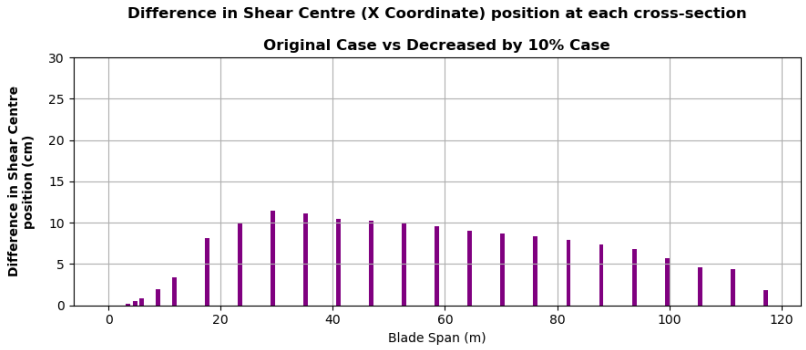

(b)

Figure 4.14: Absolute differences in shear centre (x coordinate) position.

Therefore, the **outcomes** of this thesis **suggest** that:

1) **In the design phase of the blade, small modifications (i.e., some centimetres) to the shear centre location could be considered, as they revealed potential to considerably decrease the fatigue loads, without significantly decreasing power production.**

   Previous studies have highlighted the impact of the shear centre on the natural frequencies and mode shapes of rotating blades [121], as well as on the aeroelastic damping of wind turbines [6]. This thesis, which is focused on fatigue loads, extends the range of phenomena where the shear centre plays a critical role.

2) **In the manufacturing phase of the blade, deviations in the shear centre location from the original design should be minimised, as slight differences (i.e., some centimetres) in its location revealed potential to considerably increase the fatigue loads.**

   Existing literature previously highlighted the importance of accurately estimating the shear centre, as even very small errors exhibited potential to cause undesirable twisting [119]. Moreover, the position of the shear centre along the chord (which corresponds to the x coordinate values in this thesis) has been recognised as sensitive to manufacturing defects [6].

Thus, the challenges associated with the **shear centre** location remain, and this research further emphasises the **importance of its precise location**, during both the design and manufacturing phases, as it has a **meaningful effect on fatigue loads.**

5
Conclusions and Recommendations

This chapter summarises the main findings of this thesis and provides recommendations for future work.

5.1. Main Findings

In this research, a sensitivity analysis was conducted on the IEA 15 MW RWT to investigate which blade parameters have the greatest influence on fatigue loads during normal turbine operation under turbulence.

This work serves as a preliminary, low-cost analysis of the parameters' individual effects on the turbine response. The insights provided by this research aim to support blade manufacturers in improving their blade designs by tuning the parameters in new blade models to achieve lower fatigue loads at different positions of the turbine structure. Furthermore, this study aims to highlight parameters that should receive special attention during the manufacturing phase, as slight deviations in their values from the original blade design may considerably increase the fatigue loads.

Based on the results obtained, **four main conclusions** can be drawn:

- **Modifications to the shear centre location along the chord can be key to reducing fatigue loads without significantly decreasing power production.**

  The **shear centre** exerts a **dominant influence** among the different blade parameters **at below, near, and above rated wind speeds** in critical load components related to fatigue damage, such as the **flapwise moment at the blade root and the fore-aft moment at the tower-bottom**.

  Additionally, the impact of the shear centre stands out compared to other parameters across the different wind speeds for the fore-aft force at the tower-top, as well as for the torsional moments at the tower-top and tower-bottom.

  Lastly, the shear centre holds high importance at below and near rated wind speeds for the side-side force and moment at the tower-top, as well as for the fore-aft and side-side forces and the side-side moment at the tower-bottom.

- **Deviations in the shear centre position along the chord from the original design should be minimised, as slight differences in its location revealed potential to considerably increase fatigue loads.**

  As an **indicator** of the change caused in the magnitude of the loads, the **DEL results** for the **fore-aft moment at the tower-bottom** are assessed **at near rated wind speed.**

  It is found that a **12% increase** in the original shear centre values (i.e., towards the leading edge) **reduces the DEL by about 8%**. In contrast, a **decrease of 10%** (i.e., towards the trailing edge) **increases the DEL by around 5%**.

  The **12% increase** and **10% decrease** in the original shear centre values do not result in alterations greater than **14 centimetres** and **12 centimetres**, respectively, for the different cross-sections along the blade span.

- **Modifications to the flapwise bending stiffness can play an important role in reducing fatigue loads without significantly decreasing power production.**

  The **flapwise bending stiffness**, together with the shear centre, share a **dominant influence** on the **flapwise moment at the blade root and the fore-aft moment at the tower-top across the different wind speeds**.

  Furthermore, the **flapwise bending stiffness** exerts the **greatest influence at below and near rated wind speeds on the torsional moment at the blade root**, which is a critical load component for the long and flexible modern blades.

  Finally, the flapwise bending stiffness is of significant importance for the torsional moments at the tower-top and tower-bottom, closely following the shear centre levels across different wind speeds.

- **Modifications to the edgewise bending stiffness can contribute to reducing fatigue loads without significantly decreasing power production.**

  The **edgewise bending stiffness** holds a **significant importance at below and near rated wind speeds for the torsional moment at the blade root**, closely following the flapwise bending stiffness levels at these wind speeds.

  Moreover, the impact of the edgewise bending stiffness prevails over the other parameters at above rated wind speeds and stands out at below rated wind speeds for the edgewise moment at the blade root.

Additionally, it is valuable to highlight that the **edgewise swept** exerts the **greatest influence at above rated wind speeds on the torsional moment at the blade root**. Finally, the **torsional stiffness** typically plays an **important role at near and especially above rated wind speeds in several load components at the tower**, such as the fore-aft and side-side forces and the side-side moment at the tower-bottom, as well as the side-side force and side-side moment at the tower-top.

The results of this work suggest that **future investigations of larger turbines should focus on the shear centre location and the flapwise bending stiffness**.

Although **the findings may vary depending on the size, type, and control of the wind turbine considered**, it is expected that the results found in this thesis can serve as a basis for the load analysis of other turbines.

5.2. Recommendations for Future Studies

First and foremost, it is recommended that future sensitivity analyses of blade parameters **include retuning the controller each time a blade parameter is modified**. Previous studies have given little or no attention to controller tuning parameters. However, as shown in Section 3.3.3, the controller significantly impacts the DELs. It was demonstrated that the controller tuning is an important part of the strategy to ensure, as much as possible, that variations in the dynamic response of the turbine result from changes in blade parameters rather than from other sources.

Additionally, the present work can be extended by:

1) **Accounting for the interaction between the parameters**

One limitation of the present work is that each parameter was considered independent across the full range, and only the dependence on wind speed was studied. Consequently, the model's parametric space was partially explored. It is therefore recommended to use more sophisticated methods (e.g., the second-order EE method) that account for interactions between the parameters and provide the necessary flexibility to include the controller tuning process in between the simulations. This approach would offer a valuable detailed understanding of the model response.

2) **Involving more blade parameters in the investigation**

There is an extensive range of blade parameters that can be evaluated. Nonetheless, due to time constraints, only a few were considered in this research.

In this work, the five blade parameters listed in Table 1.1 were prioritized, as available literature and previous simulation experiences from experts at COWI and Ørsted suggested their likely higher level of importance compared to other options. However, including additional parameters, such as the centre of mass, mass per unit length, neutral axis, and flapwise prebend, would be worthwhile. First, this would provide a more complete ranking of parameters, offering a broader overview of their importance levels. Second, the COV analysis could reveal other parameters with the potential to reduce the DEL in a specific load component. Third, this extension could unveil other parameters that are critical to having their deviations from the original design minimised.

Lastly, it is believed that variations in aerodynamic parameters (e.g., chord, thickness, and twist angle) would require changes in the aerofoil profiles to maintain the aerodynamic design of the blade. As a result, it is thought that the findings may be limited to the IEA 15 MW RWT, and no conclusions could be inferred for other turbine models.

References

[1] United Nations Climate Change. *The Paris Agreement*. 2000. URL: https://unfccc.int/process-and-meetings/the-paris-agreement#:~:text=It%20entered%20into%20force%20on,above%20pre%2Dindustrial%20levels.%E2%80%9D (visited on 01/12/2023).

[2] P. Passon et al. *Offshore Wind Turbine Foundation Design*. 2015. URL: https://orbit.dtu.dk/en/publications/offshore-wind-turbine-foundation-design (visited on 01/12/2023).

[3] Offshorewind.biz. *22 MW Offshore Wind Turbine in the Works for 2024/25*. 2023. URL: https://www.offshorewind.biz/2023/10/23/22-mw-offshore-wind-turbine-in-the-works-for-2024-25/ (visited on 01/12/2023).

[4] Ørsted. *1991-2001 The first offshore wind farms*. URL: https://orsted.com/en/insights/white-papers/making-green-energy-affordable/1991-to-2001-the-first-offshore-wind-farms (visited on 01/12/2023).

[5] G. E. M. Beshay and K. Y. Maalawi. *Structural Optimization of Wind Turbine Blades for Improved Dynamic Performance*. IntechOpen, 2000.

[6] H. Verdonck et al. "Uncertainty quantification of structural blade parameters for the aeroelastic damping of wind turbines: a code-to-code comparison". In: *Wind Energy Science Discussions* (2023).

[7] P. Veers et al. "Grand challenges in the science of wind energy". In: *Science* 366.6464 (2019).

[8] R. Liang et al. "Multiaxial Strain Analysis in Large Wind Turbine Blades under Full-scale Fatigue Testing". In: *Journal of Failure Analysis and Prevention* 23 (2023), pp. 2554–2574.

[9] L. Mishnaevsky. "Root Causes and Mechanisms of Failure of Wind Turbine Blades: Overview". In: *Materials* 15.9 (2022).

[10] M. A. Eder, R. D. Bitsche, and F. Belloni. "Effects of geometric non-linearity on energy release rates in a realistic wind turbine blade cross section". In: *Composite Structures* 132 (2015), pp. 1075–1084.

[11] P. Noever-Castelos, L. Ardizzone, and C. Balzani. "Model updating of wind turbine blade cross sections with invertible neural networks". In: *Wind Energy Open Access* 25.3 (2022), pp. 573–599.

[12] IEAWindTask37. *IEA-15-240-RWT: 15MW reference wind turbine repository*. URL: https://github.com/IEAWindTask37/IEA-15-240-RWT (visited on 06/12/2023).

[13] P. J. Schubel and R. J. Crossley. "Wind Turbine Blade Design". In: *Energies* 5.9 (2012).

[14] L. Schröder. "Towards digital twins: wind farm operation analysis and optimization using model-supported data analytics". In: *DTU Wind Energy* (2020).

[15] International Electrotechnical Commission. "Wind energy generation systems – Part 1: Design requirements". In: *IEC 61400-1* (2019).

[16] NEN.nl. *NEN-EN-IEC 61400-1:2019 en*. URL: https://www.nen.nl/en/nen-en-iec-61400-1-2019-en-257967 (visited on 07/12/2023).

[17] N. Dimitrov et al. "From wind to loads: wind turbine site-specific load estimation with surrogate models trained on high-fidelity load databases". In: *Wind Energy Science* 3.2 (2018), pp. 767–790.

[18] P. van der Male. "Wind Turbine Loading". In: *Applied Dynamics of Structures, TU Delft lecture slides* (2022).

[19] N. Khlaifat et al. “A review of the key sensitive parameters on the aerodynamic performance of a horizontal wind turbine using Computational Fluid Dynamics modelling”. In: *AIMS Energy* 5.3 (2020), pp. 493–524.

[20] DTU Wind Energy. “Aerodynamic Input in HAWC2”. In: *HAWC2 E-learning course* (2018).

[21] DTU Wind Energy. “An Introduction to Beam Cross Section Stiffness and Mass Properties”. In: *HAWC2 E-learning course* (2018).

[22] R. Gasch and J. Twele. *Wind power plants: fundamentals, design, construction and operation*. Springer Science & Business Media, 2011.

[23] F. M. Jensen and K. Branner. “Introduction to wind turbine blade design”. In: *Advances in Wind Turbine Blade Design and Materials* (2023), pp. 3–53.

[24] P. A. Meehan. “Prediction and suppression of chaos following flutter in wind turbines”. In: *Nonlinear Dynamics* 111 (2023), pp. 22153–22176.

[25] T. Farsadi and A. Kayran. “Classical flutter analysis of composite wind turbine blades including compressibility”. In: *Wind Energy Open Access* 24.1 (2021), pp. 69–91.

[26] B. Chen et al. “Enhancement of flutter stability in wind turbines with a new type of passive damper of torsional rotation of blades”. In: *Journal of Wind Engineering and Industrial Aerodynamics* 173 (2018), pp. 171–179.

[27] J. P. A. A. Blasques. “User’s Manual for BECAS: A cross section analysis tool for anisotropic and inhomogeneous beam sections of arbitrary geometry”. In: *DTU Wind Energy* (2012).

[28] F. M. Jensen et al. “Torsional Effects on Wind Turbine Blades and Impact on Field Damages”. In: *IOP Conference Series: Materials Science and Engineering* (2023).

[29] K. Branner et al. “Anisotropic beam model for analysis and design of passive controlled wind turbine blades”. In: *DTU Wind Energy* (2012).

[30] F. Momeni et al. “Plant leaf-mimetic smart wind turbine blades by 4D printing”. In: *Renewable Energy* 130 (2019), pp. 329–351.

[31] J. B. de Vaal, T. A. Nygaard, and R. Stenbro. “Developing a passive load reduction blade for the DTU 10 MW reference turbine”. In: *Journal of Physics: Conference Series* 753.4 (2016).

[32] C. Pavese et al. “Aeroelastic multidisciplinary design optimization of a swept wind turbine blade”. In: *Wind Energy* 20.12 (2017), pp. 1941–1953.

[33] A. Rezaeiha, R. Pereira, and M. Kotsonis. “Fluctuations of angle of attack and lift coefficient and the resultant fatigue loads for a large Horizontal Axis Wind turbine”. In: *Renewable Energy* 114 (2017), pp. 904–916.

[34] National Renewable Energy Laboratory. *OpenFAST*. URL: `https://www.nrel.gov/wind/nwtc/openfast.html` (visited on 12/03/2024).

[35] DTU Wind Energy. *HAWC2: An aeroelastic code*. URL: `https://www.hawc2.dk/` (visited on 12/03/2024).

[36] Bladed. *Wind turbine design software - Bladed*. URL: `https://www.dnv.com/services/wind-turbine-design-software-bladed-3775/` (visited on 12/03/2024).

[37] A. Otter et al. “A review of modelling techniques for floating offshore wind turbines”. In: *Wind Energy Open Access* 25 (2022), pp. 831–857.

[38] S. Fadaei, F. F. Afagh, and R. G. Langlois. “A Survey of Numerical Simulation Tools for Offshore Wind Turbine Systems”. In: *Preprints* (2023).

[39] Md. S. Islam et al. “Composite materials: Concept, recent advancements, and applications”. In: *Renewable Polymers and Polymer-Metal Oxide Composites* (2022).

[40] J. Pacheco et al. “Fatigue Assessment of Wind Turbine Towers: Review of Processing Strategies with Illustrative Case Study”. In: *Energies* 15.13 (2022).

[41] S. Loew, D. Obradovic, and C. L. Bottasso. “Model predictive control of wind turbine fatigue via online rainflow-counting on stress history and prediction”. In: *Journal of Physics: Conference Series* (2020).

[42] M. Matsuichi and T. Endo. “Fatigue of metals subjected to varying stress”. In: *Proceedings of the Kyushu Branch of Japan Society of Mechanical Engineering* (1968), pp. 37–40.

[43] M. A. Miner. “Cumulative Damage in Fatigue”. In: *Journal of Applied Mechanics* 12.3 (1945).

[44] International Electrotechnical Commission. “Wind Turbines - Part 3: Design Requirements for Offshore Wind Turbines”. In: *IEC 61400-3* (2009).

[45] Det Norske Veritas (DNV). “Design of Offshore Wind Turbine Structures”. In: *DNV-OS-J101* (2011).

[46] Germanischer Lloyd (GL). “Guideline for the Certification of Wind Turbines”. In: *Germanischer Lloyd* (2010).

[47] Germanischer Lloyd (GL). “Guideline for the Certification of Offshore Wind Turbines”. In: *Germanischer Lloyd* (2012).

[48] J. Liew. *Affect of Quantity, Resolution, & Scaling of Turbulence Boxes on Aeroelastic Simulation Convergence*. URL: `https://youtu.be/gIrMB4bbMkg?si=KP_tXiSfJ_u0BwC3` (visited on 05/05/2024).

[49] A. Natarajan. “Damage equivalent load synthesis and stochastic extrapolation for fatigue life validation”. In: *Wind Energy Science* 7 (2022), pp. 1171–1181.

[50] Siemens. *Rainflow Counting*. URL: `https://community.sw.siemens.com/s/article/rainflow-counting` (visited on 05/05/2024).

[51] D. Benasciutti and R. Tovo. “Comparison of spectral methods for fatigue analysis of broad-band Gaussian random processes”. In: *Probabilistic Engineering Mechanics* 21 (2006), pp. 287–299.

[52] D. Benasciutti and R. Tovo. “Spectral methods for lifetime prediction under wide-band stationary random processes”. In: *International Journal of Fatigue* 27 (2005), pp. 867–877.

[53] A. Saltelli et al. *Global Sensitivity Analysis. The Primer*. John Wiley & Sons, 2008.

[54] M. N. Macho. “Sensitivity analysis”. In: *MUDE (Modelling, Uncertainty, Data for Engineers), TU Delft lecture slides* (2022).

[55] Battelle Memorial Institute. *Sensitivity Analysis: The Basics*. 2022. URL: `https://uc-ebook.org/docs/html/3_sensitivity_analysis_the_basics.html` (visited on 10/05/2024).

[56] A. Saltelli et al. *Sensitivity Analysis in Practice: A Guide to Assessing Scientific Models*. John Wiley & Sons, Ltd, 2004.

[57] D. Li et al. “Comparison of local and global sensitivity analysis methods and application to thermal hydraulic phenomena”. In: *Progress in Nuclear Energy* 158 (2023).

[58] M. D. Morris. “Factorial Sampling Plans for Preliminary Computational Experiments”. In: *Technometrics* 33.2 (2012), pp. 161–174.

[59] D. G. Sanchez et al. “Application of sensitivity analysis in building energy simulations: Combining first- and second-order elementary effects methods”. In: *Energy and Buildings* 68 (2014).

[60] A. Robertson et al. “Sensitivity analysis of the effect of wind characteristics and turbine properties on wind turbine loads”. In: *Wind Energy Science* 4 (2019), pp. 479–513.

[61] R. J. L. Rutjens et al. “Elementary effects for models with dimensional inputs of arbitrary type and range: Scaling and trajectory generation”. In: *PLOS ONE* (2023).

[62] A. Robertson et al. “Assessment of Wind Parameter Sensitivity on Extreme and Fatigue Wind Turbine Loads”. In: *Wind Energy Symposium* (2018).

[63] W. Wiley et al. “Sensitivity analysis of numerical modeling input parameters on floating offshore wind turbine loads”. In: *Wind Energy Science* 8 (2023), pp. 1575–1595.

[64] H. Djojodihardjo. *Introduction to Aeroelasticity*. Springer, 2023.

[65] A. Ahlström. “Aeroelastic Simulation of Wind Turbine Dynamics”. In: *Swedish Royal Institute of Technology - Department of Mechanics* (2005).

[66] Technical University of Denmark. *Structual formulation*. URL: `https://www.hawc2.dk/about-hawc2/structual-formulation` (visited on 12/05/2024).

[67] C. C. Ike. “Timoshenko Beam Theory for the Flexural Analysis of Moderately Thick Beams – Variational Formulation, and Closed Form Solution”. In: *TECNICA ITALIANA-Italian Journal of Engineering Science* 63.1 (2019), pp. 34–45.

[68] DTU Wind Energy. “Introduction to flexible multibody dynamics”. In: *HAWC2 E-learning course* (2018).

[69] H. Glauert. *Airplane Propellers. In: Division L in Aerodynamic Theory*. Springer, Berlin, Heidelberg, 1935.

[70] T. J. Larsen and A. M. Hansen. “How 2 HAWC2, the user’s manual”. In: *DTU Wind Energy* (2021).

[71] Wind Energy Technologies Office. *How a Wind Turbine Works - Text Version*. URL: `https://www.energy.gov/eere/wind/how-wind-turbine-works-text-version` (visited on 01/06/2024).

[72] E. Gaertner et al. “Definition of the IEA 15-Megawatt Offshore Reference Wind Turbine”. In: *National Renewable Energy Laboratory (NREL)* (2020).

[73] M. H. Hansen et al. “HAWCStab2 User Manual”. In: *DTU Wind Energy* (2018).

[74] IEAWindTask37. *IEA-15-240-RWT: 15MW reference wind turbine repository*. URL: `https://github.com/IEAWindTask37/IEA-15-240-RWT/tree/master/HAWC2` (visited on 03/06/2023).

[75] P. G. Jamdade, S. V. Patil, and V. B. Patil. “Assessment of Power Coefficient of an Offline Wind Turbine Generator System”. In: *International Journal of Engineering Research & Technology (IJERT)* 2.9 (2013).

[76] C. Jung and D. Schindler. “The role of the power law exponent in wind energy assessment: A global analysis”. In: *International Journal of Energy Research* 45.6 (2021), pp. 8484–8496.

[77] D. C. Bratton and C. A. Womeldorf. “The Wind Shear Exponent: Comparing Measured Against Simulated Values and Analyzing the Phenomena That Affect the Wind Shear”. In: *ASME 2011 5th International Conference on Energy Sustainability* (2012), pp. 2245–2251.

[78] O. Castro. “Fatigue strength of composite wind turbine blade structures”. In: *DTU Wind Energy* (2018).

[79] Jake Hertz. *Unlocking the Secrets of Turbulence To Mitigate Its Impact on Turbines*. 2023. URL: `https://eepower.com/tech-insights/unlocking-the-secrets-of-turbulence-to-mitigate-its-impact-on-turbines/#` (visited on 05/06/2024).

[80] A. Chougule et al. “Modeling Atmospheric Turbulence via Rapid Distortion Theory: Spectral Tensor of Velocity and Buoyancy”. In: *Journal of the Atmospheric Sciences* 74 (2017).

[81] R. M. M. Slot et al. “Effective turbulence and its implications in wind turbine fatigue assessment”. In: *Wind Energy* 22.12 (2019), pp. 1699–1715.

[82] J. Mann. “Wind field simulation”. In: *Probabilistic Engineering Mechanics* 13 (1998), pp. 269–282.

[83] SINTEF. *The Mann uniform shear turbulence model*. URL: `https://www.sima.sintef.no/doc/4.6.0/windfield/context/MannWindGenerator.html` (visited on 06/06/2024).

[84] Á. Hannesdóttir, M. Kelly, and N. Dimitrov. “Extreme wind fluctuations: joint statistics, extreme turbulence, and impact on wind turbine loads”. In: *Wind Energy Science* 4 (2019), pp. 325–342.

[85] J. Rinker et al. “Comparison of loads from HAWC2 and OpenFAST for the IEA Wind 15 MW Reference Wind Turbine”. In: *Journal of Physics: Conference Series* 1618 (2020).

[86] DTU Wind Energy. “Exercise: Wind turbulence inputs”. In: *HAWC2 E-learning course* (2018).

[87] DTU Wind Energy. “Modeling turbulence fields in HAWC2”. In: *HAWC2 E-learning course* (2018).

[88] M. H. Hansen et al. “Design Load Basis for onshore turbines - Revision 00”. In: *DTU Wind Energy* (2015).

[89] Windy Nation Inc. *Tip Speed Ratio: How to Calculate and Apply TSR to Blade Selection*. URL: https://www.windynation.com/blogs/articles/tip-speed-ratio-how-calculate-and-apply-tsr-blade-selection (visited on 10/06/2024).

[90] SKYbrary Aviation Safety. *Blade Pitch*. URL: https://skybrary.aero/articles/blade-pitch (visited on 11/06/2024).

[91] N. J. Abbas et al. “A reference open-source controller for fixed and floating offshore wind turbines”. In: *Wind Energy Science* 7 (2022), pp. 53–73.

[92] Y. Miao, M. N. Soltani, and A. Hajizadeh. “A Machine Learning Method for Modeling Wind Farm Fatigue Load”. In: *Applied Sciences* (2022).

[93] The European Union. “Eurocode 3: Design of steel structures - Part 1-9: Fatigue”. In: *EN 1993-1-9* (2005).

[94] DTU Wind Energy. *DTU-10MW-RWT: 10MW reference wind turbine repository*. URL: https://gitlab.windenergy.dtu.dk/hawc-reference-models/dtu-10mw-rwt (visited on 01/07/2024).

[95] IEA Wind Task 55 REFWIND. *IEA-22-280-RWT: 22MW reference wind turbine repository*. URL: https://github.com/IEAWindTask37/IEA-22-280-RWT (visited on 01/07/2024).

[96] P. K. Chaviaropoulos. “Similarity rules for W/T up-scaling”. In: *UpWind Report* WP 1B4 (2007).

[97] G. Sieros et al. “Upscaling wind turbines: theoretical and practical aspects and their impact on the cost of energy”. In: *Wind Energy: The UpWind Special Issue* 15.1 (2012), pp. 3–17.

[98] R. J. L. Rutjens et al. “Elementary effects for models with dimensional inputs of arbitrary type and range: Scaling and trajectory generation”. In: *PLoS ONE* 18.10 (2023).

[99] F. Campolongo, J. Cariboni, and A. Saltelli. “An effective screening design for sensitivity analysis of large models”. In: *Environmental Modelling & Software* 22 (2007), pp. 1509–1518.

[100] J. Wu. “A new sequential space-filling sampling strategy for elementary effects-based screening method”. In: *Applied Mathematical Modelling* 83 (2020), pp. 419–437.

[101] OTMORRIS 0.16 documentation. *User manual*. URL: https://openturns.github.io/otmorris/master/user_manual/user_manual.html (visited on 09/07/2024).

[102] The Mathematics Capital. *The Art of Identifying Monotonic Functions Made Simple*. URL: https://iitutor.com/monotonic-increasing-and-decreasing-how-to-find-the-inverse-of-monotonic-functions/ (visited on 01/08/2024).

[103] Bladena. *Innovative paper unveils important findings of torsional loads that will boost the performance of large wind turbines*. URL: https://www.bladena.com/news/innovative-paper-unveils-important-findings-of-torsional-loads-that-will-boost-the-performance-of-large-wind-turbines (visited on 05/08/2024).

[104] S. Larwood and M. Zuteck. “Swept Wind Turbine Blade Aeroelastic Modeling for Loads and Dynamic Behavior”. In: *University of the Pacific - Scholarly Commons* (2006).

[105] D. R. S. Verelst and T. J. Larsen. “Load Consequences when Sweeping Blades - A Case Study of a 5 MW Pitch Controlled Wind Turbine”. In: *Risø-R-1724* (2010).

[106] Christian Pavese. "Passive Loads Control in the Preliminary and Conceptual Design of Wind Turbine Blades". In: *DTU Wind Energy* (2017).

[107] J. B. de Vaal, T. A. Nygaard, and R. Stenbro. "Developing a passive load reduction blade for the DTU 10MW reference turbine". In: *Journal of Physics: Conference Series* 753 (2016).

[108] K. Skelton. "Discussion paper on managing composite blade waste". In: *WindEurope* (2017).

[109] JEC. *HOW IT'S MADE – From bottle to blade*. URL: https://www.jeccomposites.com/news/spotted-by-jec/how-its-made-from-bottle-to-blade/?news_type=business,process-manufacturing,product-technology&end_use_application=renewable-energy (visited on 05/08/2024).

[110] J. M. Gere and B. J. Goodno. *Mechanics of Materials*. Cengage Learning, 2012.

[111] W. S. Chan and K. A. Syed. "Determination of Centroid and Shear Center Locations of Composite Box Beams". In: *International Conference on Composite Materials* (2008).

[112] T. T. C. Ting. *Anisotropic Elasticity: Theory and Applications*. Oxford University Press, 1996.

[113] NitPro Composites. *Introduction to Isotropy, Quasi-Isotropy and Anisotropy*. URL: https://www.nitprocomposites.com/blog/introduction-to-isotropy-quasi-isotropy-and-anisotropy#:~:text=Anisotropy%20is%20common%20in%20composite,specific%20direction%20will%20exhibit%20anisotropy (visited on 06/08/2024).

[114] W. Yu. "VABS Manual for Users". In: *AnalySwift* (2013).

[115] DTU Wind Energy. *Beam Cross section Analysis Software*. URL: https://becas.dtu.dk/ (visited on 06/08/2024).

[116] R. M. Jones. *Mechanics of Composite Materials*. Taylor & Francis, 1998.

[117] S. E. Rohde et al. "Experimental Testing of Bend-Twist Coupled Composite Shafts". In: *Experimental Mechanics* 55 (2015), pp. 1613–1625.

[118] C. H. Yoo and S. C. Lee. *Stability of Structures: Principles and Applications*. Elsevier Inc., 2011.

[119] W. Yu et al. "Validation of the Variational Asymptotic Beam Sectional Analysis (VABS)". In: *American Institute of Aeronautics and Astronautics Journal* (2002).

[120] D. Hodges. *Nonlinear Composite Beam Theory for Engineers*. American Institute of Aeronautics and Astronautics, 2006.

[121] V. Karadag. "Dynamic analysis of practical blades with shear center effect". In: *Journal of Sound and Vibration* 92.4 (1984), pp. 471–490.

A
Appendix

Table A.1: Load Case Table for the Model Verification Process.

Turbulence Intensity [-]	**Mean Wind Speed [m/s]**	**Yaw Misalignment [°]**	**Turbulence Seeds**
Confidential	4	-10	1
Confidential	4	-10	2
Confidential	4	0	3
Confidential	4	0	4
Confidential	4	10	5
Confidential	4	10	6
Confidential	6	-10	1
Confidential	6	-10	2
Confidential	6	0	3
Confidential	6	0	4
Confidential	6	10	5
Confidential	6	10	6
Confidential	8	-10	1
Confidential	8	-10	2
Confidential	8	0	3
Confidential	8	0	4
Confidential	8	10	5
Confidential	8	10	6
Confidential	10	-10	1
Confidential	10	-10	2
Confidential	10	0	3
Confidential	10	0	4
Confidential	10	10	5
Confidential	10	10	6
Confidential	12	-10	1
Confidential	12	-10	2
Confidential	12	0	3
Confidential	12	0	4
Confidential	12	10	5
Confidential	12	10	6
Confidential	14	-10	1
Confidential	14	-10	2
Confidential	14	0	3
Confidential	14	0	4
Confidential	14	10	5
Confidential	14	10	6
Confidential	16	-10	1
Confidential	16	-10	2
Confidential	16	0	3
Confidential	16	0	4
Confidential	16	10	5
Confidential	16	10	6
Confidential	18	-10	1
Confidential	18	-10	2
Confidential	18	0	3

Table A.1: Load Case Table for the Model Verification Process (continued).

Turbulence Intensity [-]	**Mean Wind Speed [m/s]**	**Yaw Misalignment [°]**	**Turbulence Seeds**
Confidential	18	0	4
Confidential	18	10	5
Confidential	18	10	6
Confidential	20	-10	1
Confidential	20	-10	2
Confidential	20	0	3
Confidential	20	0	4
Confidential	20	10	5
Confidential	20	10	6
Confidential	22	-10	1
Confidential	22	-10	2
Confidential	22	0	3
Confidential	22	0	4
Confidential	22	10	5
Confidential	22	10	6
Confidential	24	-10	1
Confidential	24	-10	2
Confidential	24	0	3
Confidential	24	0	4
Confidential	24	10	5
Confidential	24	10	6

B
Appendix

B.1. Convergence Study Results

B.1.1. Load Components at the Blade Root

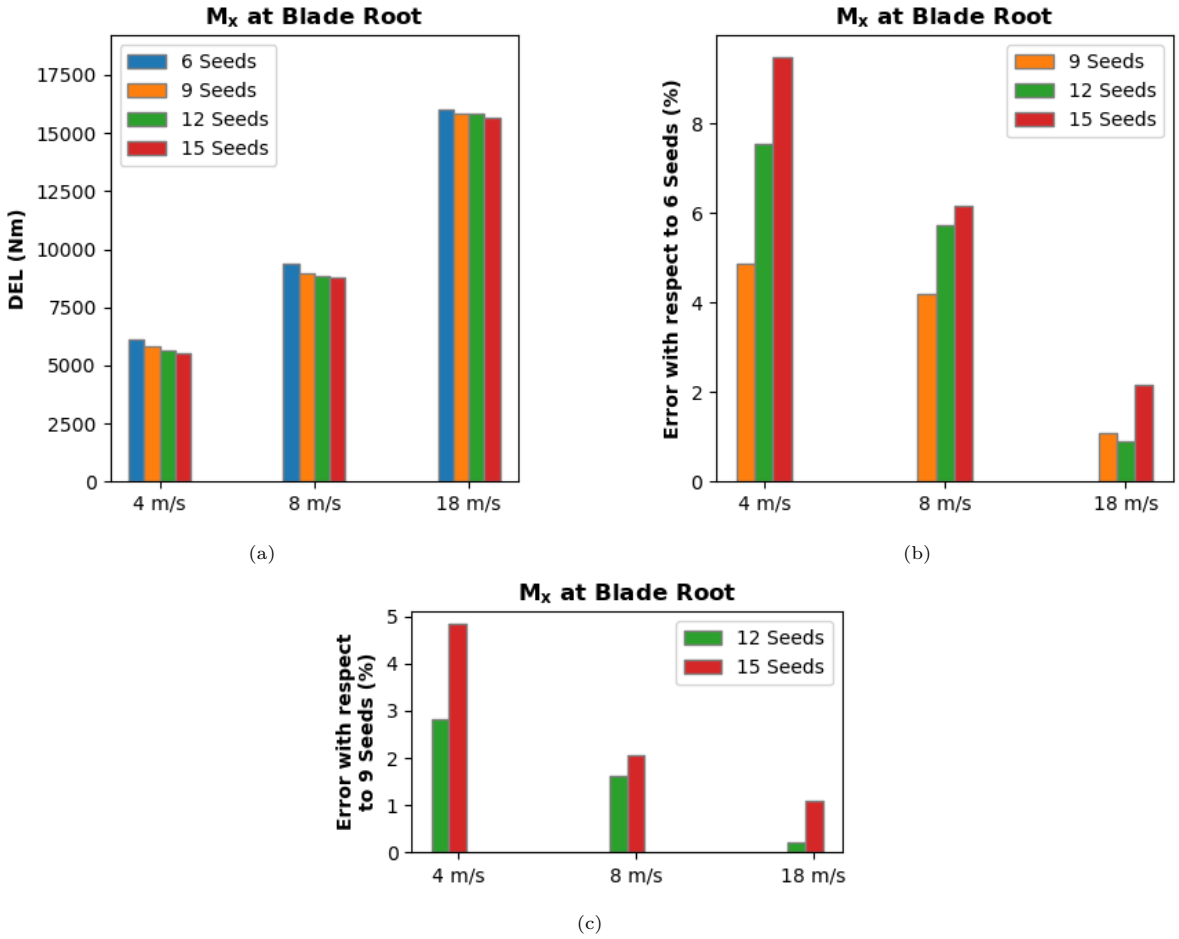

Figure B.1: Convergence study for flapwise moment, M_x, at the blade root.

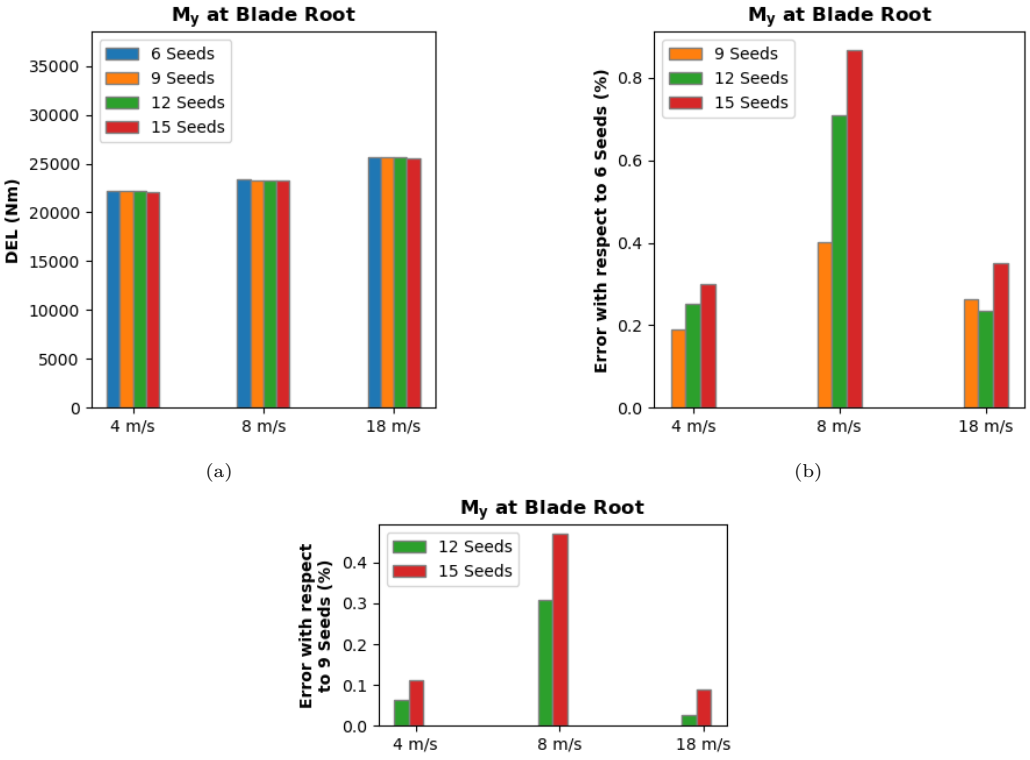

Figure B.2: Convergence study for edgewise moment, M_y, at the blade root.

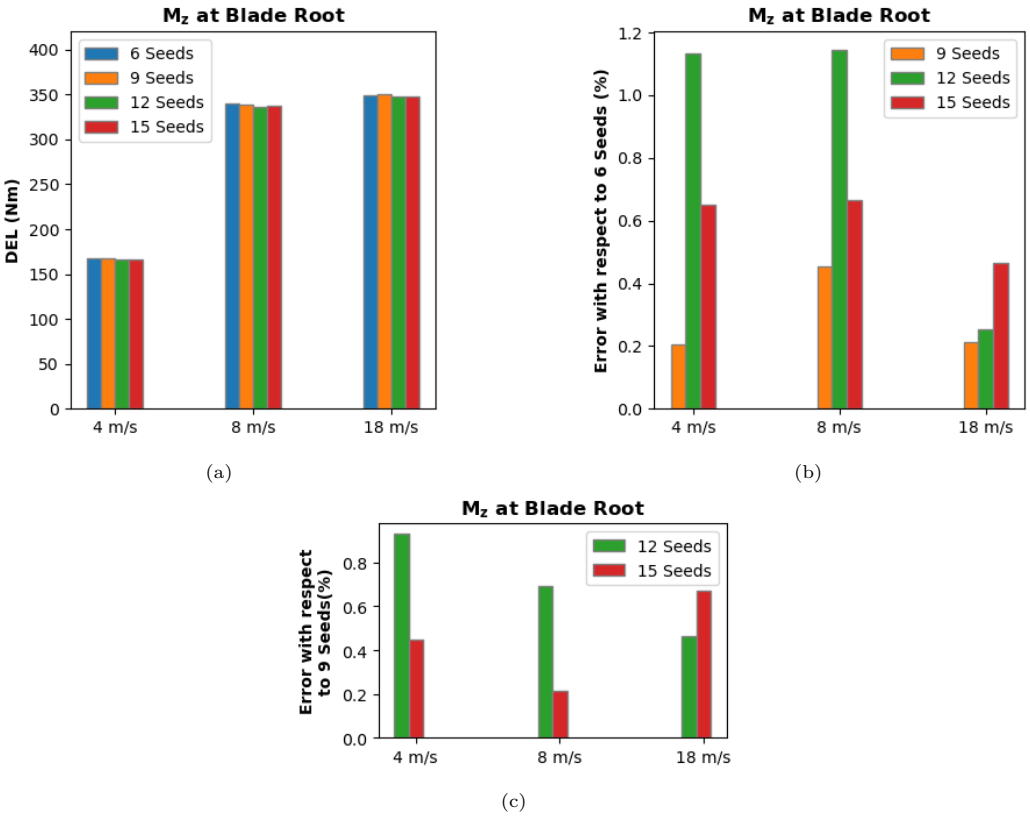

Figure B.3: Convergence study for torsional moment, M_z, at the blade root.

B.1.2. Load Components at the Tower-Top

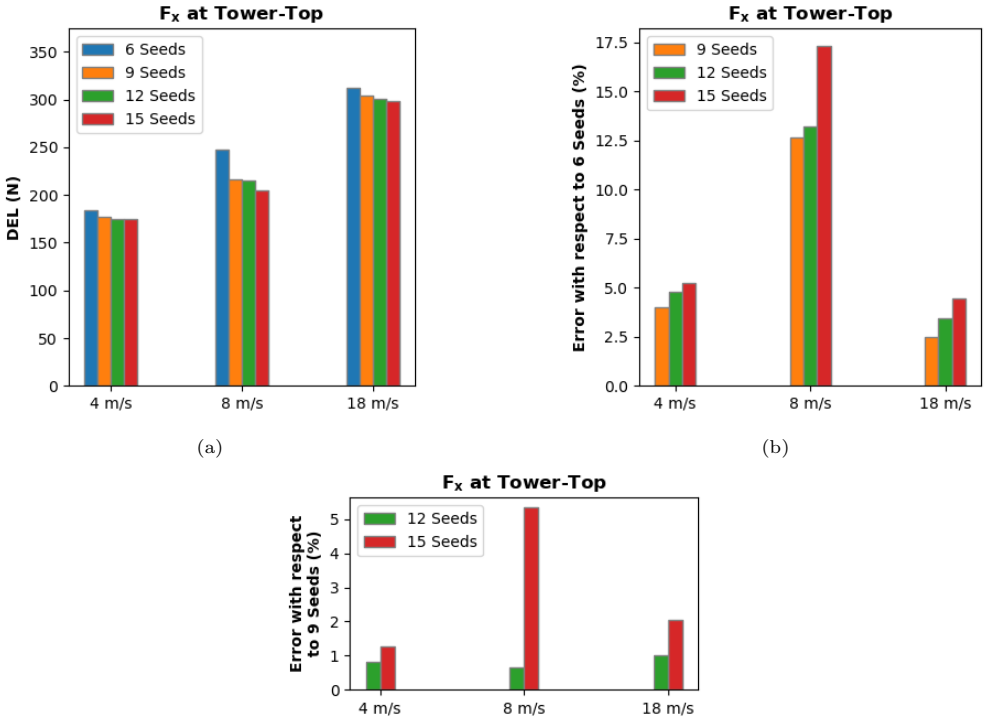

Figure B.4: Convergence study for side-side force, F_x, at the tower-top.

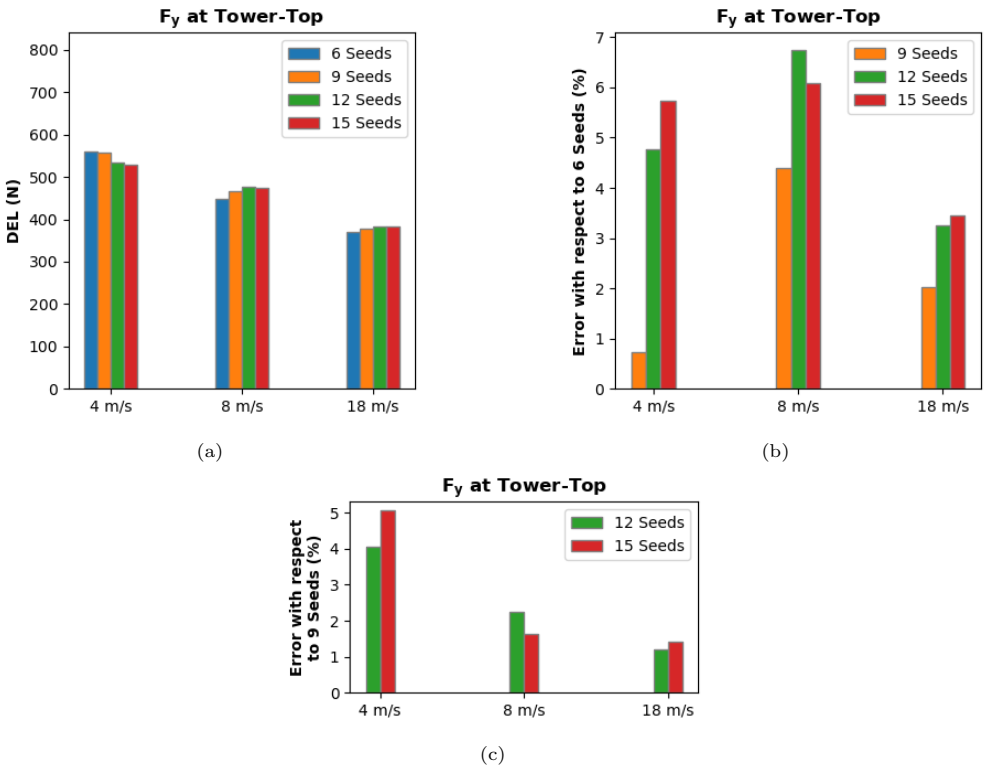

Figure B.5: Convergence study for fore-aft force, F_y, at the tower-top.

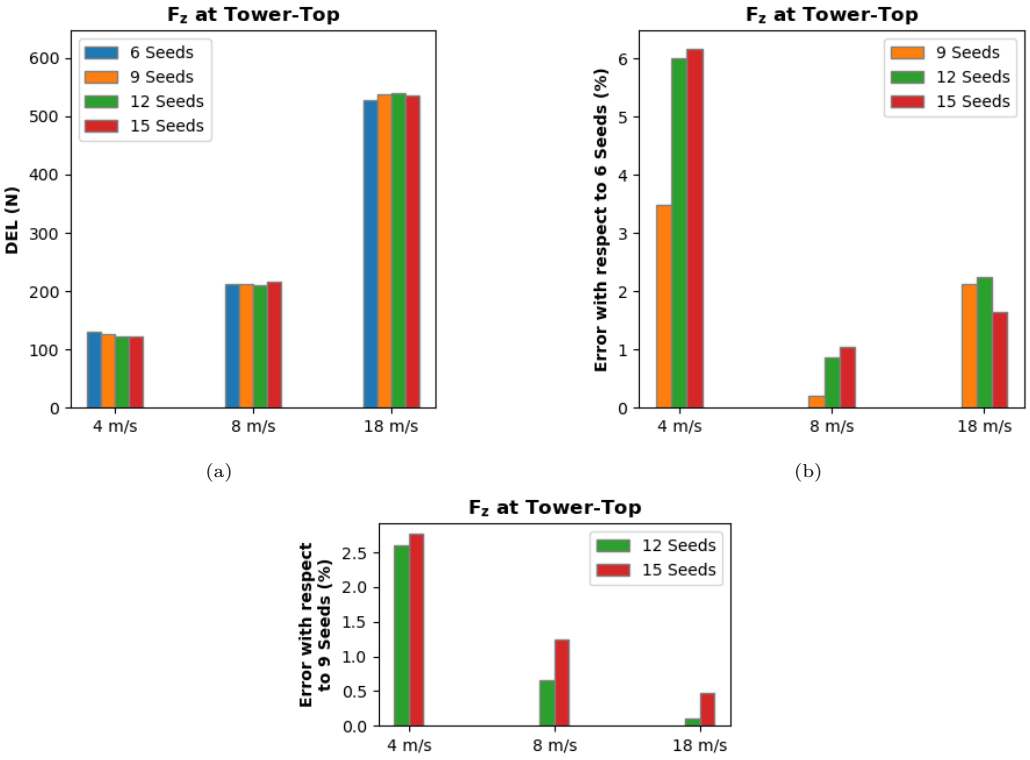

Figure B.6: Convergence study for axial force, F_z, at the tower-top.

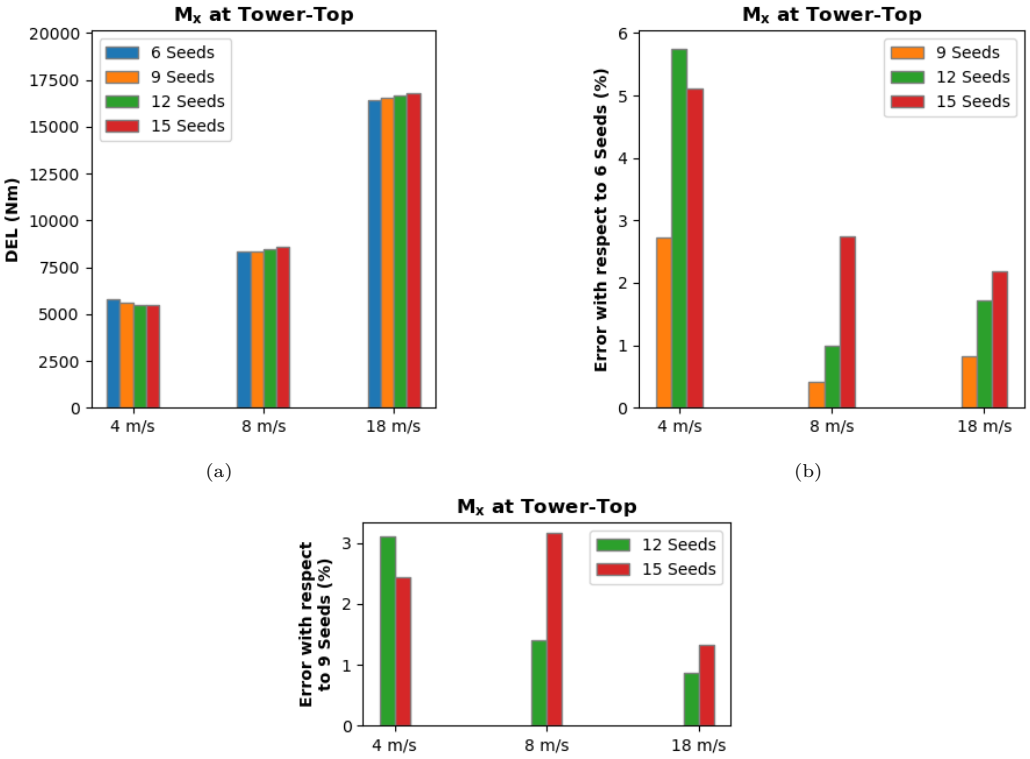

Figure B.7: Convergence study for fore-aft moment, M_x, at the tower-top.

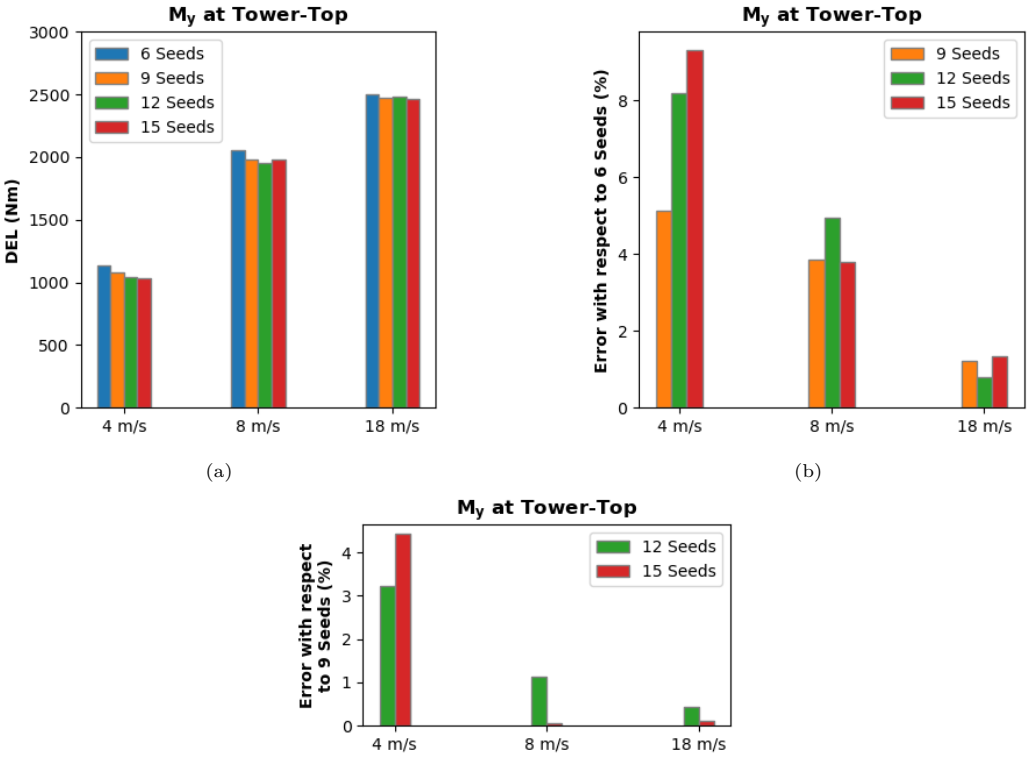

(a) (b)

(c)

Figure B.8: Convergence study for side-side moment, M_y, at the tower-top.

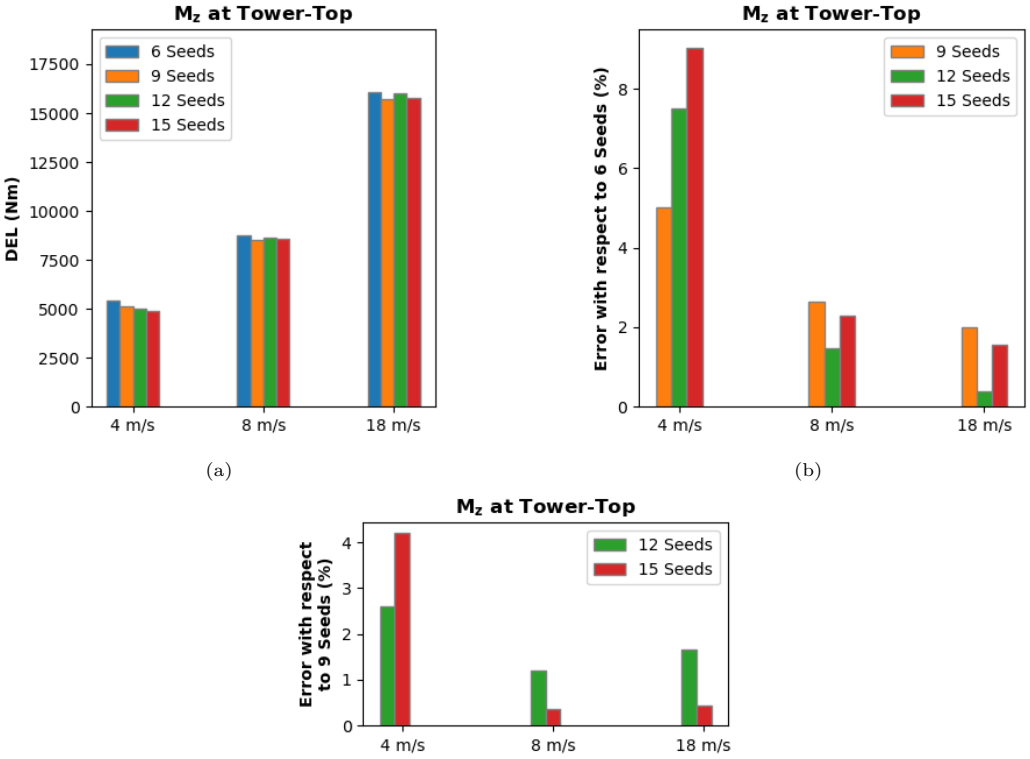

(a) (b)

(c)

Figure B.9: Convergence study for torsional moment, M_z, at the tower-top.

B.1.3. Load Components at the Tower-Bottom

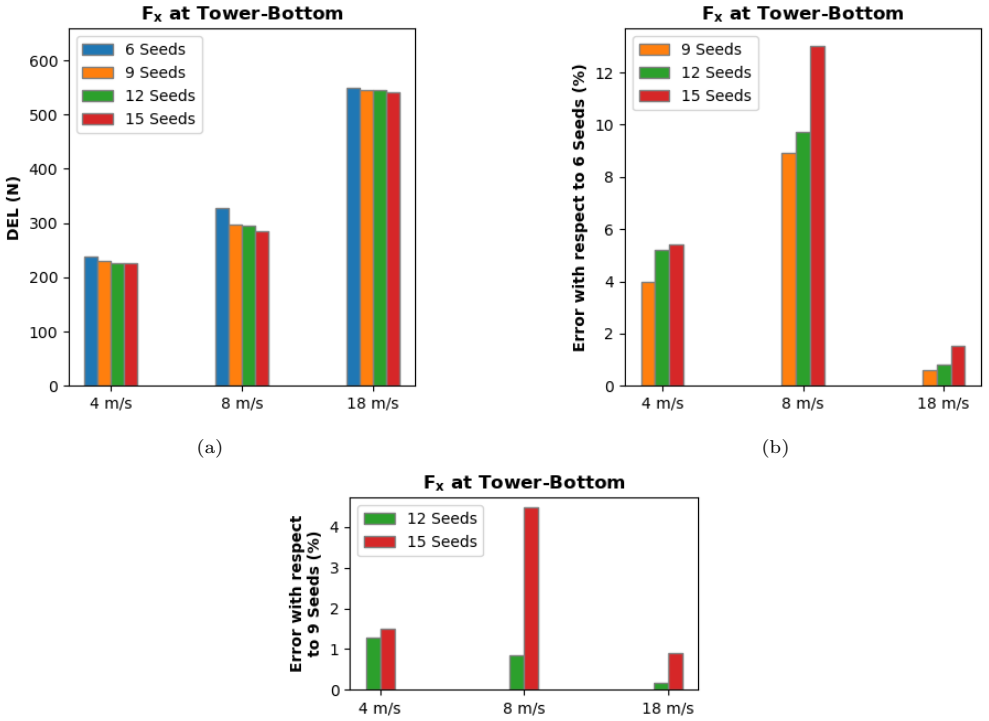

Figure B.10: Convergence study for side-side force, F_x, at the tower-bottom.

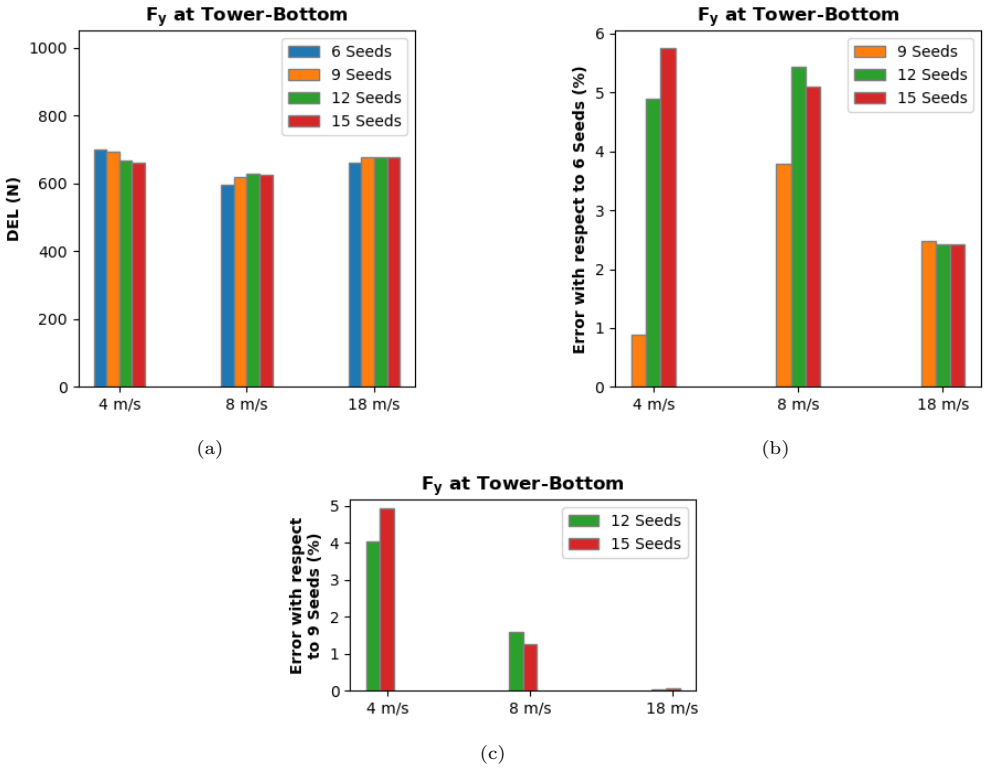

Figure B.11: Convergence study for fore-aft force, F_y, at the tower-bottom.

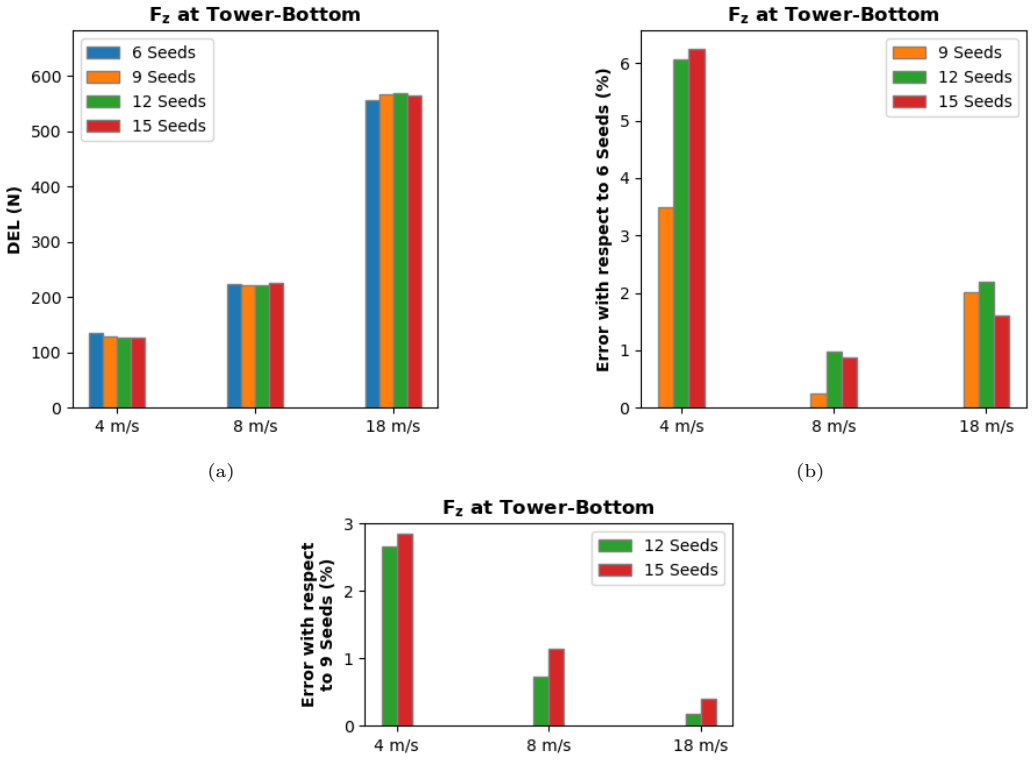

Figure B.12: Convergence study for axial force, F_z, at the tower-bottom.

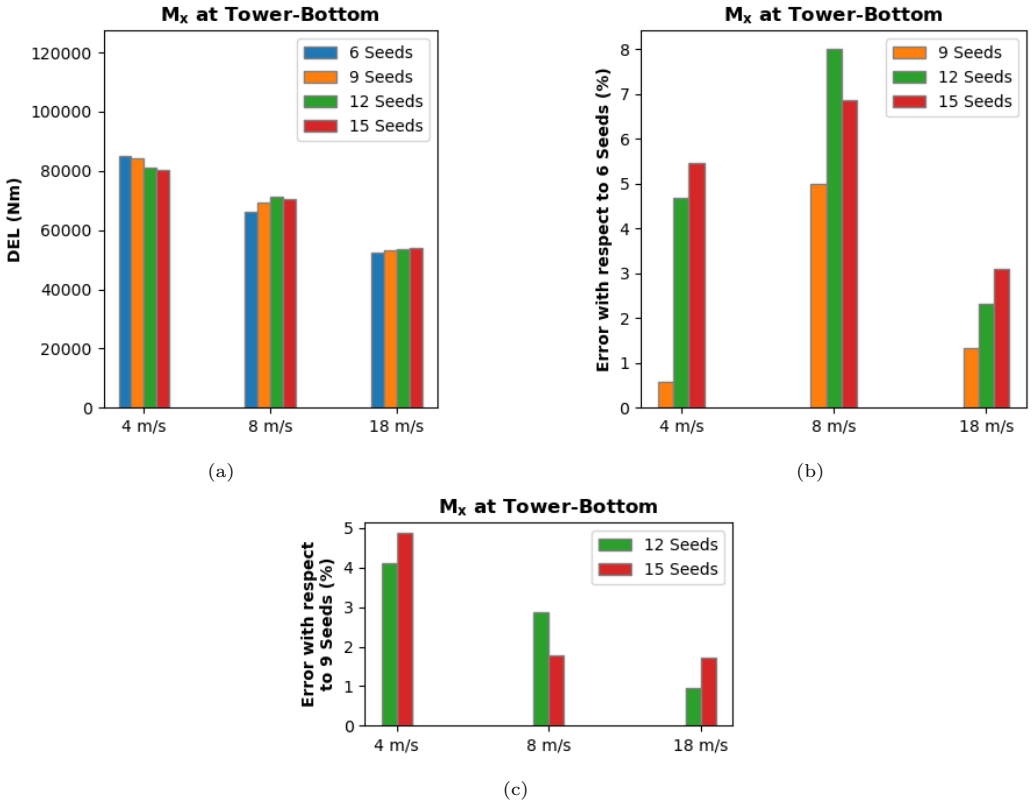

Figure B.13: Convergence study for fore-aft moment, M_x, at the tower-bottom.

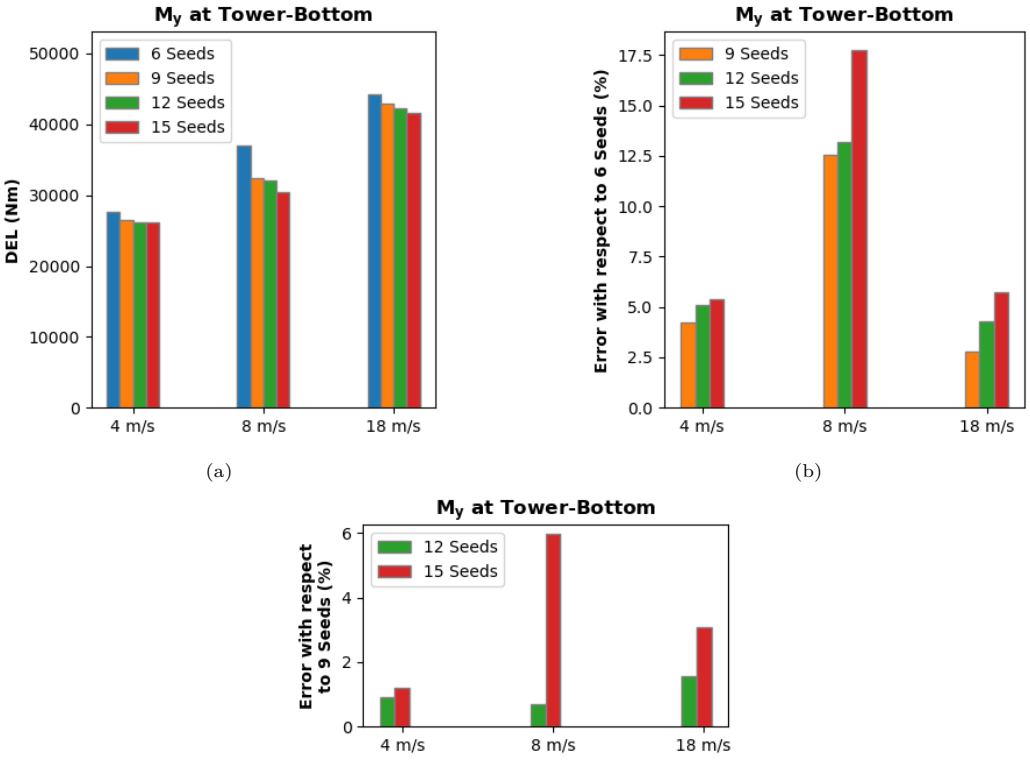

(a) (b)

(c)

Figure B.14: Convergence study for side-side moment, M_y, at the tower-bottom.

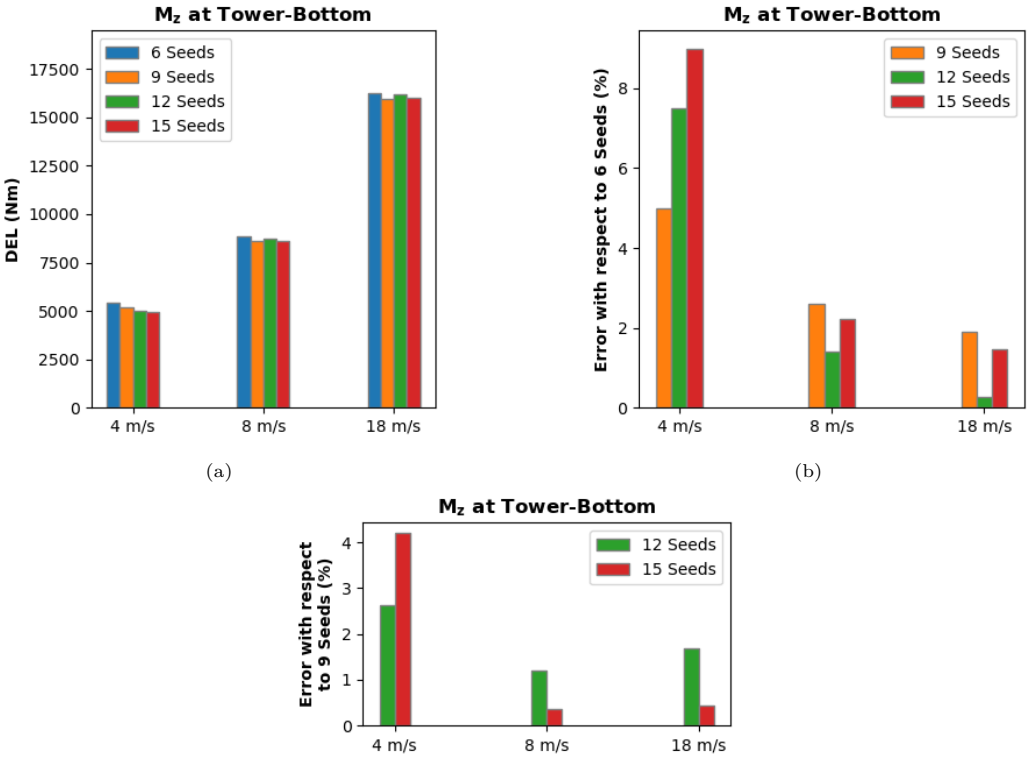

(a) (b)

(c)

Figure B.15: Convergence study for torsional moment, M_z, at the tower-bottom.

C
Appendix

Table C.1: Load Case Table for the Sensitivity Analysis.

Turbulence Intensity [-]	**Mean Wind Speed [m/s]**	**Yaw Misalignment [°]**	**Turbulence Seeds**
Confidential	4	-10	1
Confidential	4	-10	2
Confidential	4	-10	3
Confidential	4	0	4
Confidential	4	0	5
Confidential	4	0	6
Confidential	4	10	7
Confidential	4	10	8
Confidential	4	10	9
Confidential	8	-10	1
Confidential	8	-10	2
Confidential	8	-10	3
Confidential	8	0	4
Confidential	8	0	5
Confidential	8	0	6
Confidential	8	10	7
Confidential	8	10	8
Confidential	8	10	9
Confidential	18	-10	1
Confidential	18	-10	2
Confidential	18	-10	3
Confidential	18	0	4
Confidential	18	0	5
Confidential	18	0	6
Confidential	18	10	7
Confidential	18	10	8
Confidential	18	10	9

D
Appendix

Table D.1: Average power production (kW) per wind speed.

Wind Speed	Original Case	Flapwise Stiffness decreased by 40%	Difference (%)	Flapwise Stiffness increased by 40%	Difference (%)
4 m/s	802.849	797.120	- 0.713	806.090	+ 0.404
8 m/s	6872.252	6838.137	- 0.496	6872.752	+ 0.007
18 m/s	15555.951	15561.363	+ 0.035	15553.633	- 0.015

Wind Speed	Original Case	Edgewise Stiffness decreased by 40%	Difference (%)	Edgewise Stiffness increased by 40%	Difference (%)
4 m/s	802.849	803.235	+ 0.048	803.349	+ 0.062
8 m/s	6872.252	6895.718	+ 0.341	6862.238	- 0.146
18 m/s	15555.951	15554.484	- 0.009	15556.559	+ 0.004

Wind Speed	Original Case	Torsional Stiffness decreased by 8%	Difference (%)	Torsional Stiffness increased by 8%	Difference (%)
4 m/s	802.849	801.430	- 0.177	803.231	+ 0.048
8 m/s	6872.252	6832.376	- 0.580	6907.144	+ 0.508
18 m/s	15555.951	15555.106	-0.005	15556.603	+ 0.004

Wind Speed	Original Case	Shear Centre (X Coo.) decreased by 10%	Difference (%)	Shear Centre (X Coo.) increased by 10%	Difference (%)
4 m/s	802.849	802.810	- 0.005	799.667	- 0.396
8 m/s	6872.252	6987.930	+ 1.683	6747.651	- 1.813
18 m/s	15555.951	15557.667	+ 0.011	15555.288	- 0.004

Wind Speed	Original Case	Edgewise Swept decreased by 10%	Difference (%)	Edgewise Swept increased by 10%	Difference (%)
4 m/s	802.849	803.576	+ 0.091	803.121	+ 0.034
8 m/s	6872.252	6857.262	- 0.218	6886.109	+ 0.202
18 m/s	15555.951	15554.438	- 0.010	15557.400	+ 0.009

E
Appendix

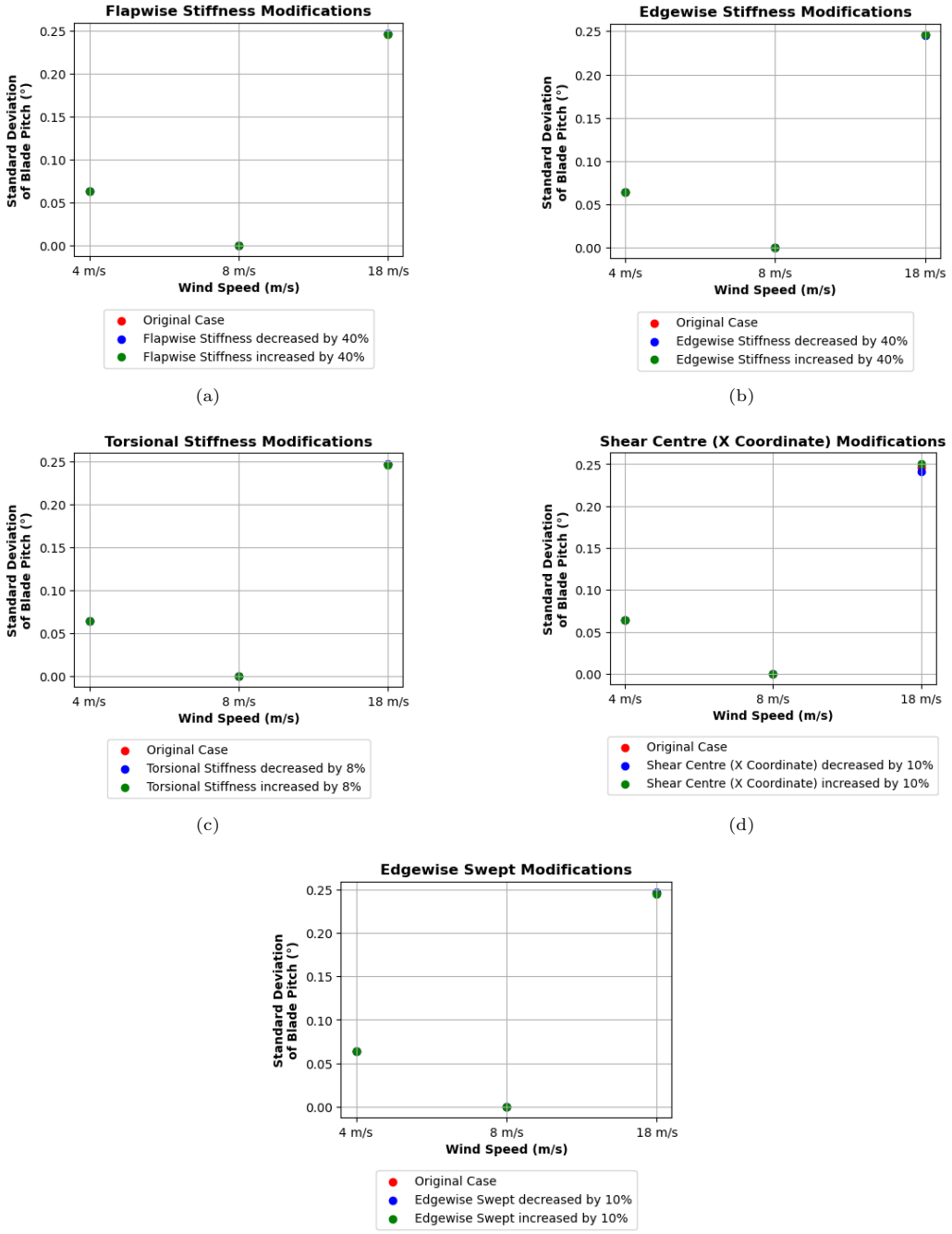

Figure E.1: Standard deviation of blade pitch for the original IEA 15 MW RWT blade compared to modified cases.

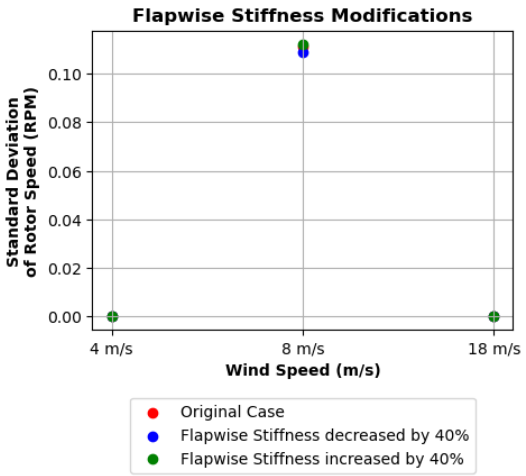

(a)

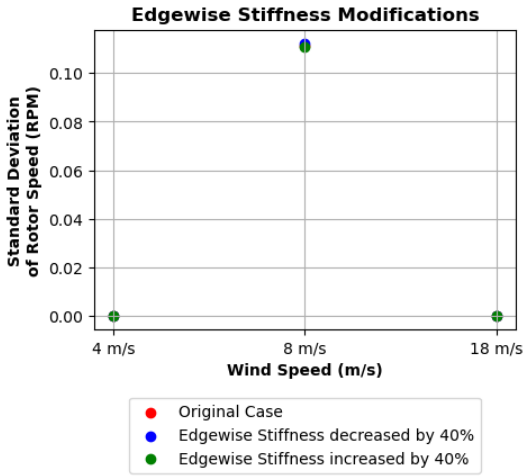

(b)

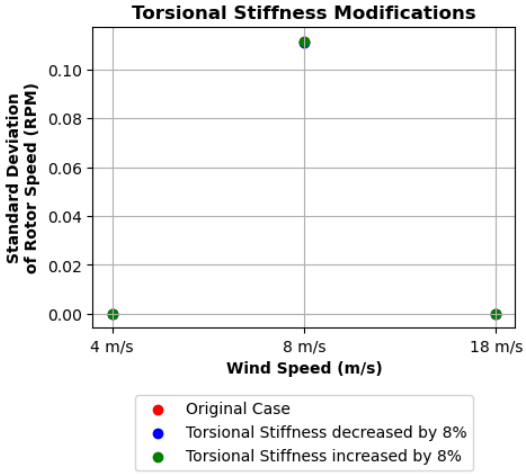

(c)

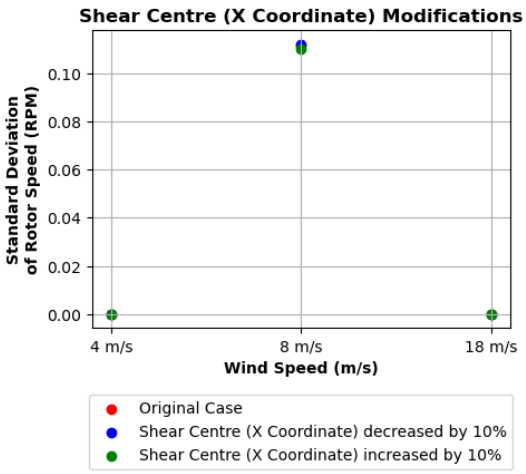

(d)

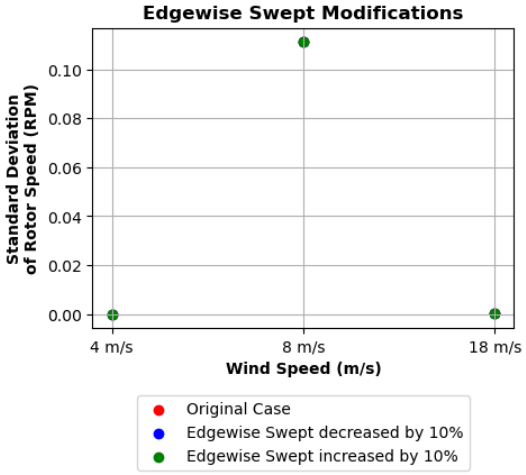

(e)

Figure E.2: Standard deviation of rotor speed for the original IEA 15 MW RWT blade compared to modified cases.

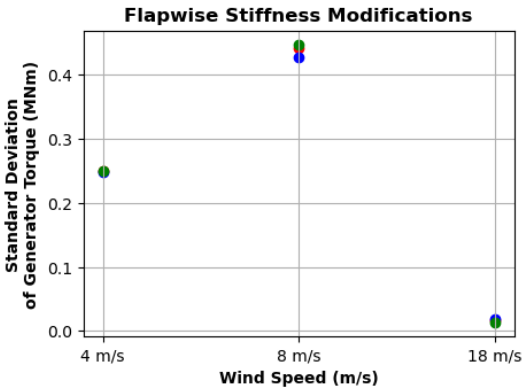

(a)

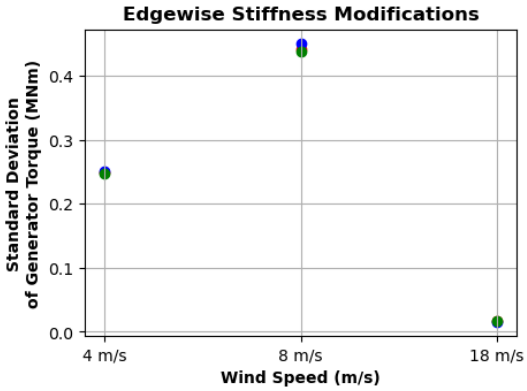

(b)

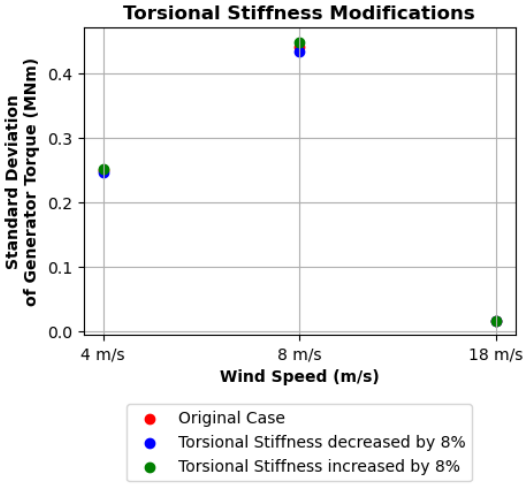

(c)

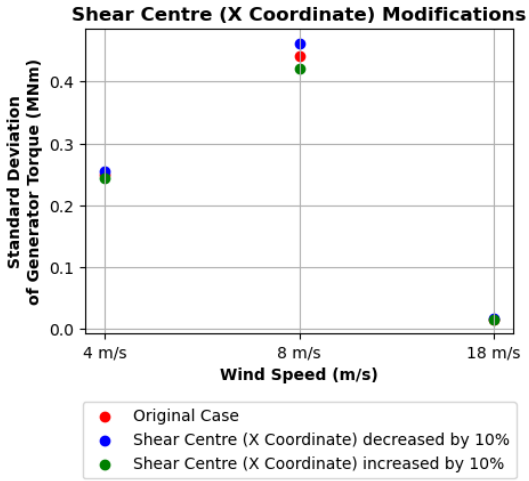

(d)

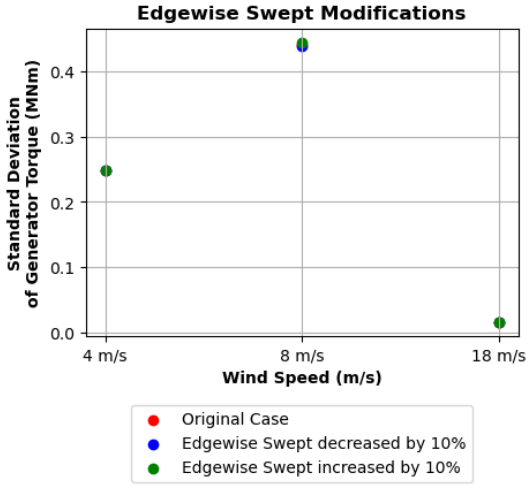

(e)

Figure E.3: Standard deviation of generator torque for the original IEA 15 MW RWT blade compared to modified cases.

F
Appendix

F.1. Controller Tuning Parameters

F.1.1. Description

Table F.1: Controller tuning parameters of the Basic DTU Wind Energy controller. (Adapted from [73])

HAWC2	Variable	Units	Description
`constant 11`	`K`	$kNm/(rad/s)^2$	Optimal C_P tracking K factor
`constant 12`	`Kp`	$Nm/(rad/s)$	Proportional gain of torque controller
`constant 13`	`Ki`	Nm/rad	Integral gain of torque controller
`constant 16`	`Kp`	$rad/(rad/s)$	Proportional gain of pitch controller
`constant 17`	`Ki`	rad/rad	Integral gain of pitch controller
`constant 21`	`K1`	deg	Coefficient of linear term in aerodynamic gain scheduling
`constant 22`	`K2`	deg^2	Coefficient of quadratic term in aerodynamic gain scheduling

F.1.2. Static Calibration for Controller Design

F.1.2.1. Results for Flapwise Bending Stiffness Modifications

Table F.2: Controller Tuning Parameters for the Sensitivity Analysis: Flapwise Bending Stiffness Modifications - Part 1.

Case	Constant 11	Constant 12	Constant 13
IEA 15 MW RWT decreased by 40%	0.294497E+08	0.150563E+09	0.337863E+08
IEA 15 MW RWT decreased by 32%	0.296381E+08	0.150686E+09	0.338139E+08
IEA 15 MW RWT decreased by 30%	0.296745E+08	0.150709E+09	0.338189E+08
IEA 15 MW RWT decreased by 22%	0.297894E+08	0.150776E+09	0.338341E+08
IEA 15 MW RWT decreased by 20%	0.298119E+08	0.150788E+09	0.338368E+08
IEA 15 MW RWT decreased by 12%	0.298834E+08	0.150824E+09	0.338448E+08
IEA 15 MW RWT decreased by 10%	0.298974E+08	0.150830E+09	0.338462E+08
IEA 15 MW RWT decreased by 2%	0.299418E+08	0.150847E+09	0.338500E+08
IEA 15 MW RWT	0.299504E+08	0.150851E+09	0.338509E+08
IEA 15 MW RWT increased by 8%	0.299775E+08	0.150855E+09	0.338518E+08
IEA 15 MW RWT increased by 10%	0.299827E+08	0.150855E+09	0.338519E+08
IEA 15 MW RWT increased by 18%	0.299984E+08	0.150854E+09	0.338516E+08
IEA 15 MW RWT increased by 20%	0.300013E+08	0.150853E+09	0.338514E+08
IEA 15 MW RWT increased by 28%	0.300094E+08	0.150847E+09	0.338501E+08
IEA 15 MW RWT increased by 30%	0.300107E+08	0.150846E+09	0.338497E+08
IEA 15 MW RWT increased by 38%	0.300137E+08	0.150837E+09	0.338479E+08
IEA 15 MW RWT increased by 40%	0.300138E+08	0.150835E+09	0.338473E+08
IEA 15 MW RWT increased by 48%	0.300134E+08	0.150826E+09	0.338452E+08

Table F.3: Controller Tuning Parameters for the Sensitivity Analysis: Flapwise Bending Stiffness Modifications - Part 2.

Case	Constant 16	Constant 17	Constant 21	Constant 22
IEA 15 MW RWT decreased by 40%	0.874553E+00	0.920179E-01	10.06951	1006.43510
IEA 15 MW RWT decreased by 32%	0.851126E+00	0.894943E-01	10.93111	852.79842
IEA 15 MW RWT decreased by 30%	0.847947E+00	0.891870E-01	11.05334	834.22796
IEA 15 MW RWT decreased by 22%	0.837716E+00	0.882034E-01	11.47618	776.12433
IEA 15 MW RWT decreased by 20%	0.835655E+00	0.880064E-01	11.56721	764.72805
IEA 15 MW RWT decreased by 12%	0.828392E+00	0.873209E-01	11.90059	726.39071
IEA 15 MW RWT decreased by 10%	0.827206E+00	0.872096E-01	11.96069	719.45312
IEA 15 MW RWT decreased by 2%	0.823348E+00	0.868520E-01	12.16580	696.22332
IEA 15 MW RWT	0.822580E+00	0.867822E-01	12.20921	691.34737
IEA 15 MW RWT increased by 8%	0.820025E+00	0.865524E-01	12.35941	674.46468
IEA 15 MW RWT increased by 10%	0.819504E+00	0.865065E-01	12.39171	670.82097
IEA 15 MW RWT increased by 18%	0.817925E+00	0.863730E-01	12.47425	661.65087
IEA 15 MW RWT increased by 20%	0.817565E+00	0.863425E-01	12.49827	658.86479
IEA 15 MW RWT increased by 28%	0.814695E+00	0.860769E-01	12.65810	645.26258
IEA 15 MW RWT increased by 30%	0.814366E+00	0.860491E-01	12.67944	643.02862
IEA 15 MW RWT increased by 38%	0.813287E+00	0.859603E-01	12.75355	635.01229
IEA 15 MW RWT increased by 40%	0.811613E+00	0.857892E-01	12.83777	630.49576
IEA 15 MW RWT increased by 48%	0.810937E+00	0.857395E-01	12.89188	624.16146

F.1.2.2. Results for Edgewise Bending Stiffness Modifications

Table F.4: Controller Tuning Parameters for the Sensitivity Analysis: Edgewise Bending Stiffness Modifications - Part 1.

Case	Constant 11	Constant 12	Constant 13
IEA 15 MW RWT decreased by 40%	0.302032E+08	0.150855E+09	0.338517E+08
IEA 15 MW RWT decreased by 32%	0.301267E+08	0.150853E+09	0.338514E+08
IEA 15 MW RWT decreased by 30%	0.301015E+08	0.150853E+09	0.338514E+08
IEA 15 MW RWT decreased by 22%	0.300549E+08	0.150852E+09	0.338511E+08
IEA 15 MW RWT decreased by 20%	0.300428E+08	0.150852E+09	0.338510E+08
IEA 15 MW RWT decreased by 12%	0.300005E+08	0.150851E+09	0.338508E+08
IEA 15 MW RWT decreased by 10%	0.299912E+08	0.150850E+09	0.338508E+08
IEA 15 MW RWT decreased by 2%	0.299579E+08	0.150850E+09	0.338506E+08
IEA 15 MW RWT	0.299504E+08	0.150851E+09	0.338509E+08
IEA 15 MW RWT increased by 8%	0.299235E+08	0.150849E+09	0.338504E+08
IEA 15 MW RWT increased by 10%	0.299174E+08	0.150849E+09	0.338503E+08
IEA 15 MW RWT increased by 18%	0.298952E+08	0.150848E+09	0.338502E+08
IEA 15 MW RWT increased by 20%	0.298901E+08	0.150849E+09	0.338502E+08
IEA 15 MW RWT increased by 28%	0.298715E+08	0.150847E+09	0.338501E+08
IEA 15 MW RWT increased by 30%	0.298672E+08	0.150847E+09	0.338500E+08
IEA 15 MW RWT increased by 38%	0.298513E+08	0.150847E+09	0.338499E+08
IEA 15 MW RWT increased by 40%	0.298477E+08	0.150847E+09	0.338499E+08
IEA 15 MW RWT increased by 48%	0.298340E+08	0.150846E+09	0.338498E+08

Table F.5: Controller Tuning Parameters for the Sensitivity Analysis: Edgewise Bending Stiffness Modifications - Part 2.

Case	Constant 16	Constant 17	Constant 21	Constant 22
IEA 15 MW RWT decreased by 40%	0.828343E+00	0.874165E-01	11.92419	711.19988
IEA 15 MW RWT decreased by 32%	0.826858E+00	0.872521E-01	11.99806	705.65843
IEA 15 MW RWT decreased by 30%	0.826523E+00	0.872151E-01	12.01463	704.46041
IEA 15 MW RWT decreased by 22%	0.825373E+00	0.870879E-01	12.07192	700.37595
IEA 15 MW RWT decreased by 20%	0.824508E+00	0.869954E-01	12.11202	697.73087
IEA 15 MW RWT decreased by 12%	0.823603E+00	0.868954E-01	12.15724	694.71794
IEA 15 MW RWT decreased by 10%	0.823400E+00	0.868730E-01	12.16731	694.07034
IEA 15 MW RWT decreased by 2%	0.822710E+00	0.867966E-01	12.20213	691.81141
IEA 15 MW RWT	0.822580E+00	0.867822E-01	12.20921	691.34737
IEA 15 MW RWT increased by 8%	0.822060E+00	0.867242E-01	12.23562	689.63904
IEA 15 MW RWT increased by 10%	0.821940E+00	0.867109E-01	12.24178	689.24327
IEA 15 MW RWT increased by 18%	0.821489E+00	0.866609E-01	12.26500	687.75605
IEA 15 MW RWT increased by 20%	0.821385E+00	0.866493E-01	12.27038	687.41352
IEA 15 MW RWT increased by 28%	0.820995E+00	0.866060E-01	12.29050	686.14042
IEA 15 MW RWT increased by 30%	0.820907E+00	0.865963E-01	12.29503	685.85787
IEA 15 MW RWT increased by 38%	0.820592E+00	0.865612E-01	12.31139	684.83929
IEA 15 MW RWT increased by 40%	0.820515E+00	0.865528E-01	12.31533	684.59559
IEA 15 MW RWT increased by 48%	0.820230E+00	0.865211E-01	12.33012	683.67859

F.1.2.3. Results for Torsional Stiffness Modifications

Table F.6: Controller Tuning Parameters for the Risk Indicator Task: Increase in Torsional Stiffness - Part 1.

Case	Constant 11	Constant 12	Constant 13
IEA 15 MW RWT	0.299504E+08	0.150851E+09	0.338509E+08
IEA 15 MW RWT increased by 10%	0.304436E+08	0.150844E+09	0.338493E+08

Table F.7: Controller Tuning Parameters for the Risk Indicator Task: Increase in Torsional Stiffness - Part 2.

Case	Constant 16	Constant 17	Constant 21	Constant 22
IEA 15 MW RWT	0.822580E+00	0.867822E-01	12.20921	691.34737
IEA 15 MW RWT increased by 10%	0.839197E+00	0.874880E-01	12.09730	675.85425

Table F.8: Controller Tuning Parameters for the Sensitivity Analysis: Torsional Stiffness Modifications - Part 1.

Case	Constant 11	Constant 12	Constant 13
IEA 15 MW RWT decreased by 8%	0.294520E+08	0.150854E+09	0.338515E+08
IEA 15 MW RWT decreased by 6.4%	0.295605E+08	0.150853E+09	0.338513E+08
IEA 15 MW RWT decreased by 6%	0.295868E+08	0.150853E+09	0.338512E+08
IEA 15 MW RWT decreased by 4.4%	0.296896E+08	0.150852E+09	0.338511E+08
IEA 15 MW RWT decreased by 4%	0.297146E+08	0.150852E+09	0.338510E+08
IEA 15 MW RWT decreased by 2.4%	0.298119E+08	0.150851E+09	0.338508E+08
IEA 15 MW RWT decreased by 2%	0.298356E+08	0.150851E+09	0.338508E+08
IEA 15 MW RWT decreased by 0.4%	0.299280E+08	0.150850E+09	0.338506E+08
IEA 15 MW RWT	0.299504E+08	0.150851E+09	0.338509E+08
IEA 15 MW RWT increased by 1.6%	0.300380E+08	0.150849E+09	0.338503E+08
IEA 15 MW RWT increased by 2%	0.300593E+08	0.150848E+09	0.338503E+08
IEA 15 MW RWT increased by 3.6%	0.301424E+08	0.150847E+09	0.338501E+08
IEA 15 MW RWT increased by 4%	0.301626E+08	0.150847E+09	0.338500E+08
IEA 15 MW RWT increased by 5.6%	0.302416E+08	0.150846E+09	0.338498E+08
IEA 15 MW RWT increased by 6%	0.302608E+08	0.150846E+09	0.338498E+08
IEA 15 MW RWT increased by 7.6%	0.303360E+08	0.150845E+09	0.338496E+08
IEA 15 MW RWT increased by 8%	0.303544E+08	0.150845E+09	0.338495E+08
IEA 15 MW RWT increased by 9.6%	0.304261E+08	0.150844E+09	0.338493E+08

Table F.9: Controller Tuning Parameters for the Sensitivity Analysis: Torsional Stiffness Modifications - Part 2.

Case	Constant 16	Constant 17	Constant 21	Constant 22
IEA 15 MW RWT decreased by 8%	0.801852E+00	0.854848E-01	12.56735	694.50854
IEA 15 MW RWT decreased by 6.4%	0.805499E+00	0.856836E-01	12.51649	693.62531
IEA 15 MW RWT decreased by 6%	0.806370E+00	0.857296E-01	12.50706	693.04822
IEA 15 MW RWT decreased by 4.4%	0.811463E+00	0.860474E-01	12.40923	693.33457
IEA 15 MW RWT decreased by 4%	0.812333E+00	0.860982E-01	12.39599	692.94269
IEA 15 MW RWT decreased by 2.4%	0.816334E+00	0.863590E-01	12.31982	693.22216
IEA 15 MW RWT decreased by 2%	0.817288E+00	0.864198E-01	12.30411	692.94857
IEA 15 MW RWT decreased by 0.4%	0.821649E+00	0.867227E-01	12.22848	690.86611
IEA 15 MW RWT	0.822580E+00	0.867822E-01	12.20921	691.34737
IEA 15 MW RWT increased by 1.6%	0.826386E+00	0.870304E-01	12.12777	693.45168
IEA 15 MW RWT increased by 2%	0.827919E+00	0.871541E-01	12.08348	695.20529
IEA 15 MW RWT increased by 3.6%	0.831326E+00	0.873641E-01	12.03186	693.80591
IEA 15 MW RWT increased by 4%	0.832201E+00	0.874195E-01	12.01589	693.90794
IEA 15 MW RWT increased by 5.6%	0.835715E+00	0.876447E-01	11.94990	694.39475
IEA 15 MW RWT increased by 6%	0.835858E+00	0.875716E-01	11.98697	691.11184
IEA 15 MW RWT increased by 7.6%	0.840588E+00	0.879144E-01	11.87863	693.85268
IEA 15 MW RWT increased by 8%	0.841367E+00	0.879582E-01	11.86954	693.39560
IEA 15 MW RWT increased by 9.6%	0.844028E+00	0.880882E-01	11.85328	690.26457

F.1.2.4. Results for Shear Centre (X Coordinate) Modifications

Table F.10: Controller Tuning Parameters for the Sensitivity Analysis: Shear Centre (X Coordinate) Modifications - Part 1.

Case	Constant 11	Constant 12	Constant 13
IEA 15 MW RWT decreased by 10%	0.311797E+08	0.150831E+09	0.338464E+08
IEA 15 MW RWT decreased by 7.9%	0.309292E+08	0.150836E+09	0.338475E+08
IEA 15 MW RWT decreased by 7.5%	0.308809E+08	0.150837E+09	0.338477E+08
IEA 15 MW RWT decreased by 5.5%	0.306370E+08	0.150841E+09	0.338486E+08
IEA 15 MW RWT decreased by 5%	0.305756E+08	0.150842E+09	0.338488E+08
IEA 15 MW RWT decreased by 3%	0.303277E+08	0.150845E+09	0.338496E+08
IEA 15 MW RWT decreased by 2.5%	0.302652E+08	0.150846E+09	0.338498E+08
IEA 15 MW RWT decreased by 0.5%	0.300138E+08	0.150849E+09	0.338504E+08
IEA 15 MW RWT	0.299504E+08	0.150851E+09	0.338509E+08
IEA 15 MW RWT increased by 2%	0.296953E+08	0.150852E+09	0.338511E+08
IEA 15 MW RWT increased by 2.5%	0.296313E+08	0.150852E+09	0.338512E+08
IEA 15 MW RWT increased by 4.5%	0.293749E+08	0.150854E+09	0.338516E+08
IEA 15 MW RWT increased by 5%	0.293106E+08	0.150855E+09	0.338517E+08
IEA 15 MW RWT increased by 7%	0.290523E+08	0.150856E+09	0.338520E+08
IEA 15 MW RWT increased by 7.5%	0.289876E+08	0.150856E+09	0.338521E+08
IEA 15 MW RWT increased by 9.5%	0.287299E+08	0.150857E+09	0.338523E+08
IEA 15 MW RWT increased by 10%	0.286659E+08	0.150857E+09	0.338523E+08
IEA 15 MW RWT increased by 12%	0.284107E+08	0.150858E+09	0.338525E+08

Table F.11: Controller Tuning Parameters for the Sensitivity Analysis: Shear Centre (X Coordinate) Modifications - Part 2.

Case	Constant 16	Constant 17	Constant 21	Constant 22
IEA 15 MW RWT decreased by 10%	0.318558E+00	0.336676E-01	-30.55241	444.03800
IEA 15 MW RWT decreased by 7.9%	0.181121E+01	0.191341E+00	3.39991	1893.48644
IEA 15 MW RWT decreased by 7.5%	0.361118E+00	0.381465E-01	-42.45845	452.68180
IEA 15 MW RWT decreased by 5.5%	0.845075E+00	0.888278E-01	11.51657	721.28979
IEA 15 MW RWT decreased by 5%	0.842861E+00	0.886257E-01	11.58032	718.49370
IEA 15 MW RWT decreased by 3%	0.835350E+00	0.879554E-01	11.79304	710.03911
IEA 15 MW RWT decreased by 2.5%	0.832872E+00	0.877239E-01	11.87183	706.49102
IEA 15 MW RWT decreased by 0.5%	0.824476E+00	0.869539E-01	12.14832	693.56101
IEA 15 MW RWT	0.822580E+00	0.867822E-01	12.20921	691.34737
IEA 15 MW RWT increased by 2%	0.814703E+00	0.860610E-01	12.45169	684.97419
IEA 15 MW RWT increased by 2.5%	0.813138E+00	0.859228E-01	12.49888	683.82914
IEA 15 MW RWT increased by 4.5%	0.806788E+00	0.853578E-01	12.71522	675.96987
IEA 15 MW RWT increased by 5%	0.804663E+00	0.851590E-01	12.79610	672.87264
IEA 15 MW RWT increased by 7%	0.796922E+00	0.844418E-01	13.09060	662.73957
IEA 15 MW RWT increased by 7.5%	0.792153E+00	0.839393E-01	13.33340	652.15242
IEA 15 MW RWT increased by 9.5%	0.543694E+00	0.573620E-01	60.33022	503.02144
IEA 15 MW RWT increased by 10%	0.816548E+00	0.860527E-01	13.13056	598.42073
IEA 15 MW RWT increased by 12%	0.586086E+00	0.617538E-01	39.15003	513.31199

Note: IEA 15 MW RWT decreased by 8% is replaced by IEA 15 MW RWT decreased by 7.9% because the former caused aeroelastic instability problems during the dynamic simulations.

F.1.2.5. Results for Edgewise Swept Modifications

Table F.12: Controller Tuning Parameters for the Sensitivity Analysis: Edgewise Swept Modifications - Part 1.

Case	Constant 11	Constant 12	Constant 13
IEA 15 MW RWT decreased by 10%	0.298071E+08	0.150848E+09	0.338502E+08
IEA 15 MW RWT decreased by 8%	0.298358E+08	0.150848E+09	0.338503E+08
IEA 15 MW RWT decreased by 7.5%	0.298429E+08	0.150849E+09	0.338503E+08
IEA 15 MW RWT decreased by 5.5%	0.298716E+08	0.150849E+09	0.338505E+08
IEA 15 MW RWT decreased by 5%	0.298788E+08	0.150849E+09	0.338505E+08
IEA 15 MW RWT decreased by 3%	0.299075E+08	0.150850E+09	0.338507E+08
IEA 15 MW RWT decreased by 2.5%	0.299146E+08	0.150850E+09	0.338507E+08
IEA 15 MW RWT decreased by 0.5%	0.299433E+08	0.150851E+09	0.338509E+08
IEA 15 MW RWT	0.299504E+08	0.150851E+09	0.338509E+08
IEA 15 MW RWT increased by 2%	0.299790E+08	0.150852E+09	0.338511E+08
IEA 15 MW RWT increased by 2.5%	0.299861E+08	0.150852E+09	0.338511E+08
IEA 15 MW RWT increased by 4.5%	0.300146E+08	0.150853E+09	0.338513E+08
IEA 15 MW RWT increased by 5%	0.300218E+08	0.150853E+09	0.338513E+08
IEA 15 MW RWT increased by 7%	0.300503E+08	0.150854E+09	0.338515E+08
IEA 15 MW RWT increased by 7.5%	0.300574E+08	0.150854E+09	0.338515E+08
IEA 15 MW RWT increased by 9.5%	0.300861E+08	0.150855E+09	0.338517E+08
IEA 15 MW RWT increased by 10%	0.300932E+08	0.150855E+09	0.338518E+08
IEA 15 MW RWT increased by 12%	0.301219E+08	0.150856E+09	0.338520E+08

Table F.13: Controller Tuning Parameters for the Sensitivity Analysis: Edgewise Swept Modifications - Part 2.

Case	Constant 16	Constant 17	Constant 21	Constant 22
IEA 15 MW RWT decreased by 10%	0.818070E+00	0.862991E-01	12.39370	683.21787
IEA 15 MW RWT decreased by 8%	0.819492E+00	0.864505E-01	12.33494	685.77357
IEA 15 MW RWT decreased by 7.5%	0.819699E+00	0.864727E-01	12.32635	686.16423
IEA 15 MW RWT decreased by 5.5%	0.820501E+00	0.865588E-01	12.29318	687.66019
IEA 15 MW RWT decreased by 5%	0.820700E+00	0.865801E-01	12.28497	688.03378
IEA 15 MW RWT decreased by 3%	0.821475E+00	0.866634E-01	12.25334	689.44200
IEA 15 MW RWT decreased by 2.5%	0.821661E+00	0.866834E-01	12.24576	689.78281
IEA 15 MW RWT decreased by 0.5%	0.822400E+00	0.867629E-01	12.21628	691.04926
IEA 15 MW RWT	0.822580E+00	0.867822E-01	12.20921	691.34737
IEA 15 MW RWT increased by 2%	0.823340E+00	0.868641E-01	12.17904	692.65659
IEA 15 MW RWT increased by 2.5%	0.823550E+00	0.868866E-01	12.17070	693.02332
IEA 15 MW RWT increased by 4.5%	0.824358E+00	0.869734E-01	12.13790	694.66095
IEA 15 MW RWT increased by 5%	0.824559E+00	0.869950E-01	12.12965	695.09372
IEA 15 MW RWT increased by 7%	0.825373E+00	0.870826E-01	12.09630	696.86457
IEA 15 MW RWT increased by 7.5%	0.826183E+00	0.871684E-01	12.06103	699.02392
IEA 15 MW RWT increased by 9.5%	0.826951E+00	0.872511E-01	12.03009	700.69555
IEA 15 MW RWT increased by 10%	0.827140E+00	0.872715E-01	12.02247	701.11494
IEA 15 MW RWT increased by 12%	0.827878E+00	0.873510E-01	11.99302	702.72503

G
Appendix

G.1. Sensitivity Analysis Results

G.1.1. Load Components at the Blade Root

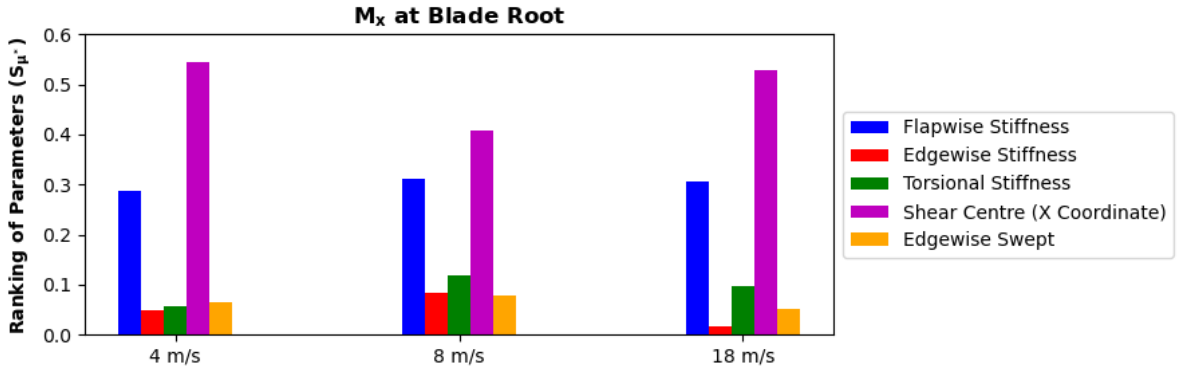

(a)

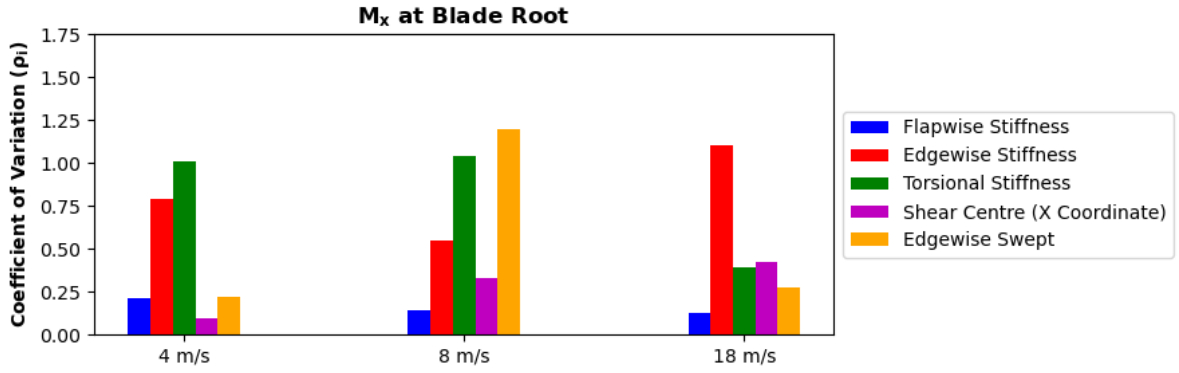

(b)

Figure G.1: (a) Ranking of parameters and (b) COV for flapwise moment, M_x, at the blade root.

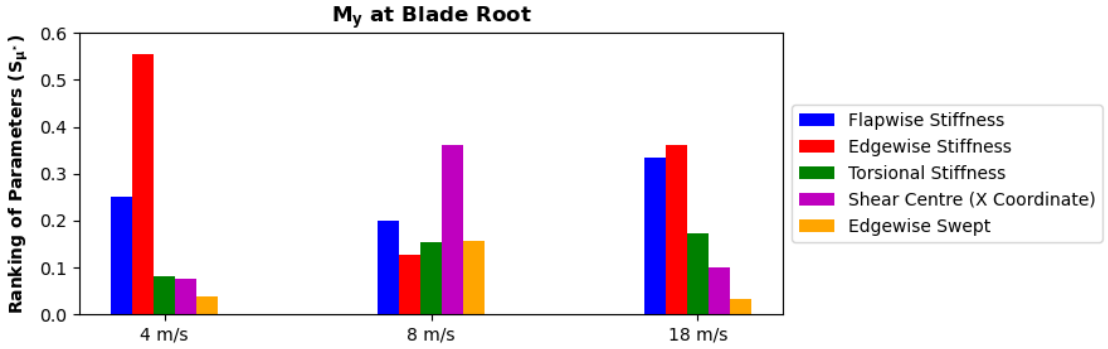

(a)

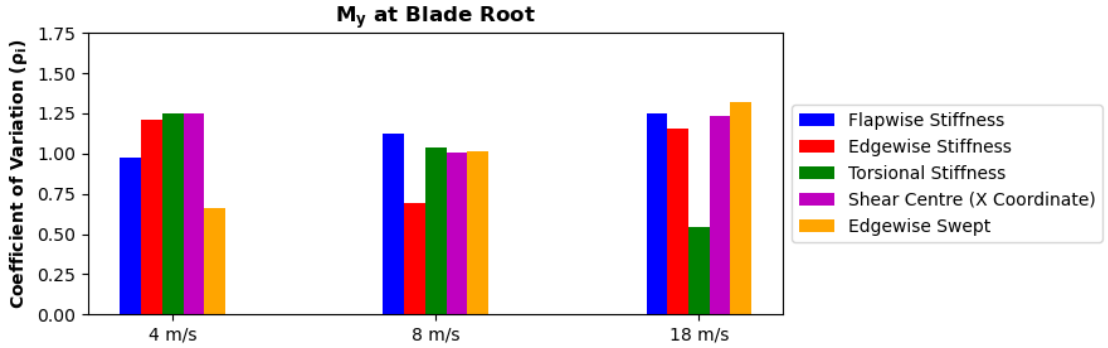

(b)

Figure G.2: (a) Ranking of parameters and (b) COV for edgewise moment, M_y, at the blade root.

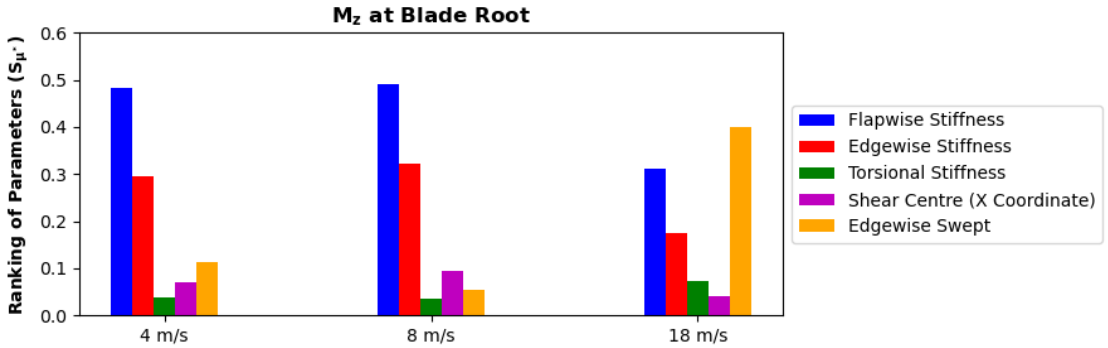

(a)

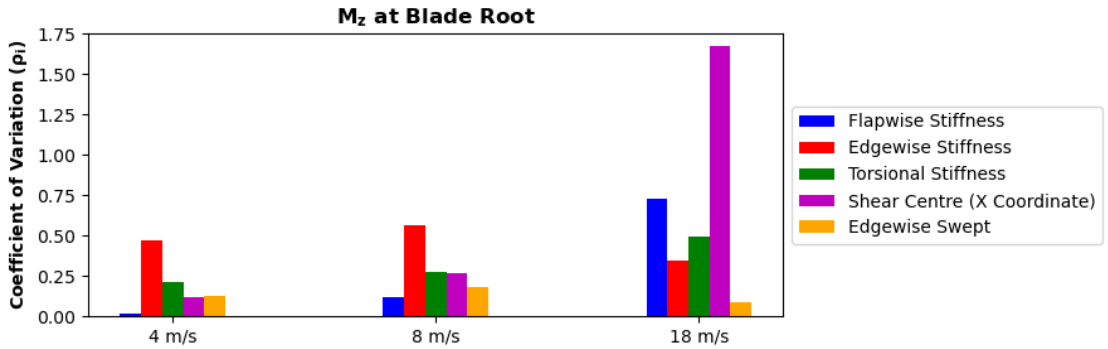

(b)

Figure G.3: (a) Ranking of parameters and (b) COV for torsional moment, M_z, at the blade root.

G.1.2. Load Components at the Tower-Top

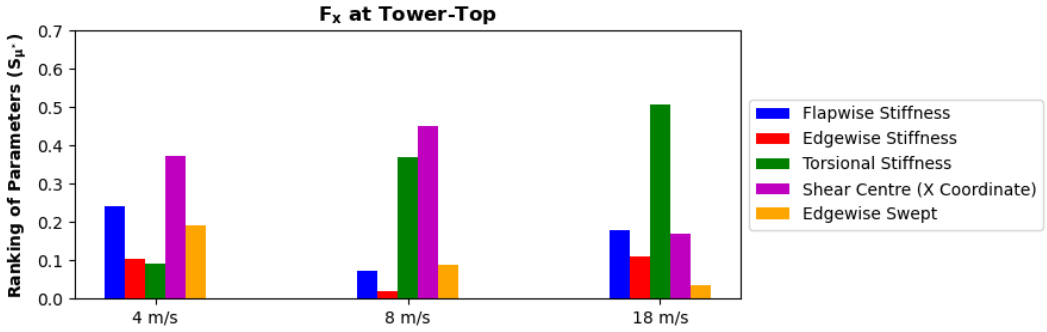

(a)

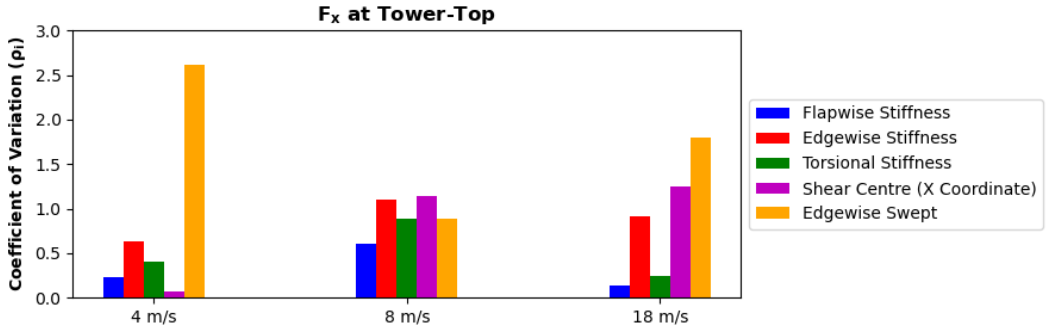

(b)

Figure G.4: (a) Ranking of parameters and (b) COV for side-side force, F_x, at the tower-top.

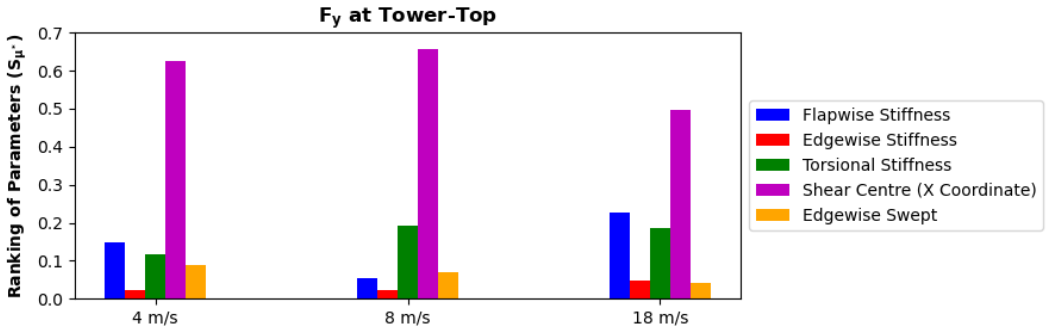

(a)

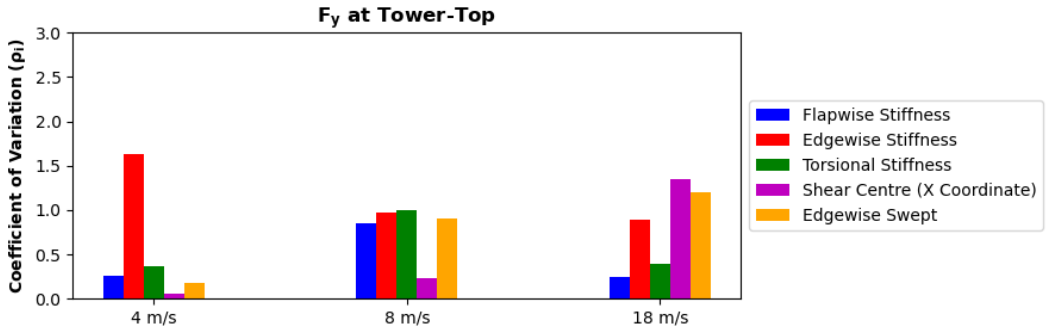

(b)

Figure G.5: (a) Ranking of parameters and (b) COV for fore-aft force, F_y, at the tower-top.

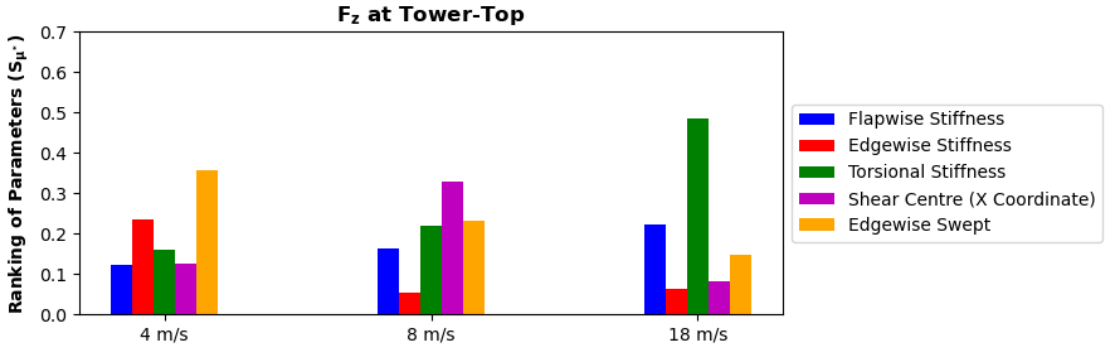

(a)

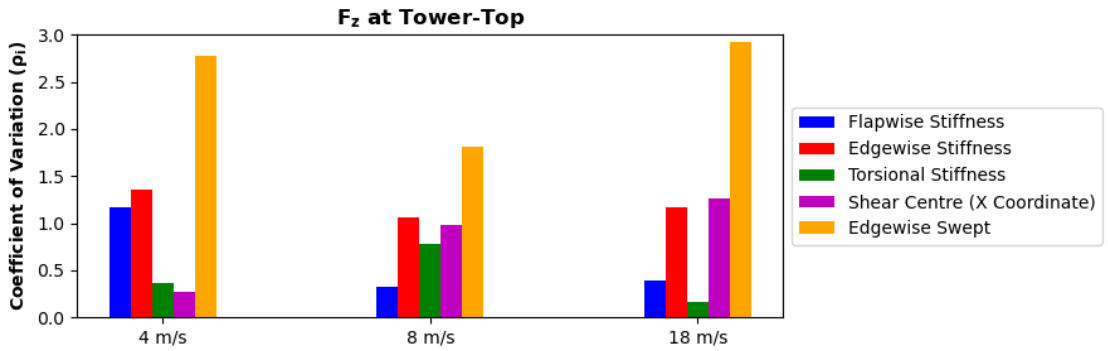

(b)

Figure G.6: (a) Ranking of parameters and (b) COV for axial force, F_z, at the tower-top.

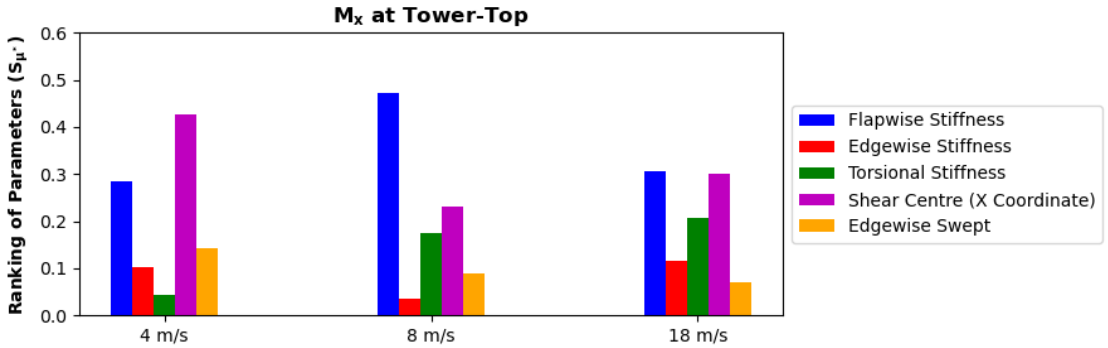

(a)

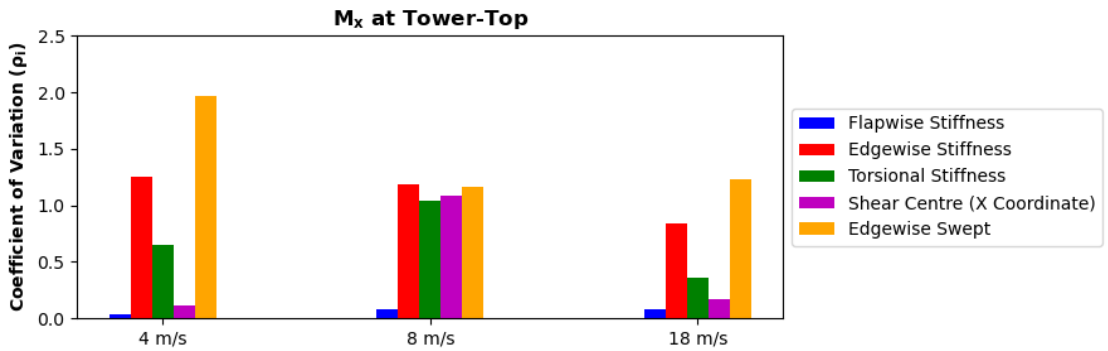

(b)

Figure G.7: (a) Ranking of parameters and (b) COV for fore-aft moment, M_x, at the tower-top.

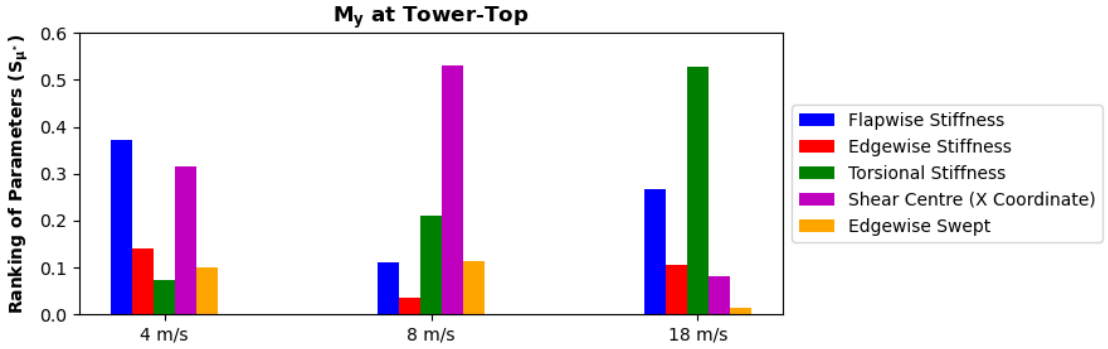

(a)

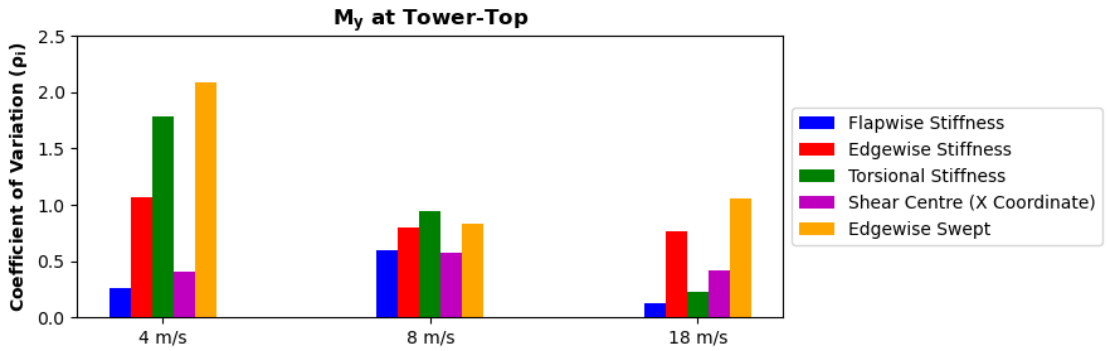

(b)

Figure G.8: (a) Ranking of parameters and (b) COV for side-side moment, M_y, at the tower-top.

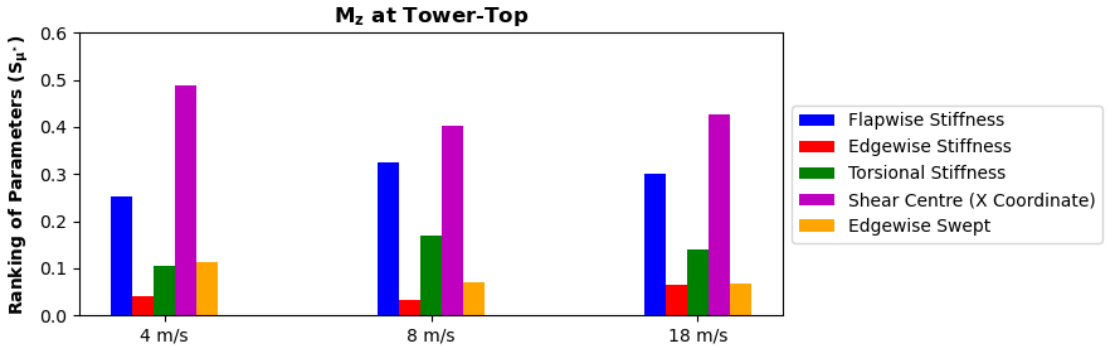

(a)

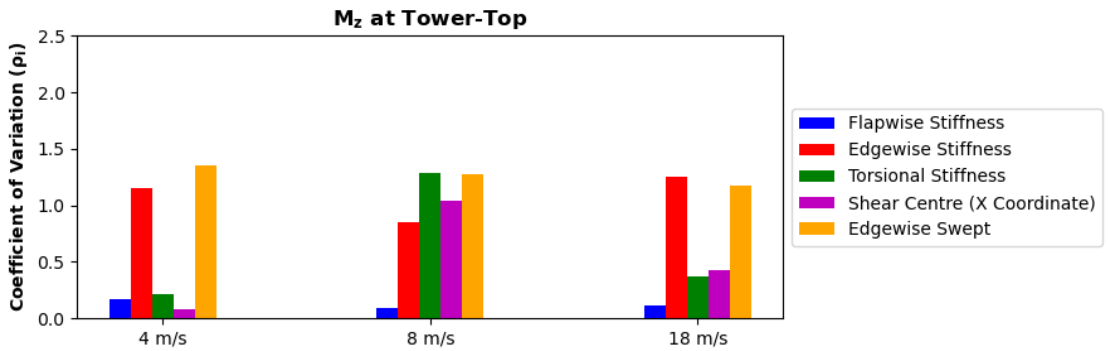

(b)

Figure G.9: (a) Ranking of parameters and (b) COV for torsional moment, M_z, at the tower-top.

G.1.3. Load Components at the Tower-Bottom

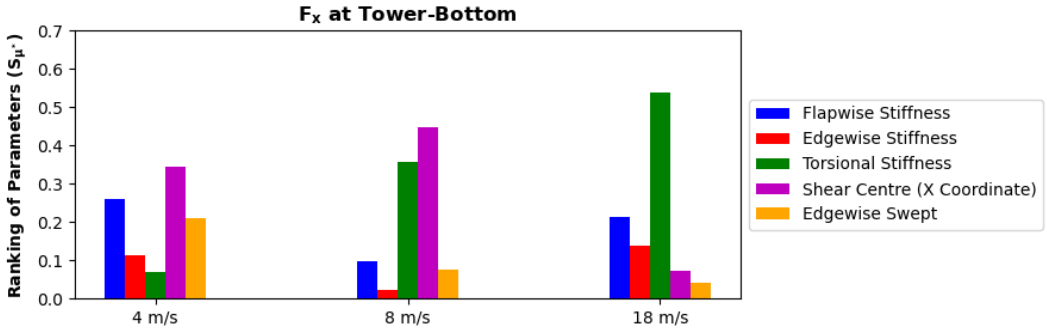

(a)

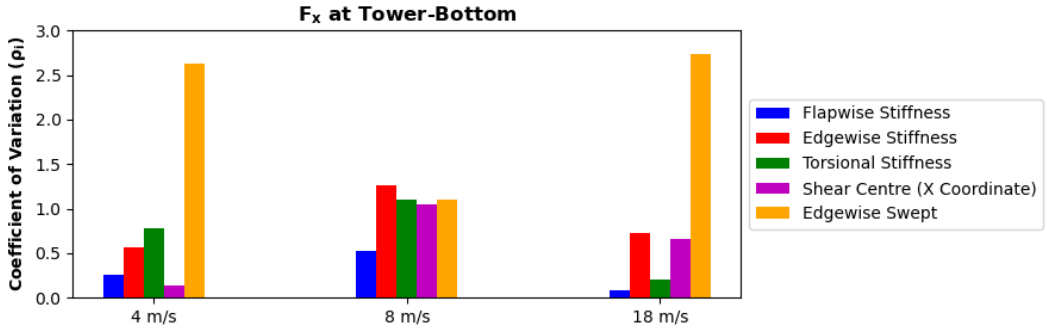

(b)

Figure G.10: (a) Ranking of parameters and (b) COV for side-side force, F_x, at the tower-bottom.

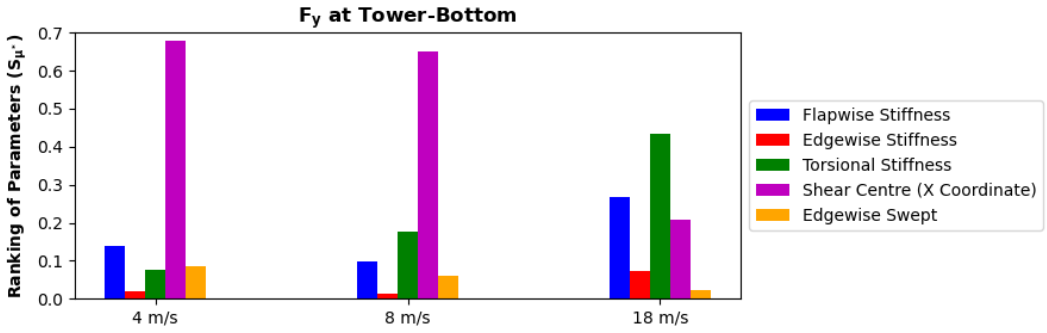

(a)

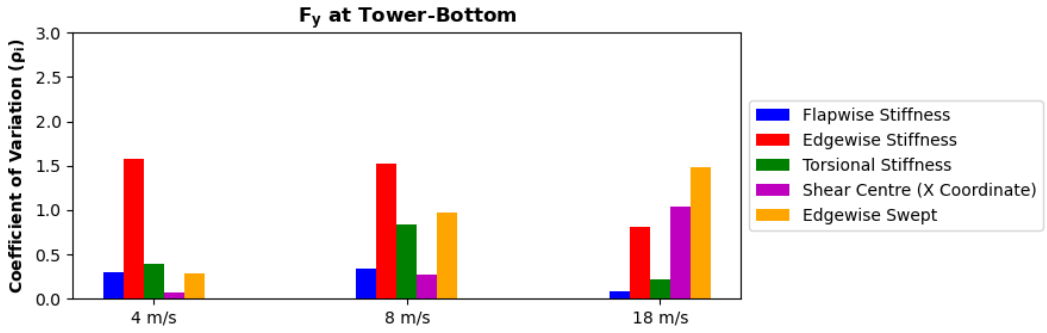

(b)

Figure G.11: (a) Ranking of parameters and (b) COV for fore-aft force, F_y, at the tower-bottom.

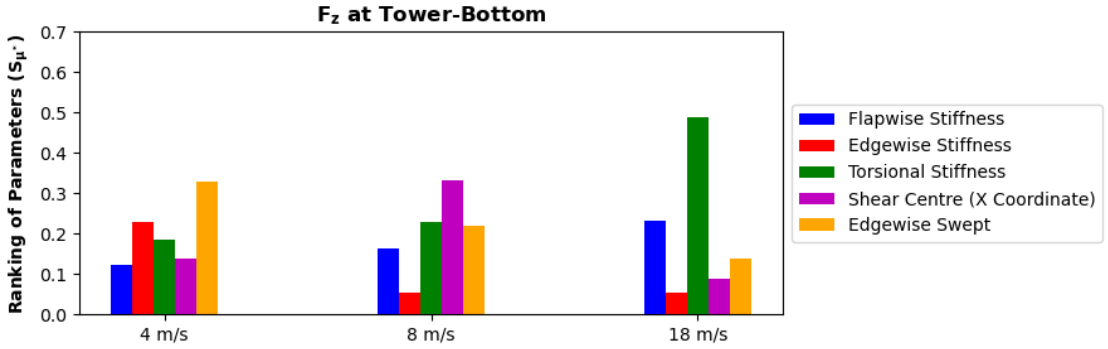

(a)

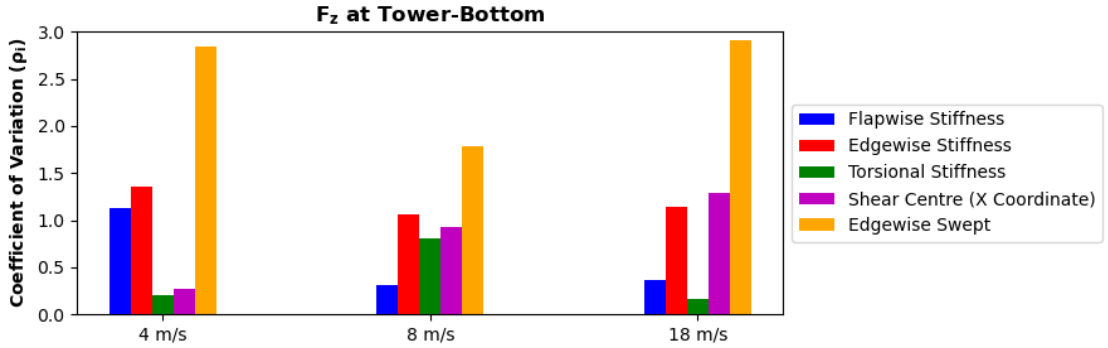

(b)

Figure G.12: (a) Ranking of parameters and (b) COV for axial force, F_z, at the tower-bottom.

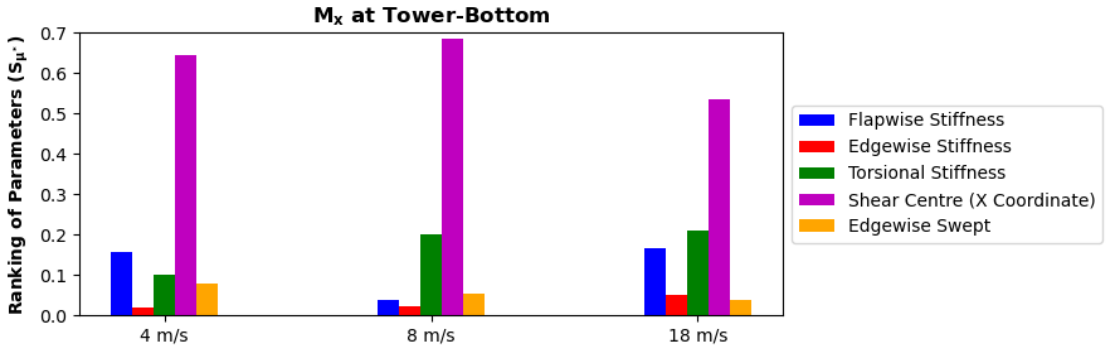

(a)

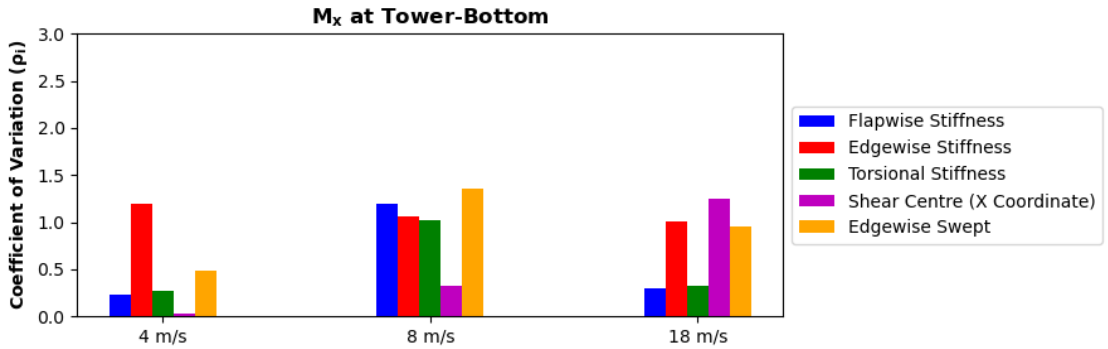

(b)

Figure G.13: (a) Ranking of parameters and (b) COV for fore-aft moment, M_x, at the tower-bottom.

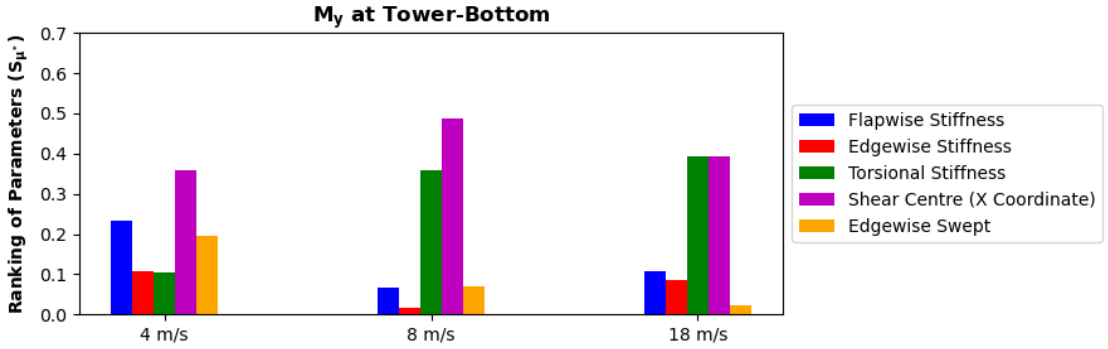

(a)

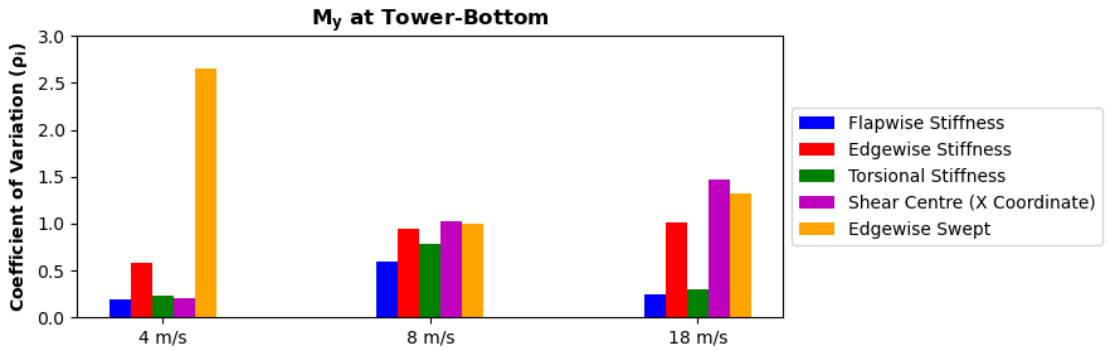

(b)

Figure G.14: (a) Ranking of parameters and (b) COV for side-side moment, M_y, at the tower-bottom.

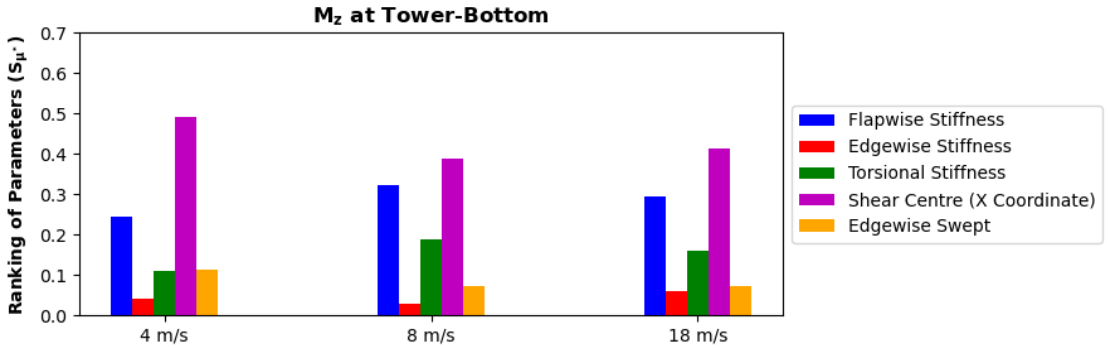

(a)

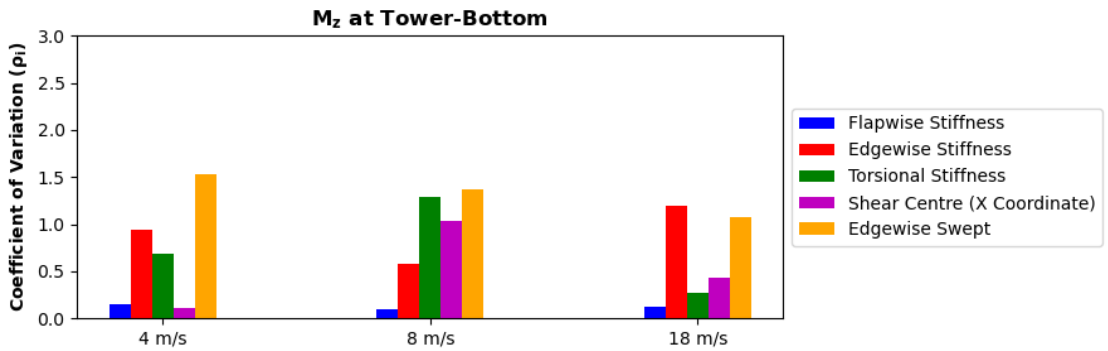

(b)

Figure G.15: (a) Ranking of parameters and (b) COV for torsional moment, M_z, at the tower-bottom.

COWI TU Delft Ørsted